UNIVERSIDAD AUTÓNOMA DE MADRID
FACULTAD DE CIENCIAS
DEPARTAMENTO DE BIOLOGÍA MOLECULAR

ROLE OF TUMOUR SUPPRESSORS IN THE CONTROL OF ENERGY HOMEOSTASIS

DOCTORAL THESIS

ELENA LÓPEZ GUADAMILLAS

MADRID, 2016

Universidad Autónoma de Madrid
Facultad de Ciencias
Departamento de Biología Molecular

ROLE OF TUMOUR SUPPRESSORS IN THE CONTROL OF ENERGY HOMEOSTASIS

DOCTORAL THESIS

Elena López Guadamillas

Madrid, 2016

Universidad Autónoma de Madrid
Facultad de Ciencias
Departamento de Biología Molecular

ROLE OF TUMOUR SUPPRESSORS IN THE CONTROL OF ENERGY HOMEOSTASIS

DOCTORAL THESIS

Elena López Guadamillas

BSc, MSc

The entirety of the work presented in this Thesis has been carried out at the Tumour Suppression Group in the Spanish National Cancer Research Centre (CNIO, Madrid), under the direction and supervision of
Dr. Manuel Serrano Marugán

Madrid, 2016

ACKNOWLEDGEMENTS

En primer lugar, quería agradecer a Manolo, mi director de tesis, por la gran oportunidad que me dio al abrirme las puertas de su laboratorio. Gracias por compartir tus grandes ideas y confiar en mí para llevarlas a cabo, por tu apoyo y por transmitirme tu ilusión por la ciencia.

Gracias a todos los miembros, pasados y presentes, de mi grupo, supresión tumoral; por toda la ayuda y apoyo recibido durante este tiempo. Pero sobre todo, gracias por todos los grandes momentos que hemos vivido juntos!!! Gracias a nuestros vecinos, el grupo de telómeros y telomerasa, por ser parte de nuestro grupo y por compartir mucho más que el laboratorio. Gracias a todas las unidades del CNIO y a Terapias Experimentales. Sin vuestra ayuda esta tesis habría sido imposible de llevar a cabo.

Por último, quería agradecer el gran trabajo y esfuerzo de todos nuestros colaboradores, en especial a Rafa y todo su laboratorio, por toda vuestra ayuda y hacerme sentir en casa durante esos dos meses de estancia en Baltimore.

Finalmente, quería agradecer a toda mi familia y amigos, por su continuo apoyo y cariño.

Muchísimas gracias!

INDEX

SUMMARY **7**

RESUMEN **11**

ABBREVIATIONS **15**

INTRODUCTION **21**

1. The insulin/IGF1 signalling pathway **23**

1.1 The insulin/IGF1 axis in longevity 23

1.2 Dietary restriction 24

2. The phosphatidylinositol 3 kinase PI3K **26**

2.1 The canonical PI3K/AKT pathway 27

2.2 Regulation of PI3K 29

2.3 Role of the PI3K pathway in cancer 30

2.4 Role of the PI3K pathway in metabolic disorders 31

2.5 Targeting the PI3K/AKT/mTOR pathway 32

3. Pathophysiological implications of obesity **33**

4. The fasting response **35**

4.1 Physiological adaptations to fasting 37

4.2 Cellular and molecular adaptations to fasting 38

5. Role of tumour suppressor genes in stress signalling pathways **41**

5.1 The tumour suppressor genes p21 42

OBJECTIVES **45**

OBJETIVOS **49**

MATERIALS & METHODS **53**

1. Mouse experimentation **55**

1.1 Animal housing 55

1.2 Transgenic mouse models 55

1.3 Administration of PI3K inhibitors 56

1.4 Metabolic characterization 56

1.5 Histology and immunohistochemistry 58

1.6 *In situ* hybridization 58

1.7 Immunophenotyping by flow cytometry 59

2. Monkey experimentation **59**

2.1 Animal housing 59

2.2 Preliminary study 60

2.3 Long-term study 60

2.4 Metabolic parameters 60

3. Characterization of the CNIO-PI3K inhibitor 61
3.1 PI3K inhibitory assay 61
3.2 Pharmacokinetics 62
4. *In vitro* procedures 62
4.1 Cell culture 62
4.2 Lentiviral transduction 62
4.2 Crystal violet staining 63
5. Biochemical assyas 63
5.1 DNA extraction 63
5.2 RNA extraction and qRT-PCR 63
5.3 Mitochondrial content 66
5.4 RNA-seq based transcriptional profiling 66
5.5 Protein extraction and immunoblots 66
6. Statistical analysis 67

RESULTS 69
1. Part 1. *In vivo* characterization of the pharmacological inhibition of PI3K 71
1.1 Effects of CNIO-PI3Ki on cellular and glucose homeostasis 71
1.2 PI3K inhibition reduces obesity, visceral fat and hepatic steatosis in mice 74
1.3 Improved metabolic syndrome after long-term CNIO-PI3Ki treatment 76
1.4 CNIO-PI3Ki protects against obesity and induces energy expenditure 81
1.5 CNIO-PI3Ki treatment reduces obesity in hyperphagic mice 82
1.6 PI3Kα inhibition promotes Ucp1 activity and causes body weight loss 84
1.7 CNIO-Pi3Ki treatment reduces adiposity in rhesus monkeys 87
2. Part 2. Role of the tumour suppressor gene p21 in the fasting response 93
2.1 Characterization of fasting-induced *p21* upregulation 93
2.2 Impaired adaptation to prolonged fasting in $p21^{Cip1}$ deficient mice 95
2.3 Enhanced energy expenditure and activity in p21KO deficient mice during fasting 97
2.4 Global transcriptome changes in $p21^{Cip1}$ deficient mice 99
2.5 Decreased immune response in 24 hours fasted p21KO mice 99
2.6 Decreased PPARα activity in the liver of p21KO mice 100
2.7 Fasting induces senescence in combination with a low oncogenic stress 102

DISCUSSION 105
1. Part 1. *In vivo* effects of pharmacological PI3K inhibition 107
1.1 PI3K inhibitors as anti-obesity treatment in obese mice 107
1.2 p110α in the regulation of energy homeostasis 110
1.3 PI3K, energy expenditure and obesity 112

1.4 CNIO-PI3Ki treatment in obese rhesus monkeys 113
1.5 Concluding remarks 114
2. Part 2. Role of p21 in the fasting response 115
2.1 p21 is a fasting-inducible factor 116
2.2 p21 enables efficient adaptation to fasting 116
2.3 p21 deficiency and transcriptional differences 117
2.4 Fasting-induced senescence 120
CONCLUSIONS 123
CONCLUSIONES 127
BIBLIOGRAPHY 131
SUPPLEMENTARY MATERIAL 155
Supplementary Table S1 157
Supplementary Table S2 164
ANNEX 165

SUMMARY

The insulin/IGF1 signalling pathway is one of the best-characterized pathways affecting longevity. Indeed, a partial reduction of the pathway has been shown to extend healthy lifespan, protect against cancer, improve insulin sensitivity and promote longevity in a great variety of organisms including worms, flies and mice. Similarly, dietary restriction is also considered a robust and conserved intervention to slow ageing and expand lifespan. In this thesis, we have focussed on two different aspects of the pathway: in the first place, we have analysed the *in vivo* effects of the pharmacological inhibition of PI3K, a key mediator of the pathway; and secondly, we have investigated the role of tumour suppressor genes in the response to fasting, the most extreme form of dietary restriction.

Genetic inhibition of PI3K signalling has been shown to increase energy expenditure, protect from obesity and the metabolic syndrome, and extend lifespan. Here, we wanted to explore whether the *in vivo* pharmacological inhibition of PI3K led to comparable effects. Interestingly, treatment with two PI3K inhibitors, CNIO-PI3Ki and GDC-0941, both preferentially selective for the α and δ isoforms, reduces adiposity of obese mice, exclusively, without affecting lean mass content. Furthermore, in the context of continuous nutritional excess, long-term treatment of obese mice with CNIO-PI3Ki reduces body weight, until reaching a new balance that is stable for months and as long as the treatment is administered, by inducing energy expenditure. CNIO-PI3Ki treatment, additionally, reverts liver steatosis, improves glycemia and reduces inflammation, thereby improving some signs of the metabolic syndrome. Finally, we have extended the use of the CNIO-PI3Ki treatment to rhesus monkeys, showing that a daily oral dose decreases adiposity and lowers glycemia of obese monkeys treated for 3 months, in the absence of detectable toxicities. Thus, pharmacological inhibition of PI3K is an effective and safe anti-obesity intervention in obese mice and monkeys that could conceivably reduce adiposity and reverse some of the symptoms of the metabolic syndrome in humans.

Fasting is a physiological stress that elicits well-known metabolic and molecular adaptations. However, little is known about the role of stress-responsive tumour suppressor genes in the fasting response. Therefore, we examined the expression of several tumour suppressors in mice upon fasting, finding that the expression of *p21* is uniquely induced in a great variety of tissues, particularly in the liver (>10 fold), in a process that is independent of p53. Remarkably, p21-deficient mice cannot efficiently adapt to long-term fasting (48 hours), becoming severely morbid and prematurely energy exhausted. Analysis of the liver transcriptome and cell-based assays revealed that the absence of p21 impairs the activity of PPARα, which is known to be critical for the adaptation to fasting by inducing fatty acid β-oxidation and ketogenesis. Therefore, we conclude that p21 is a fasting-induced factor that positively regulates PPARα and plays a relevant role in the adaptation to fasting.

RESUMEN

La ruta de señalización de la insulina/IGF1 es una de las principales vías implicadas en el envejecimiento. De hecho, su inhibición parcial protege frente al cáncer, mejora la sensibilidad a insulina y aumenta la longevidad en una gran variedad de organismos, incluyendo nematodos, moscas y ratones. De igual modo, se ha demostrado que la restricción calórica es una intervención robusta y conservada capaz de frenar el envejecimiento y alargar la longevidad. En esta tesis nos hemos centrado en dos aspectos de la ruta: por un lado, hemos analizado los efectos *in vivo* de la inhibición farmacológica de PI3K, un mediador clave de la vía; y en segundo lugar, hemos investigado el papel de los genes supresores de tumores en la respuesta al ayuno, considerado la forma más agresiva de restricción calórica.

La inhibición genética de la señalización de PI3K incrementa el gasto energético, protege frente a la obesidad y el síndrome metabólico, y aumenta la longevidad. En este trabajo hemos querido verificar si la inhibición farmacológica de PI3K *in vivo* tenía como resultado efectos similares. En concreto, observamos que el tratamiento con dos inhibidores de PI3K, CNIO-PI3K y GDC-0941, ambos inhibidores preferentes de las isoformas α y δ, reduce la adiposidad de ratones obesos. Además, en un contexto de exceso nutricional, el tratamiento prolongado con CNIO-PI3Ki, al inducir el gasto energético, reduce el peso corporal de los ratones hasta alcanzar un equilibrio que se mantiene estable mientras se administra el tratamiento. Dicho tratamiento revierte la esteatosis hepática, reduce los niveles de glucosa y la inflamación. Finalmente, hemos extendido el uso del CNIO-PI3Ki a macacos rhesus, demostrando que una dosis oral diaria durante 3 meses disminuye la adiposidad y la glucemia en monos obesos en ausencia de toxicidad. Por ello consideramos que la inhibición farmacológica de PI3K es una intervención anti-obesidad efectiva y segura en ratones y monos obesos, que podría llegar a reducir la adiposidad y revertir algunos síntomas del síndrome metabólico en humanos.

El ayuno es un estrés fisiológico que promueve múltiples adaptaciones metabólicas y moleculares. Sin embargo, teniendo en cuenta que los genes supresores de tumores se activan en respuesta a diferentes estímulos, se desconoce el papel que éstos juegan durante el ayuno. Por esta razón, analizamos la expresión de varios supresores de tumores en ratones en ayuno, descubriendo que únicamente la expresión de *p21* se induce en una gran variedad de tejidos, especialmente en el hígado (>10 veces), y de manera independiente de p53. Asimismo comprobamos que los ratones deficientes en p21 no son capaces de adaptarse eficientemente a periodos largos de ayuno (48 horas), ya que presentan síntomas graves de debilidad y una pérdida acelerada de energía. Esto es debido a que la ausencia de p21 impide la correcta actividad de PPARα, un factor crítico en la adaptación al ayuno. Por tanto, concluimos que p21 es un factor inducido en respuesta a ayuno, que regula positivamente la actividad de PPARα y que juega un papel clave en la adaptación al ayuno.

ABBREVIATIONS

4EBP1	Eukaryotic translation initiation factor 4E binding protein 1
AC	Adenylate cyclase
ACOT1/3	Acyl-CoA thioesterase 1/3
AgRP	Agouti-related peptide
AKT	V-Akt murine thymoma viral oncogene
ALT	Alanine aminotransferase
cAMP	cyclic-Adenosine monophosphate
AMPK	5' Adenosine monophosphate-activated protein kinase
ARC	Arcuate nucleus
AUC	Area under the curve
BAT	Brown adipose tissue
iBAT	Interscapular BAT
BW	Body weight
cAMP	Cyclic adenosine monophosphate
CART	Cocaine- and amphetamine-regulated transcript
CBP	CREB-binding protein
CDK	Cyclin-dependent kinase
CEBPβ	CCAAT/enhancer binding protein-β
CREB	cAMP response element-binding
CRTC2	CREB-regulated Transcription Coactivator 2
DMEM	Dulbecco's modified Eagle's medium
DMSO	Dimethyl sulfoxide
DNA	Deoxyribonucleic acid
cDNA	Complementary DNA
DR	Dietary restriction
DXA	Dual-energy X-ray absorptiometry
EE	Energy expenditure
F4/80 (Emr1)	EGF-like module-containing mucin-like hormone receptor-like 1
FFA	Free fatty acids
FGF21	Fibroblast growth factor 21
FOXO1/3	Forkhead box O 1/3
G6PC	Glucose-6-phosphatase, catalytic subunit
ChREBP	Carbohydrate-responsive element-binding protein
GLUT4	Glucose transporter type 4
GP	Glycogen phosphorylase
GPCR	G-protein coupled receptor
GSEA	Gene set enrichment analysis

GSK3β	Glycogen synthase kinase 3 β
GTT	Glucose tolerance test
GYK	Glycerol kinase
HDAC	Histone deacetylase
H&E	Hematoxylin & eosin
HFD	High fat diet
HNF4	Hepatocyte nuclear factor 4
HOMA-IR	Homeostatic model assessment-insulin resistance
IL-6	Interleukin 6
IGF1	Insulin-like growth factor 1
IHC	Immunohistochemistry
IRS1	Insulin receptor substrate 1
ITT	Insulin tolerance test
I.V.	Intravenous
I.P.	Intraperitoneal
KB	Ketone bodies
KO	Knock-out
L-PK	Liver pyruvate kinase
MCH	Mean corpuscular hemoglobin
MCV	Mean corpuscular volume
mTOR	Mammalian target of rapamycin
MYH2/4	Myosin, heavy chain 2/4
NMR	Nuclear magnetic resonance
NEFA	Non-esterified fatty acid
NF-κB	Nuclear factor-κB
NPY	Neuropeptide Y
$p16^{Ink4a}$	Cyclin-dependent kinase inhibitor 2a
$p19^{Arf}$	Cyclin-dependent kinase inhibitor 2a
$p21^{Cip1}$	Cyclin-dependent kinase inhibitor 1a
$p27^{Kip1}$	Cyclin-dependent kinase inhibitor 1b
p53	Tumour protein p53
PEPCK	Phosphoenolpyruvate carboxykinase 1
PCNA	Proliferating cell nuclear antigen
PDK1	3-Phosphoinositide dependent protein kinase-1
PDK4	Pyruvate dehydrogenase lipoamide kinase isozyme 4
PGC1α	Peroxisome proliferator-activated receptor gamma coactivator 1-α
PI3K	Phosphatidylinositol-3-kinase

PI3Ki	PI3K inhibitor
PKA	Protein kinase A/cAMP-dependent protein kinase
POMC	Pro-opiomelanocortin
PP2A	Protein phosphatase 2
PPARα	Peroxisome proliferator-activated receptor α
PRDM16	PR domain containing 16
preBAs	Pre-brown adipocytes
PTEN	Phosphatase and tensin homolog
Q-PCR	Quantitative-polymerase chain reaction
RB	Retinoblastoma
RNA	Ribonucleic acid
mRNA	Messenger RNA
shRNA	Short-hairpin RNA
RNA-seq	RNA sequencing
SREBP1c	Sterol regulatory element-binding protein 1
RTK	Receptor tyrosine kinase
S6	Ribosomal protein S6
S6K	Ribosomal protein S6 kinase
SAA3	Serum amyloid A 3
SA-β Gal	Senescence associated-β galactosidase
SD	Standard diet
Rheb	Ras homolog enriched in brain
SIRT1	NAD-dependent deacetylase sirtuin-1
SNS	Sympathetic nervous system
TG	Triglycerides
Tg	Transgenic
TNNI1	Troponin I type 1
TSC 1/2	Tuberous sclerosis protein 1/2
UCP1	Uncoupling protein 1
VPS34	Vacuolar protein sorting 34
WAT	White adipose tissue
eWAT	Epididymal WAT
iWAT	Inguinal WAT
rWAT	Perirenal WAT
scWAT	subcutaneous WAT
WT	Wild-type

INTRODUCTION

1. The insulin/IGF1 signalling pathway

The insulin/IGF1 signalling (IIS) pathway is one of the most important and highly conserved nutrient-sensing pathways. In mammals, the pathway is activated when different growth factors such as insulin or IGF1, whose production is stimulated by growth hormone (GH), bind to their correspondent receptors and activate PI3K either through a direct binding or through the IRS1 scaffold protein. Activation of PI3K is followed by phosphorylation of AKT, which, in turn, triggers a complex cascade of events that include the activation of mTORC1 and the inactivation of FOXO.

Importantly, the IIS pathway is the best characterized pathway affecting longevity, as a partial reduction of the pathway has been shown to improve healthy lifespan, protect against cancer, improve insulin sensitivity and expand lifespan in a great variety of organisms including worms, flies and mice (Houtkooper et al., 2010; Kenyon, 2010). In addition, external interventions that downregulate insulin/IGF1 signalling such as dietary restriction or rapamycin treatment have been shown to be robust anti-aging methods as well (Fontana et al., 2010).

1.1 The insulin/IGF1 axis in longevity

Ageing is a complex process that results from the accumulation of molecular, cellular and organ damage that ultimately leads to a progressive decline in physiological function. Despite this complexity, many studies suggest that most of the mutations and interventions that extend lifespan in a great variety of organisms are directly related to a downregulation of nutrient-sensing pathways, such as the insulin/IGF1 and TOR pathways (Houtkooper et al., 2010; Kenyon, 2010) (**Figure 1**).

Yeast and invertebrate models have played an important role in establishing the main genes, pathways and mechanisms involved in lifespan extension. In *S. cerevisiae*, deletion or inhibition of SCH9 (the S6K homolog) (Fabrizio et al., 2001) and TOR1 (Kaeberlein et al., 2005; Powers et al., 2006) increases lifespan by more than a 2 fold by providing increased resistance against oxidants, genotoxins and heat. Similarly, reduction of the IIS pathway in *C. elegans* by either *daf-2* (insulin/IGF1 receptor homolog) (Kenyon et al., 1993), *age-1* (PI3K homolog) mutation (Friedman and Johnson, 1988) or reduction of TOR (Jia et al., 2004), leads to an extension in the lifespan of about 65-100%. This lifespan expansion depends on the enhanced activity of the forkhead FOXO transcription factor daf-16 (Libina et al., 2003), which regulates the expression of genes like superoxide dismutase (MnSOD) and heat shock proteins (HSPs) involved in oxidative and stress resistance respectively. In *D. melanogaster*, genetic deletion of insulin-like peptides (dilps) (Gronke et al., 2010) or insulin receptor substrate Chico (Clancy et al., 2001), as well as the downregulation of the TOR pathway activity either

genetically (Kapahi et al., 2004) or by rapamycin (Bjedov et al., 2010), also increases longevity. This has been associated with an increase in stress resistance and autophagy together with a reduction in protein turnover.

As in yeast, worms and flies, reduced activity of the nutrient-sensing IIS pathway can increase lifespan in mouse in about a 20-70% depending on gender, mouse background and diet (Bartke, 2005). Mutations in genes that impair the biosynthesis, binding or activity of GH and IGF1 (Junnila et al., 2013) as well as alterations in various downstream members of the pathway such as *PTEN* upregulation (Ortega-Molina et al., 2012) or deletion of *PI3K*α (Foukas et al., 2013) lead to lifespan extension in mouse. In addition, inhibition of the mTOR pathway either with rapamycin treatment (Harrison et al., 2009) or deletion of *S6K1* (Selman et al., 2009) has been demonstrated to promote lifespan too. Some of the mechanisms thought to be involved in this lifespan extension include reduced inflammation, proliferation, oxidative damage and ER stress, accompanied by increased autophagy, regenerative capacity, and mitochondrial function.

Lastly, studies of human populations have led to the identification of a number naturally occurring deficiencies in the GH/IGF1 axis associated with reduced cancer incidence, insulin sensitivity and, possibly, increased longevity. This is the case of subjects with GH-receptor, IGF1 and IGF1-receptor deficiencies (Guevara-Aguirre et al., 2011; Laron, 2008).

1.2 Dietary restriction

To date, dietary restriction is the most robust and best-characterized intervention to extend lifespan. Numerous studies demonstrate that dietary restriction (DR), avoiding malnutrition, expands lifespan in a great variety of organisms including yeast, flies, worms, fish and rodents, and increases healthy lifespan in primates (Fontana and Partridge, 2015; Fontana et al., 2010) (**Figure 1**).

In the case of mouse, a reduction in food intake of about 25-55% results in a 30-50% lifespan extension (Weindruch et al., 1986). Of note, DR inhibits spontaneous, chemically-induced and radiation-induced tumours in several mouse models (Albanes, 1987; Thompson et al., 2003). In monkeys DR greatly delays the onset of age-associated pathologies such as sarcopenia, presbycusis and brain atrophy as well as reduces the incidence of type II diabetes, cancer and cardiovascular disease (Colman et al., 2014; Mattison et al., 2012). Importantly, in humans DR promotes healthy lifespan by reducing the incidence of type II diabetes, insulin resistance, inflammation, cancer and cardiovascular disease (Cava and Fontana, 2013; Fontana et al., 2010).

Although the mechanisms and key players responsible for the beneficial health effects observed under DR are still poorly understood, it is well accepted that, at least in part, some of them are mediated by the reduction of IGF1 levels and consequent inhibition of the PI3K/AKT pathway and enhanced FOXO activity. FOXO not only reduces proliferation but also stimulates apoptosis, DNA repair, stress resistance and autophagy (Webb and Brunet, 2014). Another key player accounting for the positive effects of DR is mTOR (Johnson et al., 2013), whose reduction improves proteostasis and increases autophagy (Rubinsztein et al., 2011). The activation of SIRT1 (Guarente, 2013) and AMPK (Burkewitz et al., 2014) are also considered key mechanisms that promote longevity under DR by enhancing genome stability together with reduced NF-κB signalling and antioxidant defences, respectively. As a consequence of all these adaptations, organisms show increased genome stability, stem cell and mitochondrial function, autophagy, stress resistance and tissue repair accompanied by a reduced inflammatory response that may eventually contribute to the observed and health- and liespan expansion (Fontana and Partridge, 2015).

Importantly, further reports have demonstrated that it is the restriction of proteins, particularly of methionine, rather than the total calorie intake restriction the leading cause that promotes lifespan extension in model organisms. This is thought to me mediated via the suppression of mTOR activity (Solon-Biet et al., 2014).

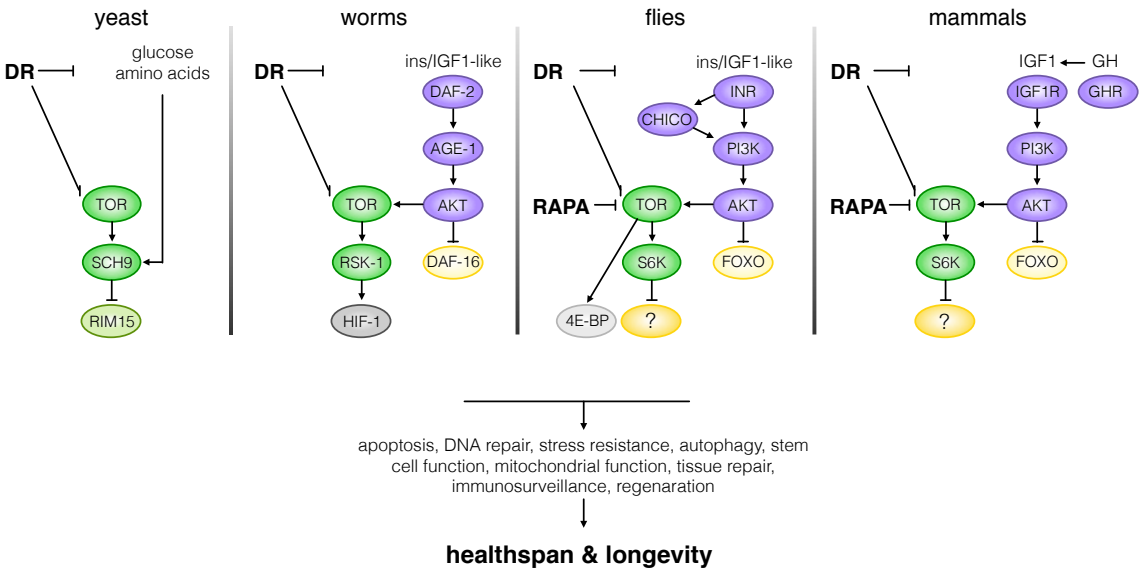

Figure 1. Conserved role of the insulin/IGF1 signalling (IIS) pathway in ageing.
The IIS pathway is conserved across various species including yeast, worms, flies and mammals. The pathway is activated upon binding of insulin/IGF1 to their receptor, which, in turn, activates PI3K and AKT. Following activation, AKT induces the activity of FOXO and TOR/S6K, two of the principal mediators of healthspan and longevity extension that stimulate apoptosis, DNA repair, stress resistance, autophagy, stem cell function, mitochondrial function, tissue repair, immunosurveillance and regeneration. External interventions such as dietary restriction (which reduces nutrients and IGF1 levels) as well as rapamycin treatment (which inhibits TOR) reduce the activity of the pathway and delay ageing and age-associated diseases.
DR: dietary restriction. Homologous pathways and proteins are indicated with the same colour code. Figure adapted from (Fontana et al., 2010).

2. The phosphatidylinositol 3 kinase PI3K

Phosphatidylinositol-3-kinases (PI3Ks) are a family of proteins involved in multiple cellular functions such as cell growth, proliferation, metabolism, glucose homeostasis, differentiation and survival (Engelman et al., 2006). They are divided into three different members according to their structural characteristics and substrate specificity (**Table 1**): class I, class II and class III (Vanhaesebroeck et al., 2010).

Class I PI3Ks, which are further divided into class IA and IB, are a group of PI3Ks located right in the centre of the insulin/IGF1 pathway that are able to phosphorylate the inositol ring of the membrane phospholipid phosphatidylinositol-4,5-bisphosphate (PI-4,5-P2) to generate phosphatidylinositol-3,4,5-trisphosphate (PIP3) upon activation. Class IA PI3Ks are composed of heterodimers consisting of a p110 catalytic subunit (p110α, p110β or p110δ) that interacts with a p85 regulatory subunit (p85α, p85β, p55α, p50α or p55γ). While p110α and p110β are ubiquitously expressed, p110δ is principally present in hematopoietic cells and, to a lesser extent, in the nervous system (Eickholt et al., 2007). Although class IA PI3K are predominantly activated by receptor tyrosine kinases (RTKs), recent data demonstrate that they can also respond to G protein-coupled receptors (GPCRs). Class IB PI3Ks consist of a single type of catalytic subunit (p110γ), which is activated by directly interacting with the Gβγ subunit of GPCRs, and a regulatory subunit (p87 or p101). In contrast to class IA PI3Ks, class IB is primarily expressed in leukocytes but can also be found in the liver, skeletal muscle, heart and pancreas. Of note, the signal transmitting small GTPase Ras plays a primordial role in the activation of both class I PI3Ks by RTKs (Katso et al., 2001; Vanhaesebroeck et al., 2010).

Class II PI3Ks consist of a single catalytic isoform (C2α, C2β or C2γ), as they do not require a regulatory subunit to function. These PI3Ks utilize phosphatidylinositol (PI) or phosphatidylinositol-4-phosphate (PI-4-P) to produce phosphatidylinositol-3-phosphate (PI-3-P) and phosphatidylinositol-3,4-bisphosphate (PI-3,4-P2) respectively. Following activation by RTKs or GPCRs, class II PI3Ks can stimulate cell migration, glucose metabolism, exocytosis and apoptosis, through a mechanism that is still unclear (Falasca and Maffucci, 2012).

Class III PI3Ks, which consist of the catalytic subunit VPS34 associated to the regulatory subunit VPS15, promote the phosphorylation of PI to form PI-3-P. VPS34 is located at autophagosomal or endosomal structures and is involved in vesicle trafficking. Even though it is not clear whether class III PI3K are regulated by extracellular stimuli, there is evidence that VPS34 activity can be regulated by GPCRs, glucose and amino acids, thereby mediating signalling through mTOR (Backer, 2008; Nobukuni et al., 2005; Schu et al., 1993).

As class I PI3K is the most studied member of the family and study-objective of this thesis, we will continue focussing on this class, referring to it as PI3K.

		catalytic sub.	regulatory sub.	activity	activator	function
class I PI3K	Type IA	p110α (ubiquitous) p110β (ubiquitous) p110δ (hemat. cells)	p85α p85β p55α p50α p55γ	PI-4,5-P2 → PIP3	receptor tyrosine kinases G-protein-coupled receptors (minor)	PI3K/AKT pathway activation
	Type IB	p110γ (principally leukocytes)	p87 p101	PI-4,5-P2 → PIP3	G-protein-coupled receptors	PI3K/AKT pathway activation
class II PI3K		PI3K-C2α (ubiquitous) PI3K-C2β (ubiquitous) PI3K-C2γ (leukocytes)		PI → PI-3-P PI-4-P → PI-3,4-P2	receptor tyrosine kinases G-protein-coupled receptors	membrane trafficking receptor internalization
class III PI3K		VPS34	VPS15	PI → PI-3-P	G-protein-coupled receptors amino acids glucose	vesicle trafficking mTOR activation

Table 1. The three PI3K classes.
The phosphatidylinositol-3-kinases (PI3Ks) are divided into three different classes characterized by specific catalytic and regulatory subunits, distribution, substrate specificity and activity, PI3K activator and function.

2.1 The canonical PI3K/AKT pathway

The PI3K/AKT pathway can be activated in response to nutrient and growth factor stimulation including insulin, IGF1, cytokines or chemokines, thereby regulating cellular growth, metabolism and survival (Manning and Cantley, 2007) (**Figure 2**). Upon binding of these factors to their correspondent RTKs and consequent activation, PI3K is recruited to the membrane by a direct interaction of the p85 subunit with the tyrosine phosphate motifs on receptors, by binding of p85 to the scaffold protein IRS1, or through the interaction with RAS. As previously mentioned, PI3K can also be activated by GPCRs through the binding to the βγ subunit (Carracedo and Pandolfi, 2008). Once active, PI3K phosphorylates the membrane phospholipid PI-4,5-P2 to generate PIP3 at the cytoplasmic face of the plasma membrane. PIP3 acts then as a second messenger by transmitting the signal to a subset of pleckstrin homology (PH) and PH-like domain containing proteins (Engelman et al., 2006) such as AKT (Franke et al., 1997) , PDK1 (Currie et al., 1999) and mTORC2 (Liu et al., 2015), this last one consisting of the mTOR, Rictor, MSin1 (PH-containing subunit) and mLST8 proteins. After PIP3 stimulation, AKT anchors to the plasma membrane together with PDK1 and mTORC2, which fully activate AKT by phosphorylating AKT in Thr308 (Alessi et al., 1997; Stephens et al., 1998) and Ser473 residue (Dos et al., 2004; Sarbassov et al., 2005) respectively. Once activated, AKT is able to phosphorylate up to 100 different substrates and is thereby responsible of modulating a great variety of cellular functions including most of the well-described PI3K responses.

AKT activity negatively regulates FOXO phosphorylating FOXO1 at Thr24, Ser256 and Ser319 (Rena et al., 1999) as well as FOXO3 (Brunet et al., 1999) and FOXO4 (Kops et al.,

1999) at equivalent sites. This phosphorylation leads to FOXO retention in the cytoplasm and inhibition of FOXO activity (Biggs et al., 1999; Tang et al., 1999). Thus, AKT is able to block the FOXO-dependent transcriptional programme of genes involved in gluconeogenesis (*PEPCK* and *G6Pc*) (Hall et al., 2000; Schmoll et al., 2000), oxidative stress resistance (*SOD* and *MnSOD*) (Kops et al., 2002), apoptosis (*PUMA* and *BIM*) (Sunters et al., 2003; You et al., 2006) and cell proliferation ($p21^{Cip1}$ and $p27^{Kip1}$) (Dijkers et al., 2000; Seoane et al., 2004). Moreover, AKT phosphorylates and inhibits PGC1α, which is a transcriptional coactivator that, together with FOXO1, promotes the transcription of genes related to fatty acid β-oxidation and gluconeogenesis (Puigserver et al., 2003). AKT plays also an important role in promoting glucose transport in response to insulin stimulation. By phosphorylating AS160, AKT is able to inhibit its GAP activity and stimulate the vesicle translocation of GLUT4 to the plasma membrane, thereby allowing the influx of glucose to the cytoplasm (Sano et al., 2003). Furthermore, AKT phosphorylates and inhibits GSK3β (Cross et al., 1995), thus promoting glycogen synthesis (through the activation of glycogen synthase) as well as lipid synthesis (through the stabilization of SREBP1). Besides, AKT also exerts an important antiapoptotic effect through the phosphorylation and inhibition of BAD (del Peso et al., 1997), MDM2 (Mayo and Donner, 2001) and members of the FOXO family (Biggs et al., 1999; Tang et al., 1999). In particular, AKT promotes the translocation of MDM2 to the nucleus by phosphorylating the Ser166 and Ser186 residues of MDM2, which finally negatively regulates p53 (Mayo and Donner, 2001; Zhou et al., 2001).

Additionally, AKT is one of the main regulators of mTORC1, a protein complex involved in autophagy, energy metabolism, protein translation and ribosome biogenesis, that is composed of the catalytic subunit mTOR, the regulatory subunit Raptor, the protein mLST8 and two endogenous inhibitors of the complex called PRAS40 (proline-rich AKT substrate of 40 kDa) and Deptor (DEP domain-containing mTOR-interacting protein) (Laplante and Sabatini, 2013). Active AKT regulates this complex in two different ways. On the one hand, AKT phosphorylates and inactivates the GTPase-activating protein (GAP) called TSC2 (Potter et al., 2002), which, in turn, forms a complex with TSC1 to inhibit the small GTPase Rheb (Ras-homolog enriched in brain) (Inoki et al., 2003a). Rheb is then responsible of activating mTORC1 through the inhibition of FKBP38, which is a negative regulator of mTORC1 (Bai et al., 2007). On the other hand, AKT regulates mTORC1 activity by phosphorylating and inhibiting PRAS40, which is a negative regulator of mTORC1 through the competition of GTPase Rheb (Sancak et al., 2007; Wang et al., 2007). Once active, mTORC1 phosphorylates and activates S6K1 and S6K2 (Brown et al., 1995) thereby triggering the phosphorylation of different substrates including the ribosomal protein S6 (Chung et al., 1992), PDCD4 (Dorrello et al., 2006), eEF2 kinase (Wang et al., 2001) and eIF4B (Raught et al., 2004) to promote

protein synthesis and ribosome biogenesis. Additionally, mTORC1 also phosphorylates and inactivates 4E-binding protein 1 (4EBP1), thereby releasing the inhibition of the eukaryotic initiation factor 4E (eIF4E) and promoting protein translation (Brown et al., 1995).

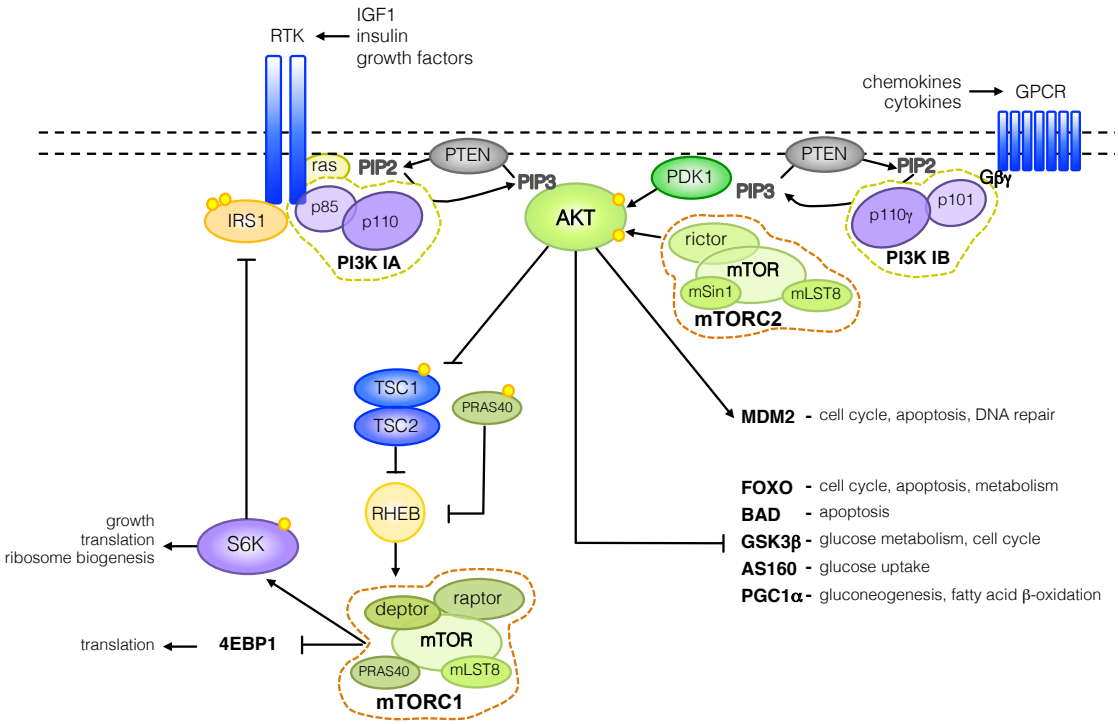

Figure 2. The PI3K/AKT signalling pathway.
Representation of the main proteins, interactions and processes involved in the PI3K/AKT signalling pathway. Small yellow circles indicate phosphoryl groups.

2.2 Regulation of PI3K

The PI3K/AKT pathway is tightly regulated at various levels, but, even though the intensity of PI3K activation is regulated by a number of proteins, the phosphatase and tensin homolog deleted on chromosome ten (PTEN) is the main negative regulator of the pathway. PTEN is a lipid phosphatase with a lipid-binding domain that allows anchorage to the plasma membrane. Importantly, PTEN counteracts the activity of PI3K by converting PIP3 back to PI-4,5-PI2 (Maehama and Dixon, 1998; Stambolic et al., 1998) (**Figure 2**). Downstream of PI3K, the activation of AKT is also negatively regulated by different proteins. While the dephosphorylation of the Thr308 residue is mediated by PP2A phosphatase (Padmanabhan et al., 2009), PHLPP phosphatase dephosphorylates AKT at Ser473 (Gao et al., 2005). Furthermore, the pseudokinase tribbles homolog 3 (TRIB3) is able to bind and inhibit AKT in response to insulin stimulation (Du et al., 2003). In contrast, some members of the FOXO family can positively regulate the PI3K/AKT pathway, through the inhibition of the PP2A phosphatase (Ni et al., 2007) and transcriptional activation of some RTKs, including the insulin receptor, upon AKT inhibition (Chandarlapaty et al., 2011).

PI3K is further controlled by downstream components of the pathway, thereby providing feedback regulation in response to extracellular signals. The most important negative feedback mechanism is the one driven by mTORC1 and S6K (**Figure 2**). First observations revealed that chronic insulin stimulation and consequent PI3K pathway hyperactivation lead to the phosphorylation and proteosomal degradation of the adaptor protein IRS1 (Haruta et al., 2000; Qiao et al., 2002; Zhande et al., 2002). Later studies showed that S6K1 phosphorylated and inhibited IRS1 on Ser302 (Harrington et al., 2004) and Ser1101 (Tremblay et al., 2007), preventing its recruitment and binding to RTKs and leading to reduced PI3K signalling. Similarly, mTORC1 can phosphorylate IRS1 on Ser636/639 (Tzatsos and Kandror, 2006), thereby reducing its activity. Altogether, this explains why the hyperactivity of the pathway caused by chronic exposure to insulin results in the desensitization of the PI3K/AKT pathway and can lead to insulin resistance.

2.3 Role of the PI3K pathway in cancer

The role of the PI3K pathway in different diseases has been widely studied since its discovery. It is not surprising that, being a central mediator of survival and growth signals, aberrations in many of the members of the pathway have specially been associated with cancer as well as with various cancer susceptibility syndromes in humans.

The first direct link between PI3K activity and human cancer was established with the study of PTEN function which was found to be highly mutated and lost in several cancers (Li and Sun, 1997; Li et al., 1997; Steck et al., 1997). PTEN is considered one of the major tumour suppressor genes due to its ability to reduce PI3K signalling and, thereby, cell growth and survival. Mutations in the catalytic domain (Sansal and Sellers, 2004) or in ubiquitinylation sites (Trotman et al., 2007) correlate with the development and progression of cancer. In fact, *PTEN* is mutated in about 38% of the endometrial carcinomas, 21% of brain tumours, 17% of skin cancers, and 13% of colon carcinomas. Similarly, 25-37% of all the glioblastomas, melanoma and gastric and breast cancers present *PTEN* heterozygosity loss (Liu et al., 2009). Furthermore, germline mutations in the *PTEN* gene cause various inherited cancer predisposition syndromes such as Cowden's syndrome, Lhermitte-Duclos and Bannayan-Riley-Ruvalcaba's syndrome (Eng, 2003). PI3K class IA is another member of the pathway that is frequently mutated and amplified in a wide variety of cancers (Samuels et al., 2004). Mutations in both, the catalytic *p110α* as well as the regulatory *p85α* subunit of PI3K, which lead to increased PI3K and AKT activity, are common alterations appearing in around 27% of breast cancers, 15% of colon cancers, 8% of pancreas cancers or 10% of glioblastomas (Liu et al., 2009). Finally, amplification of the *AKT* (Liu et al., 2009) or *PDK1* genes (Brugge et al., 2007),

have also been found in a number of different tumour types, and alterations in the *TSC* genes result in the development of an autosomal dominant disease called tuberous sclerosis, characterized by the formation of hamartomas in brain, heart, lung and kidney, angiomyolipomas and rhabdomyomas (Jozwiak et al., 2008).

2.4 Role of the PI3K pathway in metabolic disorders

As previously described, the PI3K/AKT pathway triggers a cascade of responses important for metabolic signals and glucose homeostasis.

Many studies in mouse models and the further support of clinical data have made clear that reduced PI3K activity plays a crucial role in insulin sensitivity and type II diabetes, among other metabolic disorders. In this context, p85, the regulatory subunit of PI3K IA, is involved in mediating insulin sensitivity. Despite being responsible for the stability of the catalytic subunit p110 (Yu et al., 1998) and for its recruitment to activated growth factor receptors or the adaptor protein IRS1 (Cantley, 2002), heterozygous deletion of p85α (Terauchi et al., 1999) and homozygous deletion of p85β in mouse (Ueki et al., 2002), leads to improved insulin signalling and enhanced insulin-stimulated AKT activation. This apparent contradiction can be explained by the fact that monomeric p85, which appears in excess in many cell types, competes with p85-p110 heterodimers for binding to and sequestering IRS1 in cytosolic protein complexes (Luo et al., 2005). Thus, reduced levels of monomeric p85 results in enhanced binding of p85-p110 PI3K heterodimers to IRS and increased insulin sensitivity.

Furthermore, a great number of mouse studies suggest that PI3K plays an important role in setting the balance between nutrient storage and nutrient consumption, contributing in this manner to a differential fat accumulation. In general, overall reduction of PI3K signalling due to PTEN overexpression leads to enhanced energy expenditure and, thereby, to reduced body weight and enhanced metabolic damage protection (**Figure 3**) (Garcia-Cao et al., 2012; Ortega-Molina et al., 2012). This increase in energy expenditure has been proposed to be mediated through two independent mechanisms. On the one hand, PI3K inhibition was shown to induce thermogenesis, and therefore energy expenditure, in the brown adipose tissue through the upregulation of *ucp1* directly driven by FOXO1 (Ortega-Molina et al., 2012). On the other hand, it has been suggested that PTEN overexpression leads to increased mitochondrial oxidative phosphorylation together with reduced anaerobic glycolysis, which would eventually enhance energy expenditure (Garcia-Cao et al., 2012). Notably, PTEN-overexpressing mice are characterized by a cancer-protective state, improved insulin sensitivity and extended lifespan (Ortega-Molina et al., 2012). Further reinforcing this idea, inhibition of single PI3K isoforms also achieves similar metabolic effects. In particular, mice with systemic partial decreased

PI3Kα signalling (Foukas et al., 2013), liver-specific complete loss of PI3Kα (Chattopadhyay et al., 2011), total lack of PI3Kγ activity (Becattini et al., 2011; Kobayashi et al., 2011) or combined complete loss of PI3Kγ and PI3Kβ activities (Perino et al., 2014) are protected from obesity due to an enhanced energy expenditure. Also, S6K1-deficient mice exhibit enhanced lipolysis, reduced adipose tissue and HFD-induced metabolic damage protection (Um et al., 2004) as well as extended lifespan (Selman et al., 2009).

Finally, data obtained from human patients further support a conserved role for this pathway in diabetes and obesity. For instance, p85 levels are increased in some patients with insulin resistance and AKT2 appears mutated in familiar insulin resistance. Furthermore, there is a strong association between hyperactive PI3K signalling due to germline PTEN haploinsufficiency and obesity (Pal et al., 2012).

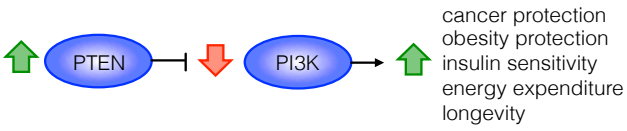

Figure 3. Effects of genetic PI3K downregulation.
Mice with reduced PI3K activity due to PTEN overexpression are characterized by cancer protection, increased energy expenditure, obesity protection, enhanced insulin sensitivity and extended longevity.

2.5 Targeting the PI3K/AKT/mTOR pathway

Developing effective inhibitors that target PI3K and other key components of the pathway represents a major goal for the treatment of a number of diseases, including (but not exclusively) cancer types with increased PI3K activity. In fact, some of these compounds are already being tested in preclinical phase I-II trials for the treatment of a great variety of tumours (Liu et al., 2009). The first generation of PI3K inhibitors, wortmannin and LY294002, were broad-spectrum inhibitors with restricted selectivity for individual PI3K isoforms and significant toxicity associated (Knight and Shokat, 2007). However, new isoform-selective PI3K inhibitors (CAL-101, selective p110δ, and BYL-719, selective p110α) or dual PI3K-mTOR inhibitors (SF1126 or BEZ235) are being introduced into preclinical trials for the treatment of advanced solid tumours and lymphomas showing more effective results (Liu et al., 2009).

Another attractive target of the pathway, and probably the most studied one since the discovery of rapamycin, is mTORC1. Rapamycin is a bacterially derived product able to suppress mTOR-mediated S6K and 4EBP1 phosphorylation by forming a complex with FKBP12, which then binds directly to the mammalian TOR complex 1 (mTORC1) but not to mTORC2 (Benjamin et al., 2011; Sabatini, 2006). Originally used as an antifungal agent (Vézina et al., 1975), rapamycin was subsequently found to have important immunosuppressant functions in humans and is therefore used to prevent rejection in organ transplantation (Yatscoff

et al., 1993). Even though rapamycin and rapamycin-related mTOR inhibitors present a low efficiency and response rate against tumour progression in some types of tumours, these have been approved for the treatment of renal cell carcinoma, soft-tissue and bone sarcomas and have also shown promising results for the treatment of TSC-associated symptoms (Faivre et al., 2006). Of note, and as previously discussed, rapamycin treatment increases lifespan in a number of organisms including mice (Fontana et al., 2010).

Interestingly, and despite the numerous reports that suggest that reduced PI3K activity may protect against obesity and symptoms of the metabolic syndrome, there are currently no PI3K inhibitors approved for the use in obesity treatment. In this context, previous studies in our laboratory demonstrated that a synthetic PI3K inhibitor (CNIO-PI3Ki) is able to increase energy expenditure and hyperactivate the BAT of mice (Ortega-Molina et al., 2012).

3. Pathophysiological implications of obesity

In contrast to the beneficial effects of dietary restriction and reduced PI3K signalling, obesity is emerging as a major global public health problem due to the numerous pathologies associated to obesity such as type II diabetes, insulin resistance, hepatic steatosis and cancer (**Figure 4**). The worldwide prevalence of obesity has nearly doubled between 1980 and 2008 (Caballero, 2007) and the incidence in developing countries has risen 3-fold (Ellulu et al., 2014). As an example, in 2011-2012, it was estimated that over one-third of the US adult population was obese or overweight (Ogden et al., 2014).

Typically, obesity appears when nutrient intake exceeds nutrient consumption. Initially, this gain in net caloric intake, driven by hypercaloric or fat-rich diets combined with a lack of physical exercise, results in obesity due to the hypertrophy and hyperplasia of the adipose tissue. However, the continuous caloric overload finally leads to the aberrant accumulation of lipids in non-adipose tissues including liver and muscle (Van Der Klaauw and Farooqi, 2015).

Obesity is tightly associated with the metabolic syndrome; a pathophysiological condition characterized by the presence of at least three of the following medical signs occurring at the same time: abdominal obesity, hypertension, hyperglycemia, and dyslipidemia, which includes hypertriglyceridemia or low high-density lipoprotein (HDL) levels (Després and Lemieux, 2006). The metabolic syndrome, as well as obesity, is correlated with a higher risk of developing insulin resistance and type II diabetes (**Figure 4**). Insulin resistance is characterized by the presence of cells that are resistant to insulin action, thereby compromising glucose uptake in the tissues and increasing glucose production in the liver, which finally gives rise to hyperglycemia (Kahn et al., 2006). Although obesity triggers insulin resistance by diverse mechanisms, it is mostly accepted that elevated non-esterified fatty acids (NEFAs) arising from

adipocytes play a key role in two different ways. On the one hand, increased intracellular NEFAs result in competition with glucose for oxidation, which leads to the downregulation of glycolysis by inhibiting pyruvate dehydrogenase, phosphofructokinase and hexokinase II (Randle, 1998). On the other hand, high NEFA levels result in the inhibitory phosphorylation of IRS1 and IRS2 and eventual suppression of the downstream insulin signalling (Solinas et al., 2006). The systemic increase in proinflammatory cytokines secreted by the adipose tissue also contributes to insulin resistance as TNFα (Zhang et al., 2002) and IL-6 (Yang et al., 2008) increase adipocyte lipolytic activity and thus, increase NEFA concentration, as well as mediate IRS1 and IRS2 inhibitory phosphorylation. Depending on pancreatic β-cell function, insulin resistance can progress to type II diabetes. In the context of healthy β-cells, elevated glucose levels lead to compensatory hyperinsulinemia and glucose tolerance through the increase of β-cell function and growth. In contrast, susceptible pancreatic β-cells carrying genetic risk factors, result in β-cell dysfunction and apoptosis in response to increased glucose levels, leading to impaired glucose tolerance and followed by the development of type II diabetes (Kahn et al., 2006).

Importantly, obesity is also considered a major risk factor not only for type II diabetes but also for other age-related pathologies including cardiovascular disease, neurodegenerative diseases and cancer (Haslam and James, 2005). In particular, several epidemiological studies have consistently shown a link between obesity and an elevated incidence of some cancer types such as colon, liver, pancreas, kidney and breast (Calle and Kaaks, 2004). Obesity increases the risk of developing cancer through a number of mechanisms and pathophysiological alterations that include changes in the production of hormones, adipokines and cytokines (Font-Burgada et al., 2016) (**Figure 4**). Obesity is characterized by systemic inflammation and a higher presence of pro-inflammatory M1 macrophages in the white adipose tissue that produce tumour-promoting cytokines such as TNF and IL6 (McNelis and Olefsky, 2014). Both are able to induce survival, proliferation, DNA damage, stemness and invasiveness by activating NF-κB/JNK and STAT3 respectively (Taniguchi and Karin, 2014; Yan et al., 2006). The altered secretion of adipokines, including low adiponectin and high leptin production, is another feature that can lead to tumourigenesis under obesity conditions. Whereas adiponectin is considered an inhibitor of tumour progression due to its ability to inhibit mTOR, activate AMPK and reduce inflammation (Dalamaga et al., 2012), leptin exerts a pro-tumourigenic effect by enhancing angiogenesis through the activation of STAT3 (Uddin et al., 2011). Furthermore, hyperinsulinemia and hypergylcemia are also two important tumour-promoting effectors derived from obesity-induced insulin resistance. Both, insulin and glucose exert an important cell survival, growth and proliferative promoting effect, especially in pre-neoplastic cells. Moreover, high glucose levels favour the increased survival of cancer cells under hypoxic

conditions due to the activation of HIF1α (Catrina et al., 2004). Similarly, high-fat diet has been shown to increase stemness and tumourigenicity of intestinal stem and progenitor cells through a PPARδ-dependent mechanism (Beyaz et al., 2016).

As a consequence of the influence of obesity on tumourigenesis, it is considered that around 14% and 20% of all cancer deaths in men and women, respectively, are due in part to overweight and obesity. And, furthermore, it is estimated that the overall risk of death from cancer is around 1.5 fold higher in obese patients (Font-Burgada et al., 2016). However, despite the increasing number of obesity and overweight incidence worldwide and the important health implications, there are currently limited pharmacological treatments available to treat obesity.

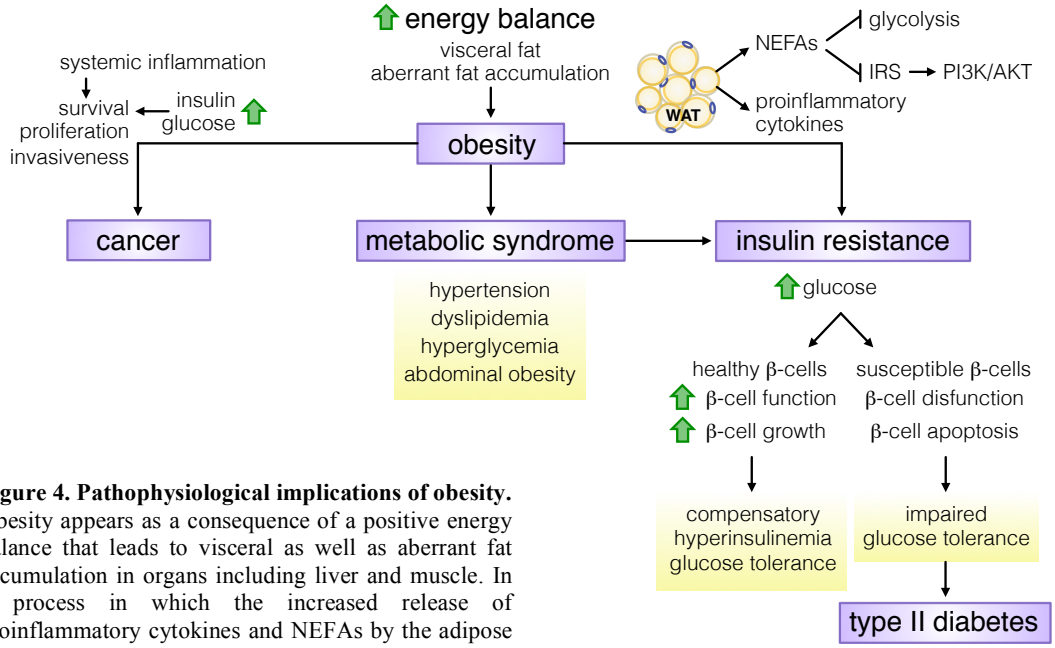

Figure 4. Pathophysiological implications of obesity. Obesity appears as a consequence of a positive energy balance that leads to visceral as well as aberrant fat accumulation in organs including liver and muscle. In a process in which the increased release of proinflammatory cytokines and NEFAs by the adipose tissue plays a determinant role, obesity is a major risk factor for the development of metabolic syndrome and insulin resistance. In turn, insulin resistance can progress to type II diabetes in the context of susceptible pancreatic β-cells. Obesity is also considered an important risk factor for cancer. NEFA: non-esterified fatty acid, WAT: white adipose tissue.

4. The fasting response

DR is a potent intervention to extend healthy lifespan and longevity in a great number of organisms. In worms, flies and mice lifespan rises to a maximum as food intake is lowered but, with further reduction of food intake, longevity is rapidly reduced. Fasting is the most extreme form of DR and requires abstinence from all food, but not from water. Nevertheless, studies in experimental organisms as well as in humans indicate that fasting periods may provide effective strategies to delay ageing and improve healthspan (Longo and Mattson, 2014).

In lower organisms such as bacteria (Gonidakis et al., 2010), yeast (Wei et al., 2008) and worms (Kaeberlein et al., 2006) food deprivation causes a 2-fold lifespan extension as well as an increase in the resistance to multiple stresses mainly driven by the downregulation of the

TOR-S6K pathway and upregulation of FOXO transcriptional activity. In the case of mammals, fasting can be applied in a chronic manner as intermittent fasting. Several studies have shown that intermittent fasting can extend lifespan up to 30% (Goodrick et al., 1990) and promote protection against several age-associated diseases in rodents. In fact, intermittent fasting reduces the incidence of neurodegenerative diseases including Alzheimer, Parkinson and Huntington, by reducing inflammation and the accumulation of oxidatively damaged molecules, as well as by improving cellular bioenergetics, neurotrophic factor signalling, and increasing synaptic plasticity (Mattson, 2012). As in the case of DR, fasting can prevent and reverse all aspects of the metabolic syndrome, reduce obesity, inflammation and blood pressure and increase insulin sensitivity (Longo and Mattson, 2014). Importantly, alternative day fasting has been demonstrated to reduce cancer incidence (Varady and Hellerstein, 2007) and improve cancer treatment by selectively protecting normal cells, but not cancerous cells, from chemotherapeutic agents (Lee et al., 2012; Raffaghello et al., 2008). This effect, called differential stress resistance, has been demonstrated on different cancer cells and mouse models treated with chemotherapy. Differential stress resistance is based on the hypothesis that, in response to fasting, normal, healthy cells enter a state characterized by low proliferation and resistance to several stresses due to the downregulation of the PI3K/AKT signalling pathway among others. In contrast, activation of oncogenic pathways renders cancer cells insensitive to growth inhibitory signals and unable to switch to a stress resistance mode. Thus, upon fasting, chemotherapeutics that target actively proliferating cells retain their efficacy on malignant, cancer cells, without causing side effects on normal cells.

Furthermore, clinical and epidemiological data support the ability of fasting to delay aging and age-associated diseases in humans. Besides promoting a reduction of oxidative damage (Johnson et al., 2007), inflammation (Müller et al., 2001) and blood pressure (Varady et al., 2009), fasting has been shown to enhance insulin sensitivity (Harvie et al., 2011) and decrease chemotherapy-induced side effects (Raffaghello et al., 2010; Safdie et al., 2009) in patients. It is thought that the inhibition of mTOR and, specially, the reduction in circulating IGF1 levels, which induce FOXO, autophagy and improved mitochondrial function among others, account for the observed positive effects of fasting (Longo and Mattson, 2014).

4.1 Physiological adaptations to fasting

Throughout evolution, organisms have developed different behavioural, physiological, biochemical and molecular mechanisms to efficiently adapt to fluctuations in nutrient availability. In particular, fasting is signalled through highly conserved nutrient-sensing

pathways that promote the arrest of energy- and nutrient-consuming anabolic processes aimed to reduce energy consumption (Wang et al., 2006).

During the adaptive response to fasting, mammals go through four different metabolic stages that are essentially controlled by the liver (Cahill, 2006; Wang et al., 2006) (**Figure 5**):

1. First, as glucose is consumed and cleared from the serum, hepatic glycogen serves as the main source of glucose. In a process called glycogenolysis, glucose, stored in the liver in the form of glycogen, is released again to the bloodstream to maintain constant blood glucose levels. Typically in humans, glucose from the diet is consumed within the first 4 hours. Glycogen becomes then the major glucose source for the next 4-16 hours, although glycogen stores last for more than 28 hours. In mice, glycogen stores are already completely consumed after 18-24 hours.
2. After liver glycogen stores are depleted, gluconeogenesis becomes necessary to cover the energetic requirements of organs, especially the brain, by allowing the production of glucose from gluconeogenic substrates. Gluconeogenesis, which is a process that takes place mainly in the liver and partially covers the reverse steps of glycolysis, generates glucose from amino acids, lactate, glycerol and pyruvate generated in hepatocytes or delivered from extrahepatic tissues through the circulation. Gluconeogenesis becomes necessary in humans after ca. 16 hours of fasting, turning into the main glucose supply for more than 24 days. In mouse, however, gluconeogenesis begins already 12 hours post-fasting.
3. At the same time, glycerol and non-esterified fatty acids (NEFAs) are released by the adipose tissue into the bloodstream upon lipolysis of triglyceride stores. NEFAs become then the major energy source not only through their β-oxidation but also through their conversion to ketone bodies in the liver via ketogenesis. Ketone bodies, consisting of β-hydroxybutyrate, acetoacetate and acetone, are produced in hepatocytes from the acetyl-CoA generated from the β-oxidation of fatty acids as well as from ketogenic amino acids (Iso, Phe, Tryp, Tyr and Thr). Ketone bodies, especially β-hydroxybutyrate, play an essential role in the adaptation to fasting as, unlike most tissues that can use fatty acids for energy, the brain relies on ketone bodies in addition to glucose for energy consumption. Ketogenesis starts to be indispensible in humans after the second day of fasting. In contrast, mice start to depend on ketone body formation already after 24 hours of fasting.
4. Finally, with prolonged fasting, fat reserves are exhausted, leading to a rapid protein degradation in the muscle that is necessary to fuel gluconeogenesis in hepatocytes (Rui, 2014; Wang et al., 2006). Normally, this process happens in human after 24 days of fasting and starts in mouse after 48 hours.

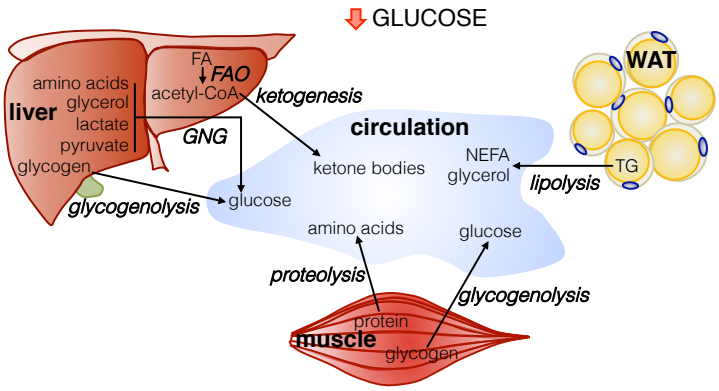

Figure 5. Physiological adaptations to fasting.
A simplified view of the major tissues and processes involved in energy homeostasis during the adaptation to fasting. NEFAs and glycerol are released to the circulation from the WAT upon lipolysis, and amino acids and glucose from the muscle through proteolysis and glycogenolysis respectively. The liver captures substrates from the bloodstream and produces glucose (through glycogen breakdown or gluconeogenesis) and generates ketone bodies through the FAO and ketogenesis of fatty acids. WAT: white adipose tissue, FAO: fatty acid β-oxidation, GNG: gluconeogenesis, TG: triglycerides, FA: fatty acids, NEFA: non-esterified fatty acids.

4.2 Cellular and molecular adaptations to fasting

Many of the molecular and cellular adaptations necessary for the adaptation to fasting are driven by insulin and glucagon, two hormones secreted by pancreatic β- and α-cells, respectively, in response to glucose availability. Under fasting conditions and hypoglycemia, reduced circulating insulin levels together with elevated glucagon levels promote a metabolic switch from an anabolic to a catabolic programme (Lempradl et al., 2015) (**Figure 6**).

The main functions of insulin, which acts by activating the PI3K/AKT pathway as previously described, is to increase glucose uptake in the tissues and promote the storage of substrates in fat, liver and muscle. Therefore, insulin is considered the primary regulator of blood glucose concentration. In the fasted state, reduced insulin levels are translated into multiple adaptations that are driven by the downregulation of the PI3K/AKT pathway by insulin. Low insulin promotes the release of glucose from glycogen liver stores in two different manners. First, reduced AKT activity leads to the activation of GSK3β, which in turn phosphorylates and inactivates glycogen synthase, thereby inhibiting glycogen synthesis (Cross et al., 1995). Second, by limiting the acetylation of glycogen phosphorylase, low insulin levels allow the phosphorylation and activation of glycogen phosphorylase, thereby promoting glycogenolysis (Zhang et al., 2012). Simultaneously, reduced insulin/PI3K/AKT signalling promotes gluconeogenesis in the liver through the increased activation of FOXO transcription factors that upregulate the expression of gluconeogenic genes such as *PEPCK* and *G6Pc* (Haeusler et al., 2010; Puigserver et al., 2003). Additionally, FOXO transcription factors transcribe *PDK4*, an enzyme that inhibits the conversion of pyruvate to acetyl-CoA. This favours the use of pyruvate as gluconeogenic substrate and reduces the glycolytic activity of cells (Jeong et al., 2012). Low insulin levels further repress glycolysis by diminishing the activity of glucokinase and the kinase activity of the bifunctional enzyme 6-phosphofructo-2-kinase/fructose-2,6-bisphosphate (PFK-2/FBP-2) (Okar et al., 2001). Finally, insulin also participates in the metabolism of lipids

by stimulating the expression and activity of SREBP1, a key transcription factor that activates the expression of genes related to fatty acid and lipid synthesis. Thus, reduced insulin signalling results in the inhibition of lipogenesis by decreasing the expression of *SREBP1* as well as by allowing the inhibitory binding of LIPIN1 to SREBP1. Of note, both processes are mediated through the reduction of mTORC1/S6K (Wan et al., 2011; Yecies et al., 2011).

At the same time, glucagon, which opposes the effects of insulin, is also responsible for many of the adaptations to fasting by activating the cAMP/PKA pathway. In response to low blood glucose levels, glucagon is secreted to the circulation by pancreatic α-cells and, when bound to GPCRs, it activates adenylate cyclase (AC). Active AC produces cAMP from ATP, which in turn triggers the activation of PKA (protein kinase A or cAMP-dependent protein kinase) and consequently the activation of a cascade of effectors including CREB (Altarejos and Montminy, 2011). Under fasting conditions, high glucagon levels promote glycogenolysis through different mechanisms mediated by PKA. First, PKA phosphorylates and activates glycogen phosphorylase directly or indirectly by inhibiting the acetylation of glycogen phosphorylase. PKA is also able to phosphorylate and activate phosphorylase kinase, which, in turn, triggers the activation of glycogen phosphorylase (Zhang et al., 2012). Glucagon also promotes hepatic gluconeogenesis by stimulating the expression of gluconeogenic genes such as *PEPCK* and *G6Pc* by CREB, which usually acts together with the coactivator CRTC2 (Herzig et al., 2001). PKA can further enhance gluconeogenesis by promoting the dephosphorylation of CRTC2, which avoids the degradation of CRTC2 (Wang et al., 2012); by stimulating the acetylation of CRTC2 via p300/CBP, which increases both the stability and gluconeogenic activity of CRTC2 (Liu et al., 2008); and by dephosphorylating and activating HDACs, which deacetylate and activate FOXO transcription factors and thereby FOXO-dependent transcription (Mihaylova et al., 2011). Moreover, glucagon supresses glycolysis by stimulating the PKA-mediated phosphorylation of PFK-2/FBP-2, thereby enhancing its phosphatase activity (Okar et al., 2001) and by reducing the expression of the liver pyruvate kinase (L-PK), which suppresses the binding of ChREBP to its promoter region (Yamashita et al., 2001). In addition, the transcription factor ChREBP is phosphorylated at Ser196 by PKA in response to glucagon stimulation, resulting in cytoplasm retention and inactivation (Kawaguchi et al., 2001). On the contrary, ChREBP is strongly activated by glucose (Yamashita et al., 2001). Furthermore, decreased ChREBP activity not only supresses glycolysis but also lipogenesis due to the reduced expression of ChREBP-dependent lipogenic genes such as *ACL, ACC, SCD1* and *FAS* (Iizuka et al., 2004).

Finally, glucagon is likewise involved in lipid metabolism by stimulating fatty acidβ-oxidation and ketogenesis in the liver. The peroxisome proliferator-activated receptor alpha (PPARα), a nuclear receptor protein activated by fatty acids (Chakravarthy et al., 2009), is the

master regulator of both, fatty acid β-oxidation and ketogenesis, as its activity promotes the expression of genes involved in fatty acid transport and binding, peroxisomal and mitochondrial fatty acid β-oxidation and ketogenesis (Kersten et al., 1999; Pawlak et al., 2015; Wahli and Michalik, 2012). Glucagon, can directly induce the transcriptional activity of PPARα by sequentially activating PKA, AMPK and p38 MAPK, leading to the dissociation from PPARα from its repressor HSP90 (Longuet et al., 2008). Multiple PPARα coactivators have been identified to promote PPARα-dependent β-oxidation and ketogenesis. The peroxisome proliferator-activated receptor gamma coactivator 1-alpha (PGC1α) is one of the best-characterized PPARα coactivators (Vega et al., 2000). PGC1α not only acts as PPARα coactivator to promote fatty acid β-oxidation and ketogenesis, but is also able to activate gluconeogenesis by building a transcriptional complex with FOXO1 and HNF4 (Finck and Kelly, 2006; Yoon et al., 2001). Upon fasting, both, reduced insulin and high glucagon blood levels induce the expression of PGC1α through the stimulation of the transcriptional activity of FOXO (Daitoku et al., 2003) and CREB (Herzig et al., 2001), respectively. In addition, the absence of insulin increases the activity of PGC1α by reducing the inhibitory phosphorylation of PGC1α by AKT (Li et al., 2007).

Moreover, AMPK and SIRT1 are further considered important energy sensors, as a low energetic status is associated with high AMPK and SIRT1 activity. Activation of AMPK, which is triggered in response to low cellular energy (high AMP to ATP ratio), results in the repression of ATP-consuming anabolic processes such as lipogenesis, glycogenesis, gluconeogenesis and protein synthesis, and the activation of ATP-producing catabolic processes such as fatty acid β-oxidation, ketogenesis and glucose uptake (Fulco and Sartorelli, 2008). While AMPK controls glucose uptake by increasing GLUT4 expression and translocation in extrahepatic tissues (Fisher et al., 2002), in the liver, it blocks lipogenesis by phosphorylating (at Ser372) and inhibiting SREBP1 (Li et al., 2011). SIRT1 is a member of the sirtuin family of proteins that uses NAD+ as substrate and that exerts its functions through the deacetylation of target proteins such as histones, transcription factors and coactivators (Fulco and Sartorelli, 2008). In turn, SIRT1 is able to promote fatty acid oxidation and gluconeogenesis by deacetylating PGC1α (Nemoto et al., 2005), thereby allowing its binding to HNF4 or PPARα. Moreover, deacetylation of SREBP1 by SIRT1 leads to the inhibition of lipogenesis (Ponugoti et al., 2010).

Finally, mTORC1 represents a main nutrient, stress and energy sensor as well. In a PI3K-independet manner, mTORC1 can also be directly regulated by nutrients, especially by amino acids (Sengupta et al., 2010). Amino acids have been proposed to activate mTORC1 through the inhibition of TSC1/TSC2 (Gao et al., 2002), through the stimulation of Rheb (Long

et al., 2005) or via VPS34 class III PI3K signalling (Nobukuni et al., 2005). In particular, amino acid deprivation leads to rapid S6K1 and 4EBP1 dephosphorylation in an mTORC1-dependent manner. Moreover, mTORC1 senses the energy status of a cell through AMP-activated protein kinase (AMPK). Activated AMPK directly phosphorylates TSC2 leading to the inhibition of mTORC1 signalling and cell growth (Inoki et al., 2003b).

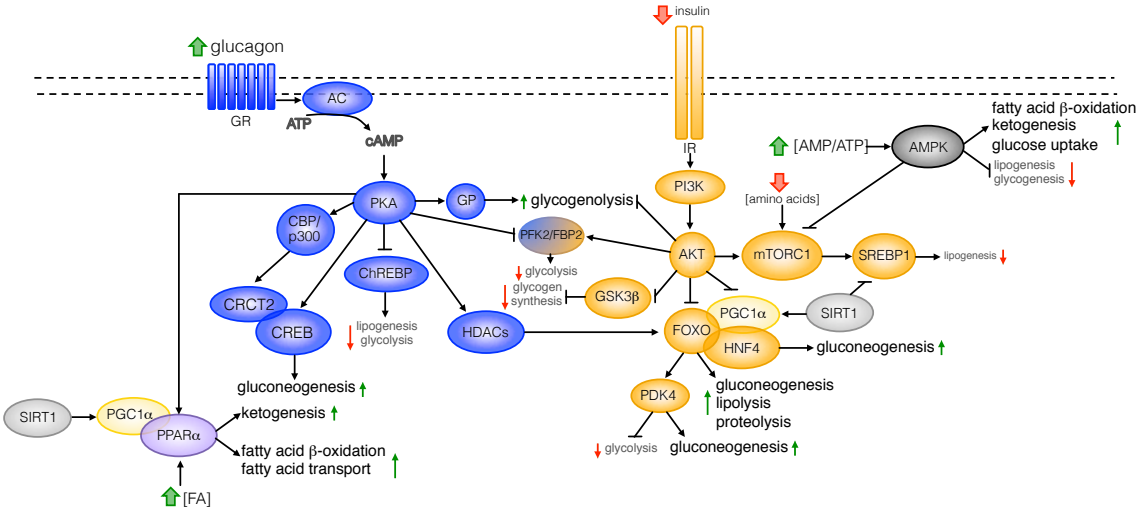

Figure 6. Cellular and molecular adaptations to fasting.
During fasting, reduced circulating insulin levels (synthesized in pancreatic β-cells) lead to the downregulation of the PI3K/AKT signalling pathway promoting gluconeogenesis, lipolysis, glycogenolysis and proteolysis and inhibiting glycolysis, lipogenesis and glycogen synthesis. At the same time, increased glucagon levels secreted by pancreatic α-cells activate the AC/PKA signalling pathway whose effectors stimulate gluconeogenesis, glycogenolysis and PPARα activity. PPARα, which is activated by fatty acids, is the master regulator of fatty acid β-oxidation and ketogensis. AMPK, SIRT1 and mTORC1 are other important energy and nutrient sensors necessary for the adaptation to fasting. GR: glucagon receptor, IR: insulin receptor, FA: fatty acids.

5. Role of tumour suppressor genes in stress signalling pathways

Tumour suppressor genes are characterized by their ability to inhibit cell proliferation and tumour development. Many of them have a major role in the cellular response to a wide range of stress signals such as DNA damage, hypoxia or oncogenic activation, leading to DNA damage repair, cell cycle arrest, differentiation, senescence or apoptosis (Sherr, 2004; Vogelstein et al., 2000; Vurusaner et al., 2012). However, little is known about the possible effects that stress associated to nutrient deprivation could exert over tumour suppressors.

Previous researchers have identified p21 (also known as $p21^{Cip1}$ or CDKN1A) as a fasting-induced factor (Tinkum et al., 2013), but, whereas its role in cell cycle regulation, senescence, apoptosis, DNA repair and transcriptional control has been widely studied, little is known about the relevance and involvement of p21 in metabolism or in the adaptation to fasting. In contrast, other tumour suppressor genes such as p53 have extensively been associated with the regulation of glucose metabolism (Kruiswijk et al., 2015; Puzio-Kuter, 2011). For instance,

p53 is phosphorylated and activated by AMPK, which leads to the induction of an important metabolic checkpoint and cell cycle arrest in response to glucose limitations (Jones et al., 2005). In addition, p53 has been implicated in modulating the balance between glycolytic and respiratory pathways. By promoting the activity of TIGAR (TP53-induced glycolysis and apoptosis regulator) (Bensaad et al., 2006) and downregulating PGM (phosphoglycerate mutase) (Kondoh et al., 2005) and GLUT4 (Zhang et al., 2013), p53 is able to limit glycolysis; whereas by inducing the expression of *SCO2* (synthesis of cytochrome c oxidase 2) (Matoba et al., 2006), p53 stimulates mitochondrial respiration. Therefore, loss of p53 is associated with low oxygen consumption by mitochondrial respiration and enhanced glycolysis for the production of energy, thereby contributing to the Warburg effect. Finally, inhibition of p53 activity in adipose tissue decreases the expression of pro-inflammatory cytokines and improves insulin resistance in mice (Minamino et al., 2009).

Given the reduced number of studies linking p21 to metabolism, and the evidence that p21 is a fasting-induced factor (Tinkum et al., 2013), we decided to further analyze the role of p21 in the fasting response.

5.1 The tumour suppressor gene p21

p21 belongs to the Cip and Kip family of cyclin-dependent kinase (CDK) inhibitors that include p27 and p57 as well. The first discovered and best-known function of p21 is mediating p53-dependent cell cycle arrest by binding to and inhibiting the kinase activity of CDKs (El-Deiry et al., 1993; Harper et al., 1993) through the direct interaction with its N-terminal domain (Chen et al., 1995) (**Figure 7**). In particular, p21 contributes to G1 arrest by inhibiting the activity of CDK2, thereby not only suppressing the formation CDK2/cyclin E and CDK2/cyclin A complexes, but also inhibiting the CDK2-dependent retinoblastoma (RB) phosphorylation and the consequent release and activation of E2F transcriptional activity of genes involved in replication and cell progression (Zhu et al., 2005). In addition, p21 also inhibits the kinase activity of CDK2/cyclin A and CDK1/cyclin A, which are required for progression to S-phase and into G2, respectively (Dutto et al., 2014). Moreover, p21 induces DNA repair through the binding of its carboxy-terminal domain to PCNA (proliferative cell nuclear antigen) (Chen et al., 1995), thus blocking DNA synthesis and S-phase progression (Moldovan et al., 2007). Even though the activation of p21 by p53 in response to DNA-damage and oncogenic stress is the main and best-characterized p21-activating pathway that primarily mediates cell cycle arrest and p53-dependent apoptosis and senescence, multiple signals and factors have been shown to regulate p21. In a p53-independent manner, p21 can also be regulated by TGFβ-activated SMAD complexes, E2F1, p300/CBP, HRAS, BRCA1, KLF4 and FOXO proteins (Abbas and

Dutta, 2009). Although best known for its growth-inhibitory functions, p21 also inhibits apoptosis in a p53-independent mechanism by interacting and inhibiting the activity of pro-apoptotic proteins such as procaspase 3, caspase 8, caspase 10 and SAPKs (stress-activated protein kinases) (Gartel and Tyner, 2002). p21 can also modulate transcription acting as a co-transcriptional factor by binding and suppressing the transcriptional activity of E2F1 (Delavaine and La Thangue, 1999), STAT3 (Coqueret and Gascan, 2000) and MYC (Kitaura et al., 2000) as well as by de-repressing and activating p300/CBP gene transcriptional activity (Snowden et al., 2000). p21 is further controlled at a post-transcriptional level by a number of protein kinases. Phosphorylation of p21 at Ser130 by CDK2/cyclin E promotes its binding to SKP2, leading to its ubiquitylation, proteolysis and consequent cellular progression (Bornstein et al., 2003). Furthermore, AKT phosphorylates p21 at Thr145 disrupting the binding with PCNA and preventing the nuclear translocation of p21 which promotes p21-dependent anti-apoptotic activity and cell proliferation through assembly of CDK/cyclin complexes (Li et al., 2002).

Despite being downregulated in some human cancers such as head and neck, colorectal and small-cell lung cancer (Abbas and Dutta, 2009), loss-of-function mutations in *p21* are extremely rare (Shiohara et al., 1994). In fact p21-deficient mice develop spontaneous tumours relatively late compared to mice lacking other tumour suppressor genes (Martin-Caballero et al., 2001) such as *Trp53* (Jacks et al., 1994), *p16* (Serrano et al., 1996) or *Arf* (Kamijo et al., 1999). However, p21KO mice exhibit accelerated development of chemically-induced tumours (Philipp et al., 1999). Importantly, p21 has been attributed to have oncogenic capacity not only due to its anti-apoptotic function. This can further be explained by its ability to stimulate cell motility through the inhibition of Rho (Ras homolog family member A kinase), thereby contributing to tumour metastasis and invasion (Lee and Helfman, 2004), and by its ability to maintain self-renewal capacity and genomic stability in stem cells (Kippin et al., 2005). Moreover, p21 promotes G1 progression and proliferation by inducing the kinase activity of CDK4 or CDK6 in complex with cyclin D (Labaer et al., 1997). The theory that p21 may act as an oncogene is supported by the fact that p21 is overexpressed in a variety of human cancers such as prostate, cervical and breast (Abbas and Dutta, 2009) and that p21 deletion in mice suppresses the development of spontaneous lymphomas in p53-KO (De la Cueva et al., 2006) and ATM-KO mice (Wang et al., 1997). This dual, contradictory effect may be explained by the cellular localization of p21 as, whereas the growth-inhibitory functions of p21 are associated with its nuclear localization, the anti-apoptotic or oncogenic activities of p21 are frequently associated with its cytoplasmic accumulation.

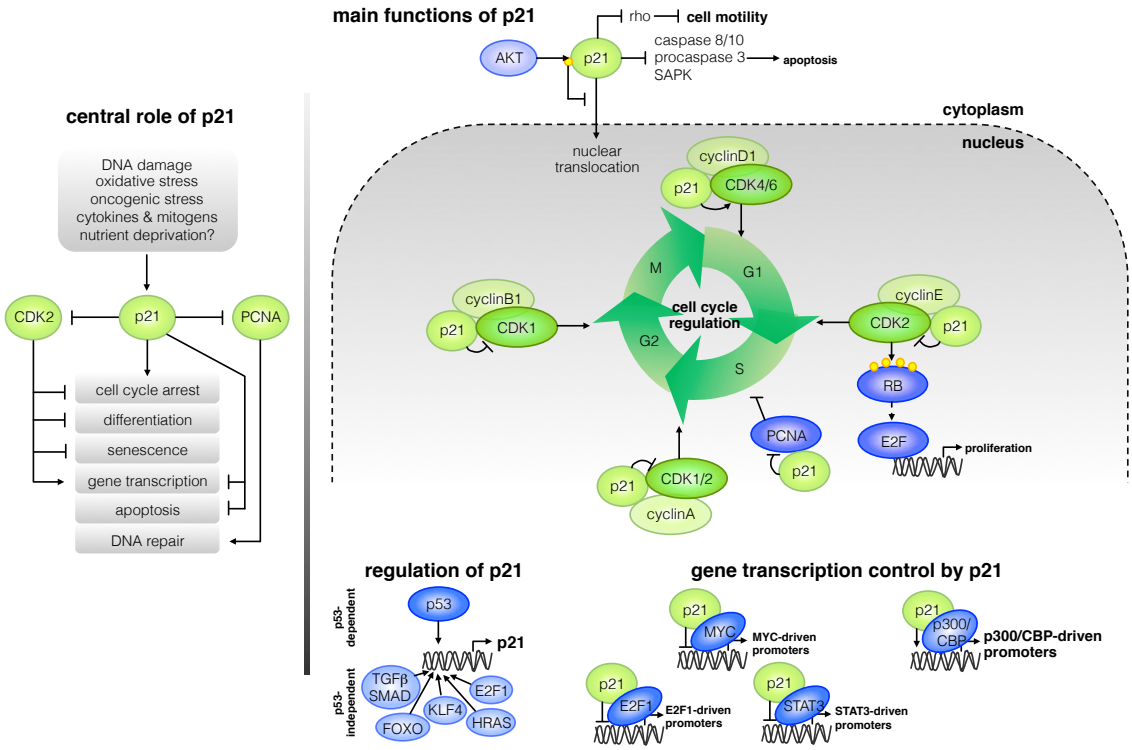

Figure 7. The central role of p21 in sensing and responding to stimuli.
Left, simplified representation of the stimuli that activate p21 and the different responses triggered either directly by p21 or mediated through the inhibition of CDK2 or PCNA. Right, regulation of p21 (p53-dependent and p53-independent), main processes in which p21 is involved and principal interactions of p21 with proteins in the nucleus

OBJECTIVES

1. Characterization of the pharmacological effects of PI3K inhibition on obesity.

1.1 Study the *in vivo* effects of the treatment with PI3K inhibitors in obese mice and rhesus monkeys.

1.2 Evaluate a possible use of PI3K inhibitors as anti-obesity treatment.

2. Role of the tumour suppressor gene p21 in the fasting response.

2.1 Analyse the role of p21 in the adaptive response to fasting.

2.2 Characterize the fasting response in p21-deficient mice.

OBJETIVOS

1. **Caracterización de los efectos de la inhibición farmacológica de PI3K sobre la obesidad.**
   1.1 Estudiar los efectos *in vivo* del tratamiento con inhibidores de PI3K en ratones y macacos rhesus obesos.
   1.2 Evaluar el posible uso de inhibidores de PI3K como tratamiento anti-obesidad.

2. **Análisis del papel del gen supresor de tumores p21 en la respuesta a ayuno.**
   2.1 Analizar el papel de p21 en la respuesta de adaptación al ayuno.
   2.2 Caracterizar la respuesta a ayuno en ratones deficientes en p21.

MATERIALS & METHODS

1. Mouse experimentation

1.1 Animal housing

All animal procedures done at the CNIO were approved by the CNIO-ISCIII Ethics Committee for Research and Animal Welfare (CEIyBA) and the Autonomous Community of Madrid, and conducted in accordance to the recommendations of the Federation of European Laboratory Animal Science Associations (FELASA). Wild type mice were originally obtained from Harlan Laboratories C57BL6/J-OlaHsd and housed at the specific pathogen-free (SPF) barrier area of the Spanish National Cancer Research Centre (CNIO), Madrid. Male mice were maintained at 22°C, and with 12 hour dark/light cycles (light cycle from 8 am to 8 pm) having free access to water and standard chow diet (18% of fat-based calorie content, Harlan Teckland 2018). When indicated, mice were fed with a high fat diet (45% fat-based calorie content, Research Diets D12451) or fasted for 24 to 48 hours with *ad libitum* water access. Mice were observed on a daily basis and sacrificed when they showed signs of morbidity in accordance to the *Guidelines for Humane Endpoints for Animals Used in Biomedical Research* from the Council for International Organizations of Medical Sciences (CIOMS).

All animal procedures done at the National Institute on Aging (NIA-NIH) were approved in the study protocol 352-TGB-2016 by the Animal Care and Use Committee of the National Institute on Aging (Baltimore, MD). Male C57BL6 mice were obtained from the NIA Aging Colony (Charles River, Bethesda MD) at 8 weeks of age. They were aged in house until they reached 7 months of age.

1.2 Transgenic mouse models

Ob/Ob C57BL6/J male mice were purchased from Charles River Laboratories with 10 weeks of age and treated with 0.1 mg/ml of CNIO-PI3Ki dissolved in drinking water at 12 weeks of age.

Transgenic $p21^{-/-}$ (Brugarolas et al., 1995), $p19^{ARF-/-}$ (Kamijo et al., 1997) and $Sirt\text{-}1^{+/-}$ (Wang et al., 2008) male mice were maintained at the CNIO in a C57BL6 background and used for experimentation at 12 weeks of age. Mouse genotyping was performed by Transnetyx enterprise (Cordova, TN 38016).

Eμ-Myc mice (Adams et al., 1985) were kindly provided by Dr. Óscar Fernández-Capetillo (CNIO) and genotyped by standard PCR procedures with the following primers that amplify a band of 850 base pairs:

Forward Primer: **5'** CAGCTGGCGTAATAGCGAAGAG **3'**

Reverse Primer: **5'** CTGTGACTGGTGAGTACTCAACC **3**'

1.3 Administration of PI3K inhibitors

For oral gavage administration, CNIO-PI3Ki, GDC-0941, BYL-719 and acalisib (all of them synthesized at the CNIO) were dissolved in 10% NMP (N-methyl-2-pyrrolidone, Sigma) - PEG-300 (Polyethyleneglycol 300, Sigma). For administration in drinking water (CNIO, Madrid), 0.1 mg/ml CNIO-PI3Ki was dissolved in 1.8% cyclodextrin (Sigma). For administration in food (NIA, Baltimore), CNIO-PI3Ki was incorporated into a high fat diet (60% calories from fat) purchased from Dyets, Inc. (Bethlehem, PA) at 0.17 g of drug per kg of food.

1.4 Metabolic characterization

1.4.1 Body composition

At the CNIO, body composition (fat and lean content) was determined by Dual energy X-ray Absorptiometry (DXA) (Lunar PIXImus Densitometer, GE Medical Systems). Image acquisition lasted 5 minutes with mice under anesthesia by inhalation of 2% isofluorane in oxygen. Whole body fat and lean mass was determined excluding head region.

At the NIA, measurements of lean and fat mass were acquired by nuclear magnetic resonance (NMR) using the Minispec LF90 (Bruker Optics, Billerica, MA).

1.4.2 Indirect calorimetry and activity studies

At the CNIO (p21 project), indirect calorimetry was performed following standard methods using Oxylet System metabolic chambers (Panlab Harvard Apparatus) at the CNIO. Acclimatization of 12-13 weeks old WT and p21KO mice to the measurement cages was three days prior to data recording. Volume of consumed O_2 (VO_2) and eliminated CO_2 (VCO_2) was recorded in *ad libitum* fed mice for 48 hours. After that, food was withdrawn and data were recorded for the next 48 hours under fasting conditions with *ad libitum* water access. Room temperature was constantly kept at 21°C and light/dark cycles were of 12 hours. Respiratory Quotient (RQ) was calculated as $RQ=VCO_2/VO_2$ from volumes of consumed O_2 (VO_2) and eliminated CO_2 (VCO_2) recorded every 24 minutes (8 simultaneous metabolic chambers). Energy Expenditure (EE) was calculated as $EE=(3.815+(1.232xRQ)) \times VO_2 \times 1.44$). Mouse activity was recorded in time intervals of 20 minutes during the whole measurement period.

At the NIA, metabolic rate of mice fed with HFD or HFD supplemented with CNIO-PI3Ki was assessed by indirect calorimetry in open-circuit oxymax chambers using the Comprehensive Lab Animal Monitoring System (CLAMS; Columbus Instruments, Columbus, OH) as described previously (Mitchell et al., 2014).

1.4.3 Body temperature measurement

At the CNIO, rectal temperature of *ad libitum* fed or 48 hours fasted WT and p21KO mice was measured using a rectal probe.

At the NIA, body temperature was established by thermoimaging. Mice were lightly anaesthetized with ketamine-xylazine, which was sufficient to induce anesthesia without a drop in respiration or body temperature. Rectal temperature was measured using a rectal probe prior to anaesthesia, once the mouse was asleep, and at the end of the imaging. Temperature remained consistent from the start to the end of the experiment. Mice were placed into a chamber maintained at 37ºC for the experiment. Thermal images of mice were captured every second for 30 minutes for whole body and for the intrascapular area by the Seahorse Bioscience TSA ImagIR Thermal Imaging system (Seahorse Bioscience, N Billerica, Massachusetts, USA).

1.4.4 Glucose and insulin tolerance test

To perform the glucose tolerance test (GTT), mice were fasted overnight and i.p. injected with glucose 2 g/kg (Sigma). Tail blood glucose levels were measured 0, 15, 30, 60, 90 and 120 minutes post-injection using a glucometer (Meranini Diagnosis). For the insulin tolerance test (ITT), mice were injected with 0.75 U/kg of insulin (Eli Lilly and Co., Humalog Insulin) and tail blood glucose levels were determined 0, 15, 30, 45, 60 and 90 minutes after insulin injection.

1.4.5 Metabolic parameters in serum

Blood was collected from the tail tip for the determination of glucose (Glucocard strips; A. Meranini Diagnosis) and insulin, or from post-mortem heart puncture for the rest of parameters. Serum insulin (Ultra Sensitive Mouse Insulin ELISA kit; Crystal Chem Inc.), Igf1 (Mouse/Rat IGF-1 ELISA; Demeditec), leptin (Crystal Chem Inc.) and adiponectin levels (Invitrogen) were measured by ELISA following the manufacturer's instructions. Serum triglycerides (Serum Triglyceride Determination Kit; Sigma), free fatty acids (Wako NEFA C Kit; Wako Chemicals) and ketone bodies (Autokit 3-HB; Wako Chemicals) were quantified by colorimetric assay. ALT and cholesterol were determined by VetScan (mammalian liver profile; VetScan) or by ABX PENTRA 400 clinical chemical analyser (Horiba ABX Diagnostics). Insulin resistance was evaluated by the HOmeostatic Model Assessment index (HOMA-IR = [(fasting insulin, μU/ml) x (fasting glucose, mg/dl] / 405).

1.4.6 Free fatty acids in liver

Lipids were extracted from the liver as followed: 10-20 mg of tissues was homogenized with 200 μl of Chloform/1% Triton. After centrifugation, lower, organic phase was collected and

vacuum air dried at 50ºC to remove Chloroform. Afterwards, fatty acids were quantified using Wako NEFA C Kit (Wako Chemicals) and following the manufacturer's instructions.

1.4.7 Nuclear magnetic resonance

Mice blood for serum isolation was collected by post-mortem heart puncture. After coagulation in ice, 100 µl of serum were mixed with 100 µl ice-cold 2X PBS buffer in deuterium oxide (D_2O), centrifuged for 10 min at 16000 x g and transferred to a 3 mm NMR sample tube. NMR spectra were recorded at 20ºC in 9 mins on a Bruker Avance 700 MHz spectrometer. Metabolite levels in serum samples were determined from the integrals of the most resolved and largest signals of each metabolite (for example methyl groups of lactate, alanine and pyruvate, and H4 proton of glucose) in 1D ^{1}H NMR spectra acquired with a transversal relaxation filter (CPMG of 200 ms, t=0.4 ms) that attenuates the fast relaxing signals of macromolecules (proteins, lipids and lipoproteins) signals and optimises the NMR signals of low mass metabolites for their quantification (Beckonert et al., 2007). Thus, the obtained values of integrals are not absolute concentrations but relative concentrations in arbitrary units (AU).

1.5 Histology and immunohistochemistry

Tissues were fixed overnight in 10% buffered formalin (Sigma), embedded in paraffin blocks and sectioned at a thickness of 2.5 µm. Tissue sections were stained with hematoxylin/eosin (H&E), with anti-UCP1 (AbCam, #ab10983), anti-F4/80 (Monoclonal Antibodies Core Unit, CNIO #AM-D10 or ABD Serotec, #MCA497), Ki-67 (Master Diagnostica #0003110QD) or active-Caspase 3 (Cell Signaling #9661) following standard procedures. OCT frozen 10 µm liver sections were stained for Oil Red O (Sigma).

Senescence associated β-galactosidase staining (X-gal) in spleen of Eµ-Myc mice was performed following the manufacturer's instructions (Senescence β-Galactosidase Staining Kit #9860; Cell Signaling). Shortly, tissues frozen in OCT tissue freezing medium (Leica) were sectioned at a thickness of 10 µm, fixed for 10 minutes, stained with X-Gal solution at 37ºC overnight and counter-stained with nuclear fast red.

1.6 *In situ* hybridization

Coronal mouse brain sections (16 µm) were probed with a specific oligonucleotide for AgRP (*GenBank Accession Number*: NM_007427; 5'-CGA CGC GGA GAA CGA GAC TCG CGG TTC TGT GGA TCT AGC ACC TCT GCC-3'), CART (*GenBank Accession Number*: NM_013732; 5'-ACA GTC ACA CAG CTT CCC GAT CCT GGC CCC TTT C-3'), NPY

(*GenBank Accession Number*: AF273768; 5'-GGG CGT TTT CTG TGC TTT CCT TCA TTA AGA GGT CTG-3') and POMC (*GenBank Accession Number*: NM_008895; 5'-CTT GAT GAT GGC GTT CTT GAA GAG CGT CAC CAG GGG CGT CTG GCT CTT-3') as previously published (López et al., 2008, 2010; Martínez De Morentin et al., 2014; Whittle et al., 2012). Sections were scanned and the hybridization signal was quantified by densitometry using *ImageJ-1.33* (*NIH;* Bethesda, MD, USA). We used between 12 sections for each animal (3 slides with four sections per slide). The mean of these 12 values was used as the densitometry value for each animal.

1.7 Immunophenotyping by flow cytometry

Cells from *ad libitum* fed or 24 hour fasted WT and p21KO mice (12-16 weeks old, n=6) were isolated from spleen and liver by disaggregating tissues through a 70 μm or 100 μm strainer, respectively. Following erythrocyte lysis with Red Blood Cell Lysis Buffer (Qiagen), immune cells from the liver were further isolated using a 38-70% Percoll gradient (GE Healthcare). Cells were then blocked in Fc block (CD16/CD32, BD Biosciences #553141) diluted 1:400 on ice for 30 minutes and incubated with the following conjugated antibodies for 1 hour at 4ºC in a rotating platform: CD8a-FITC (eBioscience #11-0081-82), CD4-PE (eBioscience #12-0041-82), CD45-PerCP (Biolegend #103130), CD11b-PerCP/Cy5.5 (eBioscience #45-0112-82), Gr1-PECy7 (eBioscience #25-5931-82), NK1.1-PECy5 (Biolegend #108715), F4/80-AF647 (eBioscience #12-0041-82), CD3-AF700 (eBioscience #56-0032-82), CD19-APC/EF780 (eBioscience #47-0193-80) and B220-APC/EF780 (eBioscience #47-0452-82). Splenocytes were used as Fluorescence Minus One (FMO) to gate cell populations and commercial anti-mouse or anti-rat IgG beads (BD Biosciences #552843 or # 552844) to compensate for fluorochrome spectral overlap. We used pulse processing to exclude cell aggregates and an amine reactive live/dead dye (Aqua, Invitrogen) to exclude dead cells. At least 10,000 cells from the CD45 gate were collected. Cells were analyzed in an LSR-Fortessa (BD Biosciences; FACS Diva software) and all data analyzed using FlowJo v9.6.2 software (Trestar, Oregon).

2. Monkey experimentation

2.1 Animal housing

All procedures were approved by the Animal Care and Use Committee of the NIA Intramural Research Program. Rhesus monkeys (*Macaca mulatta*) were housed at the NIH Animal Center (Poolesville, MD, USA) in standard primate caging with controlled temperature and humidity and a 12-hour light cycle.

2.2 Preliminary study

A preliminary study was performed to determine the appropriate dosing of the CNIO-PI3Ki compound for rhesus monkeys (*Macaca mulatta*) based on allometric scaling of the mouse dosing. Here, physiological parameters of six healthy monkeys (n=6; 3 males and 3 females) were monitored during dose escalation treatment of CNIO-PI3Ki administered intravenously under anesthesia. The test doses ranged from 0.2 mg/kg to 2.1 mg/kg. Animals were under anesthesia for 2 hours, while serum was collected at various time points.

2.3 Long-term study

For the 12-week study, subjects were 19 male and female rhesus monkeys aged 12 to 27 years (18 ± 5.4 years old) randomized into two groups: 9 control (5 females + 4 males) and 10 CNIO-PI3Ki treated (6 females + 4 males). All monkeys were considered naturally obese with baseline body weights between 7 and 18 (11.8 ± 2.5) kilograms and body fat > 27% (Hansen et al., 2013). Monkeys were fed commercially prepared monkey chow that was distributed twice daily along with daily food enrichment, and water was available *ad libitum*. Additionally, study animals were supplemented with 5 or 6 PRIMA-treat® wafers (Bio-Serv®, assorted fruit flavors, F0345; each wafer weighs 5 g with 3.28 kcal/gr). The PRIMA-treat wafers were used as vehicle for CNIO-PI3Ki. Individually weighed doses of CNIO-PI3Ki were reconstituted in water and then distributed, via syringe, onto the PRIMA-treats. Once absorbed, they were fed to the animals. Drug administration continued daily (weekends included) for 12 weeks.

Monkeys were anesthetized at baseline to measure body weight, blood pressure, heart rate, temperature, to collect anthropometric measures (i.e., abdominal circumference and crown-rump length), and to extract blood samples. These parameters were subsequently evaluated every one to two weeks during the study. In addition, food consumption data were collected daily for three to five days at baseline and again at weeks 3, 6, 8, and 11.

2.4 Metabolic parameters

Fasting blood samples were obtained by venipuncture of the femoral artery after anesthesia with intramuscular ketamine (7-10 mg/kg) and sent to Antech Diagnostics for chemistry panel and complete blood count testing. The following measurements were performed: glucose, total protein, albumin, globulin, alkaline phosphatase, gamma guanine triphosphate, alanine and aspartate transaminases, bilirubin, BUN, creatinine, phosphorus, calcium, magnesium, sodium, potassium, chloride, cholesterol, triglycerides, amylase, lipase, creatining phosphokinase, white blood cells, red blood cells, hemoglobin, hematocrit, MCV, MCH, MCHC, neutrophils, platelets, lymphocytes, monocytes, eosinophils, and basophils.

Trunk body composition (fat and lean content) was determined by Dual energy X-ray Absorptiometry (DXA) using the GE Lunar Prodigy® (GE Healthcare, Wauwatosa, WI).

At baseline and week 10, monkeys were fasted overnight and anesthetized for two-hour Intravenous Glucose Tolerance Test (IVGTT). During each test, serial blood samples were collected following a dose of 300 mg/kg of 50% dextrose administered IV through the saphenous vein. Glucose values were promptly measured in whole blood using an Ascensia® Breeze 2 blood glucose monitoring system (Bayer HealthCare LLC., Mishawaka, IN). Samples were then centrifuged and serum samples were aliquoted and stored at -80°C for subsequent analysis using a commercially available Insulin ELISA (Mercodia, Inc., Uppsala, Sweden). Insulin resistance was evaluated by the HOmeostatic Model Assessment index (HOMA-IR = [(fasting insulin, μU/ml) x (fasting glucose, mg/dl] / 405).

3. Characterization of the CNIO-PI3K inhibitor

The low molecular weight compound CNIO-PI3Ki is described in patent WO2010/119264 (files available at the World Intellectual Property Organization, http://www.wipo.int/pctdb/en/wo.jsp?WO=2010119264).

3.1 PI3K inhibitory assay

The kinase activity of PI3K isoforms was measured by using the commercial PI3kinase (h) HTRF™ assay available from Millipore, following the manufacturer´s recommendations. PI3Kα (p110α/p85α) and PI3Kδ (p110δ/p85α) were used at 100 pM; PI3Kα (p110β/p85α) and PI3Kγ isoforms (p110γ) at 500 pM and 4 nM respectively. ATP concentration was 50 times KMATP: 200 mM for PI3Kα and PI3Kδ, 250 mM for PI3Kβ and 100 mM for PI3Kγ. PIP2 was held at 10 mM. Values were normalized against the control activity included for each enzyme (i.e, 100% PI3K activity, without compound). These values were plotted against the inhibitor concentration and were fitted to a sigmoidal dose-response (variable slope) curve by using GraphPad Software. The obtained IC_{50} were converted to k_{iapp} according to Cheng-Prusoff equation for competitive inhibitors (Cheng and Prusoff, 1973).

Mammalian target of rapamycin (mTOR) was assayed by monitoring phosporylation of GFP-4EBP using a LanthaScreen™ kinase activity assay (Invitrogen). The enzyme and reagents were purchased from Invitrogen. Reaction conditions used were those recommended by the manufacturer. Values were plotted against the inhibitor concentration and fitted to a sigmoid dose-response curve by using GraphPad Prism version 5.03 (GraphPad Software CA, USA).

3.2 Pharmacokinetics

Male C57BL6 mice (n=3) were treated intravenously with 2 mg/kg or orally with 10 mg/kg CNIO-PI3Ki. Drug concentration was measured by mass spectrometry. Pharmacokinetic parameters were estimated by fitting the experimental data to a bicompartmental model using WinNonlin software for pharmacokinetic analysis.

4. *In vitro* procedures

4.1 Cell culture

Primary large-T immortalized pre-brown adipocyte cell lines were kindly provided by Dr. Ángela Martínez-Valverde (IIB-Madrid) and obtained from the interscapular BAT of 3-5 day-old neonates as previously described (Fasshauer et al., 2000; Lorenzo et al., 1993). Primary large-T immortalized WT and p21KO hepatocytes were also provided by Dr. Ángela Martínez-Valverde (IIB-Madrid) and obtained from the liver of 3-5 day-old neonates as previously described (Gonzalez-Rodriguez et al., 2007). HepG2 cells (human hepatocellular carcinoma) were obtained from ATCC® (HB-8065) (Knowles et al., 1980).

All cell lines were cultured in DMEM (Dulbecco's Modified Eagle's Medium; Gibco) supplemented with 10% heat inactivated FBS (Fetal Bovine Serum; Gibco) and 1% antibiotic/antimycotic (Gibco) if not otherwise specified. Cells were incubated in 20% O_2 and 5% CO_2 at 37ºC.

4.2 Lentiviral transduction

Lentiviral supernatants were produced in HEK293T cells (ATCC® number CRL-11268™) plated at 2.5 x 10^6 cells per 100 mm-diameter dish and transfected with the packaging plasmids pLP1 (1.95 µg), pLP2 (1.3 µg), pLP/VSVG (1.65 µg) (Invitrogen), and one of the following lentiviral constructs (5 µg) expressing shRNAs against PIK3Cα (pLKO.1; Thermo Scientific TRCN0000025615), PIK3Cβ (pLKO.1; Thermo Scientific TRCN0000024793), PIK3Cγ (pLKO.1; Thermo Scientific TRCN0000024569) and PIK3Cδ (pLKO.1; Thermo Scientific TRCN0000024644). Transfections were performed using Fugene HD transfection reagent (Promega) according to the manufacturer's instructions. Supernatants from HEK293T cells used for infection of pre brown-adipocytes were collected 48, 56 and 72 hours after transfection. Primary immortalized pre-brown adipocytes were plated (8 x 10^5 per 100 mm-diameter dish) the day prior to infection and selected with puromycin (2 mg/ml, Sigma) after 48 hours.

4.3 Treatments

Primary immortalized pre-brown adipocytes were stimulated with DMSO (Dimethyl Sulfoxide, Sigma) or forskolin 10 μM (Sigma) for 4 hours. HepG2 and primary immortalized hepatocytes (plated at 5 x 10^5 cells per 6-well plate the previous day) were washed twice with PBS (Phosphate Buffer Saline, Gibco) and nutrient starved in starvation medium consisting of glucose-free DMEM (Gibco #11966025) without FBS supplementation for 24 or 48 hours. When indicated, cells were stimulated with forskolin 10μM (Sigma) or CNIO-PI3Ki 10 μM, both dissolved in DMSO, for 5 hours.

4.4 Crystal violet staining

For crystal violet staining, cells cultured for 48h in complete or starvation medium were fixed in 1% glutaraldehyde (Sigma) for 10 minutes and stained with 0.1% crystal violet (Sigma) for 30 minutes. After washing with distilled H_2O, plates were scanned.

5. Biochemical assays

5.1 DNA extraction

For the genotyping of Eμ-Myc mice, DNA was extracted from mouse-tail. After overnight incubation with proteinase K (0.4 mg/ml; Roche), DNA was isolated following standard phenol:chloroform:isoamyl alcohol (25:24:1) (Sigma) extraction protocol and performing genotyping PCR as specified in section 1.2.

5.2 RNA extraction and qRT-PCR

Total RNA from tissues or cells was isolated using TRIZOL (Invitrogen), chloroform and isopropanol standard extraction protocol. RNA extraction of monkey biopsies was optimized as followed: tissue was homogenized using an Omni Polytron Homogenizer and aqueous phase isolated with the help of Phase Lock Gel Tubes (5PRIME). RNA was precipitated overnight at -20ºC and pelleted by centrifugation at 20000 g, at 4ºC, during 30 minutes. DNA synthesis was performed with 1-2 μg of RNA using iScript First Strand cDNA synthesis kit (BioRad #170-8891) according to the manufacturer's instructions. Quantitative real time-PCR (qRT-PCR) was carried out using *GoTaq Q-PCR* Master Mix (Promega) in a 7500 Fast Real-Time PCR System (Applied Biosystems). Reactions were performed in triplicate, normalized to *β-actin* or *Gapdh* in the case of muscle, and calculations were made using the ΔΔCt method as described (Yuan et al., 2006).

Primer sequences used for mouse, monkey and human transcripts are described below:

PCR primers for mouse transcripts

Primer	Forward sequence 5' → 3'	Reverse sequence 5' → 3'
β-Actin	GGCACCACACCTTCTACAATG	GTGGTGGTGAAGCTGTAGCC
Gapdh	TTCACCACCATGGAGAAGGC	CCCTTTTGGCTCCACCCT
CD68	TGTCTGATCTTGCTAGGACCG	GAGAGTAACGGCCTTTTTGTGA
Emr1	TGACTCACCTTGTGGTCCTAA	CTTCCCAGAATCCAGTCTTTCC
IL-6	AGTTGCCTTCTTGGGACTGA	TCCACGATTTCCCAGAGAAC
Ucp1	ACTGCCACACCTCCAGTCATT	CTTTGCCTCACTCAGGATTGG
G6pc	ACTGTGGGCATCAATCTCCT	AGGTGACAGGGAACTGCTTT
Pgc1α	GGGTTATCTTGGTTGGCTTTATG	AAGTGTGGAACTCTCTGGAACTG
PI3Kα	AAAGTGTGTGGCTGTGACGA	CTTTCTTTGGCCATCAGCAT
PI3Kβ	TACAGGTCAGTGGGAGAGTG	GAAGTGGGGCAGGGTTCTAT
PI3Kγ	CGAAACCATTGGAATCATCTT	CCAGAGATTCAGTCTCCCAAA
PI3Kδ	CAGGGGTCTACTTGAACTTCC	CTGAGCATGTGGAAGAGTGG
Tnni1	GCCTCCACAACACCAGAGAG	GCCAGACATAGCCTCCACAT
Myh2	GCAAACACGAGAGACGAGTG	CAGCTTGTTGACCTGGGACT
Myh4	AACCTGATGCAGGCTGAGAT	TCCTGCTCCTTCTTCAGCTC
$p21^{Cip1}$	GTGGGTCTGACTCCAGCCC	CCTTCTCGTGAGACGCTTAC
$p16^{Ink4a}$	TACCCCGATTCAGGTGAT	TTGAGCAGAAGAGCTGCTACGT
$p19^{ARF}$	GCCGCACCGGAATCCT	TTGAGCAGAAGAGCTGCTACGT
$p27^{Kip1}$	TCAAACGTGAGAGTGTCTAACG	CCGGGCCGAAGAGATTTCTG
p53	GCGTAAACGCTTCGAGATGTT	TTTTTATGGCGGGAAGTAGACTG
Fgf21	GTGTCAAAGCCTCTAGGTTTCTT	GGTACACATTGTAACCGTCCTC
CD36	ATGGGCTGTGATCGGAACTG	TTTGCCACGTCATCTGGGTTT
Abcd2	TGTGGAGCAGCTGTGGACTA	ATCAGCTCCAGAGGCCAGTA
Saa3	TAAAGTCATCAGCGATGCCAGAG	CAACCCAGTAGTTGCTCCTCTTC
Acacb	GTATCCGCAAGGCTGAGAGT	GTTCTGGGCCAGCTTCATTA
Srebp1	TAGAGCATATCCCCCAGGTG	GGTACGGGCCACAAGAAGTA
Gyk	TGAAGAAAGCGAAATCCGTTACT	CCCAAAGGCAGACTACAGAAG
Cpt1a	TCAATCGGACCCTAGACACC	CTTTCGACCCGAGAAGACCT
Acot1	TGCACGAGCGTCACTTCTT	GATACTCCAGAAGGCCACCTC
Acot3	GCACGAGCGTCACTTCAT	CGATACTCCAGAAGGCCACT
Pparα	AGCCTCAGCCAAGTTGAAGT	TGGGGAGAGAGGACAGATGG
Pparγ	TGGCCACCTCTTTGCTCTGCTC	AGGCCGAGAAGGAGAAGCTGTTG
Pparδ	ACCAGAACACACGCTTCCTT	TTGCGGTTCTTCTTCTGGAT
Itgal	CCAGACTTTTGCTACTGGGAC	GCTTGTTCGGCAGTGATAGAG
Icam	TCCGCTACCATCACCGTGTAT	TAGCCAGCACCGTGAATGTG
Tlr1	TGTGAATGCAGTTGGTGAAGA	CATTCCTGAGGTCCCTGCTA
Ccl3	CTCCCAGCCAGGTGTCATTTT	CTTGGACCCAGGTCTCTTTGG

Rantes	GCTGCTTTGCCTACCTCTCC	TCGAGTGACAAACACGACTGC
Ifnγr1	GTGGAGCTTTGACGAGCACT	TTCCCAGCATACGACAGGGT
IL-5	CTCTGTTGACAAGCAATGAGACG	TCTTCAGTATGTCTAGCCCCTG
IP10	CCAAGTGCTGCCGTCATTTTC	GGCTCGCAGGGATGATTTCAA
Mig	GGAGTTCGAGGAACCCTAGTG	GGGATTTGTAGTGGATCGTGC
Nos2	AATCTTGGAGCGAGTTGTGG	CAGGAAGTAGGTGAGGGCTTG
CD301	TGAGAAAGGCTTTAAGAACTGGG	GACCACCTGTAGTGATGTGGG
CD163	TCCACACGTCCAGAACAGTC	CCTTGGAAACAGAGACAGGC

PCR primers for rhesus monkey transcripts

Primer	Forward sequence 5' → 3'	Reverse sequence 5' → 3'
Ipo8	GCTCCTTCCTGATTCCTCCTATT	CATCCACGTTGTCATGGTTTG
Tnni1	GGTTCCAAGCACAAGGTGTC	AAGTGAGTGAGCTGGGTTGG
Myh2	TGACAAGATCGAGGACATGG	CTGTCACCACCTCAGGGTTA
Myh4	GTTCATTGACTTCGGGATGG	GGAGGTATCTGTTGCCTTGG
Pgc1α	GCTGACAGATGGAGACGTGA	CCACTGCATTCATTATAACTTAGCTG
Pck1	GCTCTCAGGATAGCCAGTCG	AAATGCAGCTGCCAGGTACT
Adiponect.	CGAGAAGGGTGAGAAAGGAGA	CATGTTGGGGACAGTAACGTAG
Ucp1	GTGTGCCCAACTGTGCAAT	TGCCTTGACTTTGACAGTTCTC
Prdm16	CCTGGCTGAGGAGCTCAAG-	GGCACTGGTCGCATTTGTA
Emr1	CTTCCTGGAGAGCGTGGA	CTGCCAAGCTCAAGTTCACA
CD68	CTCGACCTGCTCTCCCTGAG	TGATGAGAGGCAGCAAGATG
CD11c	TTGATGCTCTGAAAGATATTCAAAA	CTGCGCCATCTCCAATTC
CD206	ACAAGGGATCGGGTTTATGG	GGCGTTGCCCAGTAGTGTAT

PCR primers for human transcripts

Primer	Forward sequence 5' → 3'	Reverse sequence 5' → 3'
β-Actin	CAAGGCCAACCGCGAGAAGAT	CCAGAGGCGTACAGGGATAGCAC
$p21^{Cip1}$	TGTCCGTCAGAACCCATG	TGCCTCCTCCCAACTCATC

5.3 Mitochondrial content

Mitochondrial content in monkeys was analysed as previously described (Lagouge et al., 2006). Shortly, DNA was extracted from muscle biopsies by overnight incubation with proteinase K (0.4 mg/ml; Roche), followed by standard phenol:chloroform:isoamyl alcohol (25:24:1) extraction protocol. PCR was performed in a 7500 Fast Real-Time PCR System (Applied Biosystems) in triplicate and expression of the mitochondrial gene *Cox2* was normalized to the expression of the nuclear gene *Mrsp18a* using the following primers:

Cox2 Forward Primer: **5'** TAGCATCACAGATGCCCAAG **3'**
Cox2 Reverse Primer: **5'** CCCGTAGTCCGTGTATTCGT **3'**
Mrps18a Forward Primer: **5'** GCTGGAACAAGGTGTGCAT **3'**
Mrps18a Reverse Primer: **5'** GGGCTTATGAGTGTGCCTCT **3'**

5.4 RNA-seq based transcriptional profiling

Livers of *ad libitum* fed or 24 hours fasted WT and p21KO mice (n=2-3 per group) were snap-frozen in liquid nitrogen and RNA was prepared using Trizol (Invitrogen) and further purified with RNeasy Mini kit (Qiagen) following the manufacturer's instructions. RNA Integrity Number (RIN) was in the range of 9.1-9.5 (Agilent 2100 Bionalyzer). 2–8 ng of total RNA was used to synthesize the cDNA (SMARTer Ultra Low Input RNA Kit, version 3, Clontech #634848). After amplification with SeqAmp DNA Polymerase (Clontech), 10 ng of cDNA was used to prepare the adaptor-ligated library following the ''TruSeq DNA sample preparation guide'' (part #15005180). The resulting cDNA libraries were sequenced for 50 bases in a single-read format (Illumina HiSeq2000). Reads were aligned to the mouse genome (GRCm38/mm10) with TopHat-2.0.10 (Trapnell et al., 2012) using Bowtie 1.0.0 (Langmead et al., 2009) and Samtools 0.1.19 (Li et al., 2009), allowing two mismatches and five multihits. Transcripts assembly, estimation of their abundances and differential expression were calculated with Cufflinks 2.2.1 (Trapnell et al., 2012), using the mouse genome annotation data set RCm38/mm10 from the UCSC Genome Browser. Gene Set Enrichment Analysis (GSEA) was performed using annotations from the KEGG, Reactome and NCI databases. Genes were ranked using the t statistic. After Kolmogorov-Smirnoff correction for multiple testing, only those pathways bearing a FDR<0.25 were considered significant. Enrichment plots were also obtained with GSEA and ranked according to their enrichment score (ES).

5.5 Protein extraction and immunoblots

Protein lysates were prepared using lysis buffer (150 mM NaCl, 10 mM Tris pH 7.2, 0.1% SDS, 1% Triton X-100, 1% deoxycholate, 5 mM EDTA, protease inhibitors). In the case of tissue extracts, lysates were homogenized using a Precellys 24 tissue homogenizer (Bertin Technologies). Immunoblot analyses were performed according to standard procedures. Membranes were stained with antibodies anti-P-Ser473-AKT (Cell Signaling, #4058), anti-P-Thr24/Thr32-FOXO1/3 (Cell Signaling, #9464), anti-total-AKT1 (Millipore, #07-416), anti-UCP1 (AbCam, #ab10983), anti-P-Thr1462-TSC2 (Cell Signaling, #3616), anti-TSC2 (Cell Signaling, #3612), anti-P-Thr389-p70S6K (Cell Signaling, #9206), anti-P-Ser240/Ser244-S6 (Cell Signaling, #5364), anti-P-Ser65-4EBP1 (Cell Signaling, #9451), anti-4EBP1 (Cell Signaling, #9644), anti-β-actin (Sigma, #AC-15), and anti-γ-tubulin (Sigma, #T6557).

6. Statistical analysis

Data are expressed as mean ± s.d. or mean ± s.e.m. and differences are considered significant with *P* value < 0.05 (* $p<0.05$, ** $p<0.01$, *** $p<0.001$). Statistical significance between two groups was assessed using the two-tailed unpaired Student's t test. In the longitudinal fat and lean content measurement in the monkey study statistical significance was determined using the paired Student's t test, as specified in the figure. For survival curves, we used the Log-rank (Mantel-Cox) test. These statistical analyses were performed using GraphPad Prism software.

RESULTS

PART1. EFFECT OF PHARMACOLOGICAL PI3K INHIBITION ON METABOLIC SYNDROME AND OBESITY

Various research lines focussed on longevity, dietary restriction, obesity and metabolic syndrome have converged on the concept that a partial downregulation of PI3K signalling activity has the potential to improve health and provide protection from obesity and its associated pathologies. PI3K inhibitors have recently entered clinical use for cancer treatment, but, likewise, it is of great importance to determine the potential beneficial effects of pharmacological PI3K inhibition on obesity and healthspan.

1.1 Effects of CNIO-PI3Ki on cellular and glucose homeostasis

For our studies, we took advantage of CNIO-PI3Ki, a PI3K inhibitor developed by the Experimental Therapeutics Programme at the Spanish National Cancer Research Centre (CNIO), characterized by high PI3Kα (IC50 2.4 nM), PI3Kδ (IC50 2.5 nM) and modest PI3Kγ (IC50 44 nM) inhibitor activity (**Figure 8A**); no relevant or modest inhibitory activity against other 284 tested kinases (data not shown) including mTOR (**Figure 8A)**; minimal access to the brain (**Figure 8B**); and a good pharmacokinetic profile in mice (**Figure 8C**). To compare the effects and efficiency of our compound, we also used the well-characterized PI3K inhibitor GDC-0941 (also called pictisilib) that shows inhibitory activity restricted to PI3Kα (IC50 3 nM), PI3Kδ (IC50 3 nM), PI3Kβ (IC50 33nM) and PI3Kγ (IC50 75 nM), little access to the brain and a good pharmacokinetic profile as well (Salphati et al., 2012; Workman et al., 2010).

A

molecule	PI3Kα IC50 (nM)	PI3Kβ IC50 (nM)	PI3Kγ IC50 (nM)	PI3Kδ IC50 (nM)	MTOR IC50 (nM)
CNIO-PI3Ki	2.4	212	44	2.5	6700

B

administration route	dose (mg/kg)	time (h)	CNIO-PI3Ki in serum (ng/ml) (*)	CNIO-PI3Ki in brain (ng/g) (*)
I.V.	2	1	469 ± 64	7 (**)
oral	10	1	1154 ± 240	20 ± 4

*All values correspond to average ± s.d. (n=3)
(**) in this case, only one sample was detectable

C

parameter	I.V.	oral
F	-	62%
Cmax (ng/ml)	-	3728.41
Tmax (h)	-	0.29
AUCinf (h*ng/ml)	5185.44	16020.84
T1/2 (h)	0.9	1.45
T1/2 elimination phase (h)	1.67	4
Cl (l/h/kg)	0.39	-
Vd (l)	0.018	-

Figure 8. Pharmacological characterization of CNIO-PI3Ki.
(A) Inhibitory activity (IC_{50}) of CNIO-PI3Ki towards the four PI3K isoforms and mTOR. All assays were performed in triplicates (n=3). **(B)** CNIO-PI3Ki concentration in serum and brain of mice after 1-hour i.v. (2 mg/kg) or oral (10 mg/kg) CNIO-PI3Ki administration. All values correspond to average ± s.d. n=3, except for brain where CNIO-PI3Ki after i.v. was detectable only in one sample. **(C)** Pharmacokinetic data of CNIO-PI3Ki upon i.v. (2 mg/kg) or oral (10 mg/kg) administration. Measured parameters are: bioavailability (F); maximum plasmatic concentration (Cmax); time for maximum plasmatic concentration (Tmax); area under the curve (AUC); plasmatic half-life of the product (T ½); plasmatic clearance (Cl) and volume of distribution (Vd). Values correspond to average ± s.d. n=3.

As a first step to use CNIO-PI3Ki in mice, we began by measuring its serum levels by mass spectrometry. After a single oral dose of 15 mg/kg, the drug reached a serum concentration of 2-3 µg/ml (4-6 µM) 1 to 6 hours post-administration, being completely cleared after 24 hours (**Figure 9A**). Given the direct role of PI3K in insulin signalling and glucose homeostasis (Crouthamel et al., 2009), we next examined the effect of CNIO-PI3Ki on glucose levels of overnight fasted mice treated with a dose of 15 mg/kg. We observed a glucose peak of about 150 mg/dl 30 minutes to 2 hours post-administration (**Figure 9B**). Importantly, these glucose levels are comparable to those of *ad libitum*-fed mice (**Figure 9B**).

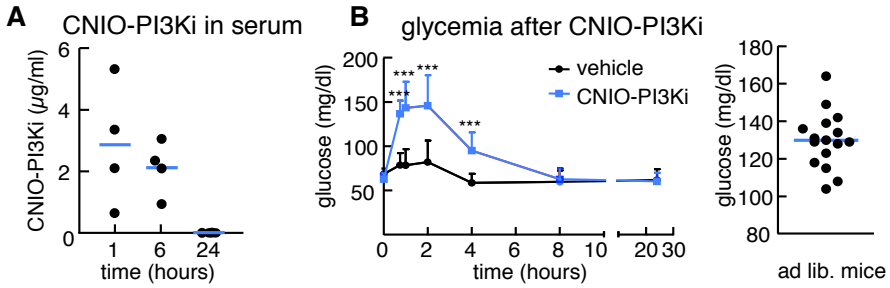

Figure 9. Effects of PI3K inhibition on glucose homeostasis.
(A) Detection of CNIO-PI3Ki in serum by mass spectrometry at the indicated times. Mice (C57BL6 males n=4 per group, 3-4 months old) were orally administered with CNIO-PI3Ki (15 mg/kg). Dots correspond to individual values and blue line to average. **(B)** Left panel, glucose serum levels at the indicated times after CNIO-PI3Ki (15 mg/kg) orally administered by gavage. Mice (C57BL6 males n=8-9 per group, 4 months old) were fasted overnight prior to gavage and maintained under fasting. Values correspond to average ± s.d. Right panel, glucose serum levels of *ad libitum*-fed mice (C57BL6 males n=16, 3 months old). Dots correspond to individual values and blue line to average. Statistical significance was determined by the two-tailed Student's t test: *p < 0.05, **p < 0.01, ***p < 0.001.

From a molecular point of view, both PI3Kis, GDC-0941 (75 mg/kg) and CNIO-PI3Ki (15 mg/kg), significantly reduced phosphorylated AKT (P-Ser473-AKT) (**Figure 10A**) and phosphorylated FOXO1, FOXO3 (P-Thr24/Thr32-FOXO1/3) and 4EBP1 (P-Ser65-4EBP1) levels in the liver and, especially, in the interscapular brown adipose tissue (iBAT) of mice 1 hour after treatment (**Figure 10B**). Inhibition of P-AKT was still detectable, although less notably, in both tissues 6 h post-administration (**Figure 10A**). Similarly, PI3K inhibition resulted in remarkable upregulation of the hepatic gluconeogenic transcriptional programme (measured by *G6pc* mRNA) 1 hour post-treatment, although *G6pc* levels returned close to basal after 6 hours (**Figure 10C**). Hence, we conclude that, at the administered dose, PI3K inhibitors produce a transient glycemic response within physiological range and a measurable downregulation of the PI3K/AKT signalling.

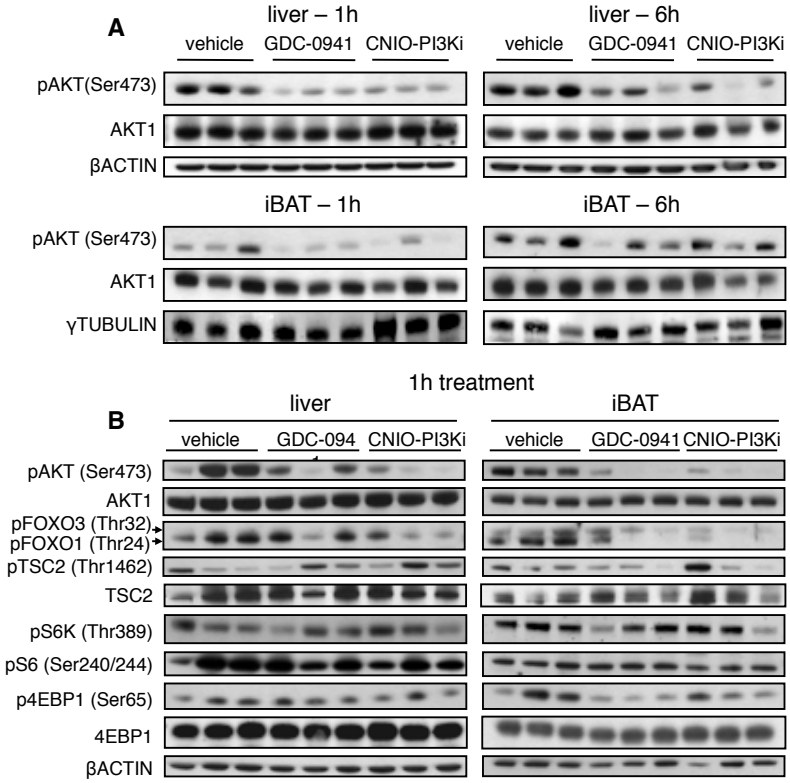

Figure 10. *In vivo* effects of PI3K inhibition.
(A) and **(B)** immunoblot analyses of the indicated proteins of liver and iBAT extracts, 1 or 6 h after oral gavage of vehicle, GDC-0941 (75 mg/kg), or CNIO-PI3Ki (15 mg/kg). **(C)** Expression of *G6pc* relative to *β-actin* in the liver of mice treated by gavage with vehicle, GDC-0941 (75 mg/kg), or CNIO-PI3Ki (15 mg/kg) 1 or 6 hours post-administration. In (A) and (C), mice were fed *ad libitum* during the whole assay. In (B), mice were fasted overnight, fed for 1 hour *ad libitum*, food removed and dosed by gavage.
Statistical significance was determined by the two-tailed Student's t test: *p < 0.05, **p < 0.01, ***p < 0.001.

In agreement with our previous data (Ortega-Molina et al., 2012), CNIO-PI3Ki treatment led to increased UCP1 protein levels in the BAT after 6 h administration, together with reduced P-AKT and P-FOXO1 (**Figure 11A**). After 24 h, and despite normalized P-AKT and P-FOXO1 levels and cleared serum PI3K inhibitor, UCP1 levels were still elevated (**Figure 11A**). Also, extending our previous findings on the ability of CNIO-PI3Ki to promote brown-like features within white adipose depots (Ortega-Molina et al., 2012), we also observed increased *Ucp1* expression in subcutaneous inguinal white adipose tissue (iWAT) and in visceral epididymal (eWAT) and perirenal white adipose tissue (rWAT) 6 hours after treatment (**Figure 11B**).

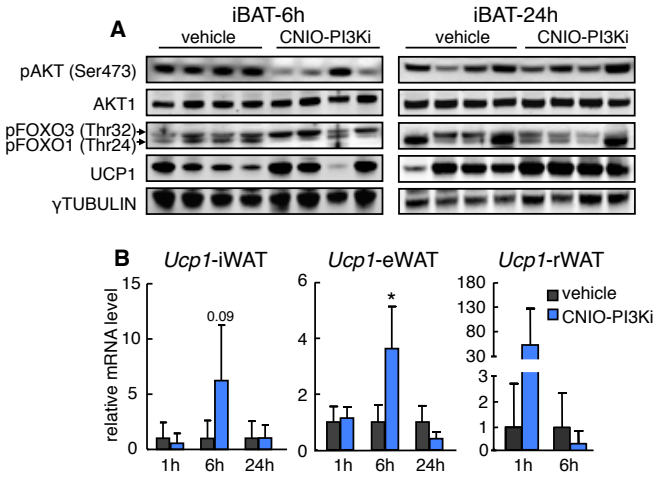

Figure 11. Effects of CNIO-PI3Ki on UCP1 expression in brown and white adipose tissue.
(A) Immunoblot analyses of the indicated proteins in iBAT lysates after treatment with vehicle or CNIO-PI3Ki (15 mg/kg) at the indicated times. **(B)** *Ucp1* expression in inguinal (iWAT), epididymal (eWAT), and perirenal (rWAT) white adipose tissue of mice (C57BL6 males n=4 per group, 12 weeks old) treated orally by gavage with vehicle or CNIO-PI3Ki (15 mg/kg) at the indicated times. Data are expressed as mean ± s.d.
Mice were fed *ad libitum* during the whole experiment. Statistical significance was determined by the two-tailed Student's t test: *p < 0.05.

As already shown, both PI3K inhibitors have limited access to the brain (**Figure 8B**), but still, the arcuate nucleus of the hypothalamus (ARC), a master regulator of metabolism (Sohn et al., 2013; Yeo and Heisler, 2012), is exposed to peripheral circulation through the median eminence, a circumventricular organ lacking brain-blood barrier (Cone et al., 2001). Thanks to the collaboration established with Dr. Miguel López from de CIMUS (Santiago de Compostela), we were able to verify unaltered expression of the main orexigenic (NPY and AgRP) and anorexigenic (CART and POMC) neuropeptides by *in situ* hybridization in the arcuate nucleus after oral PI3K inhibitor administration (**Figure 12**). These results indicate lack of hypothalamic effects, at least at the level of the ARC, and represent an important safety feature of both PI3K inhibitors.

As a conclusion, we show that PI3K inhibitors produce a transient cellular and molecular response accompanied by a glycemic peak within physiological range and without detectable effects on the hypothalamus.

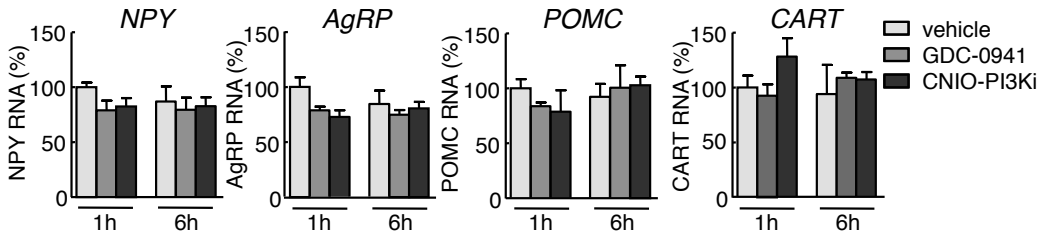

Figure 12. Hypothalamic effects of PI3K inhibition.
Effects of oral administration of vehicle, GDC-0941 (75 mg/kg) and CNIO-PI3Ki (15 mg/kg) on *NPY, AgRP*, *POMC* and *CART* mRNA expression measured by *in situ* hybridization in the arcuate nucleus of the hypothalamus (ARC) of mice. Data are expressed as mean ± SEM, n=4 per group (male C57BL6). No statistical significant differences were observed relative to vehicle by two-tailed Student's t-test.

1.2 PI3K inhibition reduces obesity, visceral fat and hepatic steatosis in mice

In order to test whether pharmacological PI3K inhibition could reduce obesity in mice, we started by performing a 10 days short-term treatment protocol, in which obese mice that had been on a HFD for 8 months were daily treated with 10 or 15 mg/kg CNIO-PI3Ki or 10 or 75 mg/kg GDC-0941 by gavage (**Figure 13A**). These diet-induced obese mice did not only weight around 44% more than control animals on a SD, but also presented insulin resistance and elevated levels of leptin (data not shown). Interestingly, mice significantly decreased their body weight upon treatment with PI3K inhibitors (**Figure 13B**) despite continuing on a HFD and maintaining their food intake constant (**Figure 13C**). In the most efficient case (15 mg/kg CNIO-PI3Ki), mice lost more than 20% body weight within the 10-day treatment and even reached the same weight as lean SD-fed mice (**Figure 13B**). Although to a lesser extent, treatment with 10 mg/kg CNIO-PI3Ki and 75 mg/kg GDC-0941 significantly reduced body

weight, too (**Figure 13B**). In all cases, mice displayed *ad libitum* glucose levels similar to vehicle treated mice 3 days after the end of the treatment (**Figure 13D**), meaning that glucose homeostasis had completely been restored. We also performed dual-energy X-ray absorptiometry (DXA) before, during and after treatment, which allowed us to follow fat and lean mass content of mice as well as distinguish the tissue responsible for the observed body weight loss. Importantly, this loss was exclusively due to a reduction in adiposity, while lean mass content remained stable throughout the whole experiment (**Figure 13E**).

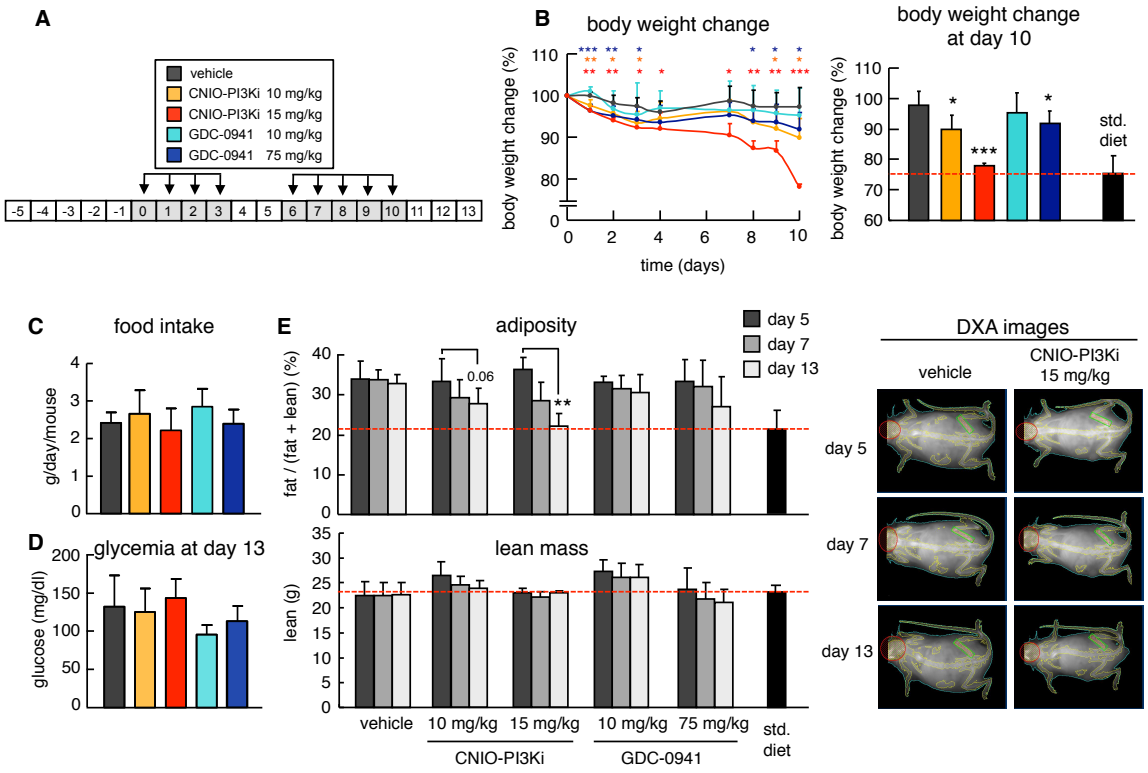

Figure 13. Body weight reduction and decreased adiposity after PI3Ki treatment.
(A) Schematic diagram showing administration regime of vehicle or PI3K inhibitors by gavage at the indicated days (grey boxes) to diet-induced obese mice (C57BL6/CBA males, n=4-7 per group, 10 months old). **(B)** Body weight change relative to day 0 (left) or to the last day of treatment (day 10) (right). For reference, right panel includes a dotted red line corresponding to the relative body weight of control male mice fed SD. **(C)** Average food intake per day during treatment. **(D)** *Ad libitum* glucose serum levels at the end of the treatment (day 13) with PI3K inhibitors. **(E)** Adiposity (top) and lean mass (bottom) at the indicated times measured by DXA. Adiposity values correspond to the fat percentage relative to the sum of lean and fat masses. For reference, graphs include dotted red lines corresponding to adiposity and lean mass of control male mice fed with SD. Right panel, representative DXA images at the indicated days of two mice treated with vehicle or CNIO-PI3Ki (15 mg/kg), respectively.
All values correspond to average ± s.d. All panels follow colour code as in (A). Statistical significance was determined by the two-tailed Student's t test: *p < 0.05, **p < 0.01, ***p < 0.001.

Examination of a number of tissues at the end of the treatment revealed important macroscopical as well as histological differences between groups. Whereas vehicle treated mice showed a pale coloured liver characteristic of obese animals and a great amount of fat surrounding the heart (pericardial fat), 15 mg/kg CNIO-PI3Ki treated mice exhibited normal,

healthy liver coloration and almost absent pericardial fat (**Figure 14A**). Both features seemed to be partially improved in 10 mg/kg CNIO-PI3Ki or 75 mg/kg GDC-0941 treated mice compared to controls (**Figure 14A**). Furthermore, histological analyses revealed reduced lipid accumulation in liver as well as reduced adipocyte size in eWAT, iBAT and perirenal and pericardial fat of CNIO-PI3Ki (15 and 10 mg/kg) and 75 mg/kg GDC-0941 treated mice (**Figure 14B**). Also, some browning areas (Wu et al., 2013), characterized by the presence of brown-like adipocytes interspersed in the eWAT, were also distinguishable, especially in the case of 15 mg/kg CNIO-PI3Ki-treated mice (**Figure 14B**).

Altogether, these data indicate that pharmacological PI3K inhibition reduces adiposity, lipid accumulation and induces browning within the white adipose tissue, thereby reducing body weight in diet-induced obese mice.

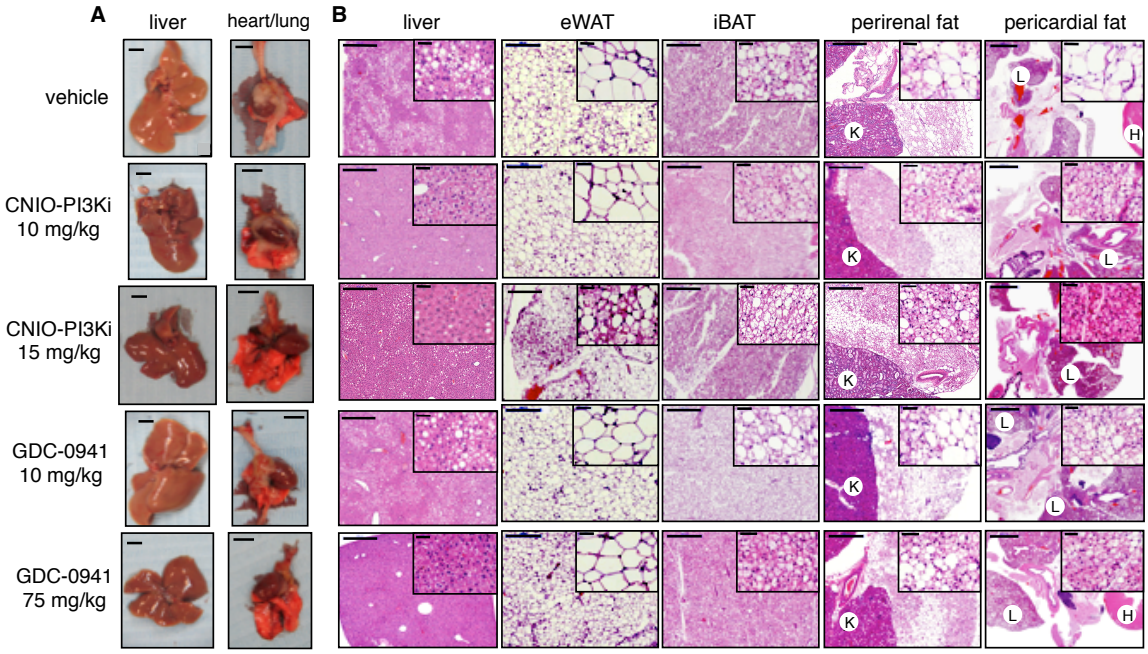

Figure 14. Reduced liver steatosis and increased browning after acute CNIO-PI3Ki treatment.
(A) Representative pictures of liver and fat surrounding lung and heart (perivascular fat) in vehicle- and PI3Ki-treated mice at day 13. Bars correspond to 0.5 cm. **(B)** Representative pictures of H&E-stained sections of the indicated tissues at day 13. eWAT is epididymal WAT and iBAT interscapular BAT. In perirenal fat K indicates kidney; in perivascular fat L indicates lung and H heart. Bars correspond to 0.5 mm with the exception of the perivascular picture, where it corresponds to 2 mm. All high-magnification insets correspond to 50 µm.
Mice are the same as in **Figure 13.**

1.3 Improved metabolic syndrome after long-term CNIO-PI3Ki treatment

A desirable feature for an anti-obesity treatment is to retain activity at low doses, which would allow its administration during prolonged periods of time and would lead to a gradual, controllable weight loss. Bearing this in mind, we formulated the CNIO-PI3Ki for administration in drinking water at a concentration of 0.1 mg/ml, which corresponds to a daily-

accumulated dose of approximately 10 mg/kg. For this experiment, diet-induced obese HFD-fed and lean SD-fed mice were either treated with vehicle or CNIO-PI3Ki for 2.5 months. Due to *ad libitum* and, consequently, heterogeneous water access of mice, the administered dose resulted in detectable but variable (63 ± 54 ng/ml) CNIO-PI3Ki levels in serum with almost no signs of accumulation in iWAT, iBAT and liver (**Figure 15A**). At this point, it is worth mentioning that the mean CNIO-PI3Ki serum concentration in this assay is about 40-fold lower than the drug's peak obtained after 1-6 hours CNIO-PI3Ki at 15 mg/kg given by gavage **(Figure 9A)**.

Soon after the beginning of the treatment, obese HFD-fed mice treated with CNIO-PI3Ki showed a progressive body weight loss (**Figure 15B**) despite continuing on a HFD and maintaining their food and water intake unaltered (**Figure 15C**). This loss represented a 20% body weight reduction compared to HFD vehicle-treated mice and takes places during the first 50 days of treatment, as body weight stabilizes after this time point (**Figure 15B**). This behaviour supports the idea that CNIO-PI3Ki increases energy expenditure, and, thereby, lowers body weight until mice reach a new energetic balance. Also, the fact that CNIO-PI3Ki treatment is only effective in HFD-fed mice and not in lean SD-fed animals suggests that the inhibitor may selectively act on energy expenditure induced by nutritional overload and represents a relevant safety feature as well.

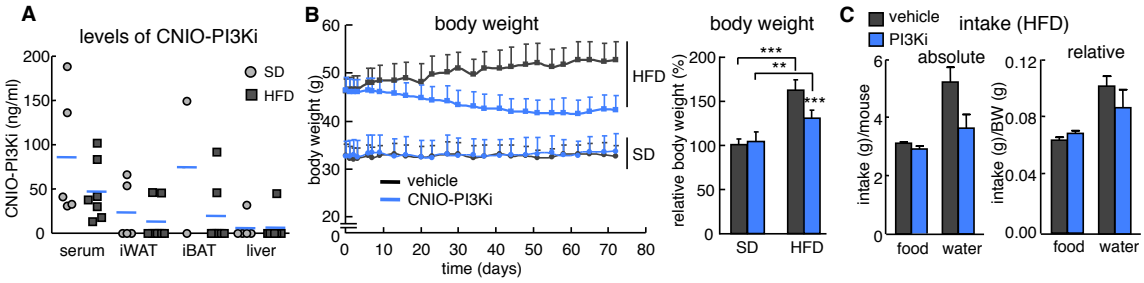

Figure 15. Obesity reduction upon long-term CNIO-PI3Ki treatment.
(A) CNIO-PI3Ki concentration measured by mass spectrometry in serum, iWAT, iBAT and liver of long-term CNIO-PI3Ki (0.1 mg/ml in drinking water) treated mice fed on a standard diet (SD, n=2-5 depending on tissue) or high fat diet (HFD, n=7). Dots and squares correspond to individual values and blue bars to average. **(B)** Left, body weight curves during 2.5 months vehicle or CNIO-PI3Ki (0.1 mg/ml) treatment in drinking water. HFD, mice fed high-fat diet since 2 months of age and throughout the whole assay; SD, mice fed SD. C57BL6 males, n=5-7 per group; 11 months at the beginning of the treatment. Right, body weights relative to SD-fed, vehicle-treated mice at the end of the treatment. Significant weight difference between groups maintained on a HFD started at day 23 ($p < 0.05$) and lasted until the end of the assay ($p < 0.001$). **(C)** Absolute (left) and relative (right) food and water intake during vehicle/CNIO-PI3Ki treatment of HFD-fed mice. Intake was measured in periods of 3 days in a total of 4 periods, distributed throughout the entire assay.
Values correspond to average ± s.d in (B) or average ± SEM in (C). Statistical significance was determined by the two-tailed Student's t test: *$p < 0.05$, **$p < 0.01$, ***$p < 0.001$.

We confirmed again that the observed body weight loss after CNIO-PI3Ki treatment was exclusively due to a reduction in adiposity %, as lean mass content was unaltered (**Figure 16A**). Verifying this data, we found reduced relative weight of eWAT and iWAT as well as

decreased pericardial and perirenal fat accumulation (**Figure 16B**), lower leptin serum levels (**Figure 16C**) and a tendency towards reduced serum triglycerides (**Figure 16D**) in CNIO-PI3Ki treated mice compared to vehicles at the end of the treatment. In contrast, cholesterol serum levels did not change **(Figure 16E)**.

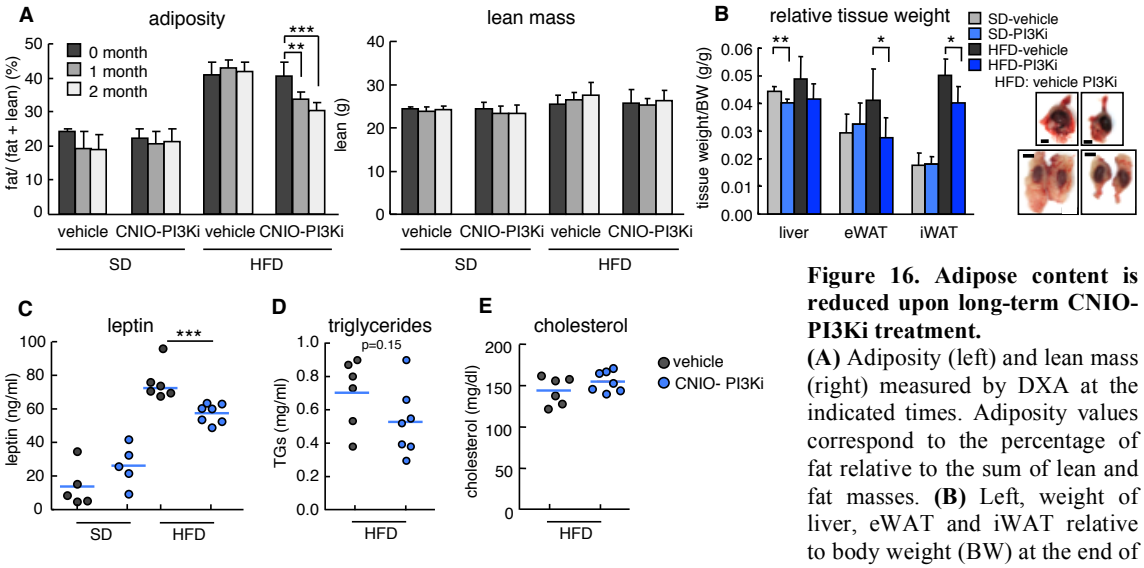

Figure 16. Adipose content is reduced upon long-term CNIO-PI3Ki treatment.
(A) Adiposity (left) and lean mass (right) measured by DXA at the indicated times. Adiposity values correspond to the percentage of fat relative to the sum of lean and fat masses. **(B)** Left, weight of liver, eWAT and iWAT relative to body weight (BW) at the end of vehicle or CNIO-PI3Ki long-term treatment. SD, n=5 in both groups; HFD, n=6 for vehicle and n=7 for CNIO-PI3Ki. Right, representative macroscopic pictures of pericardial and perirenal fat of vehicle or CNIO-PI3Ki treated mice. **(C)** *Ad libitum* leptin serum levels, **(D)** *ad libitum* triglycerides serum levels and **(E)** *ad libitum* cholesterol serum levels at the end of the long-term vehicle/CNIO-PI3Ki treatment.
Values correspond to average ± s.d in (A) and (B). In (C), (D), and (E) dots correspond to individual values and blue bars to average. Mice are the same as in **Figure 15**.
Statistical significance was determined by the two-tailed Student's t test: *p < 0.05, **p < 0.01, ***p < 0.001.

We next wanted to address if the CNIO-PI3Ki treatment had improved some of the pathological signs associated to obesity. For example, PI3K inhibition was able to revert liver steatosis by reducing fat accumulation in liver (**Figure 17A**). Other markers of liver injury such as circulating alanine aminotransferase (ALT) levels (**Figure 17B**) or *Il-6* mRNA expression in liver, indicative of chronic inflammatory reaction (**Figure 17C**), were also reduced in CNIO-PI3Ki treated mice. Regarding the adipose tissues of HFD-fed mice, iBAT as well as epididymal WAT (eWAT) of CNIO-PI3Ki-treated mice showed a clear decrease in lipid droplets compared with vehicle-treated mice (**Figure 17A**). In contrast to the previous experiment, in which CNIO-PI3Ki was administered acutely by gavage at a higher dose (15 mg/kg), we were not able to detect any browning areas in the eWAT of CNIO-PI3Ki-treated animals (**Figure 17A**). We hypothesize that a possible reason for this finding is precisely the low CNIO-PI3Ki dose administered in drinking water, which leads to a 40-fold lower serum concentration compared to the peak of drug achieved by gavage. Another feature of insulin resistance associated with obesity is the infiltration of macrophages into the white adipose tissue (Strissel et al., 2007). Interestingly, staining with macrophage-restricted glycoprotein F4/80

revealed reduced infiltration of macrophages in HFD CNIO-PI3Ki-treated mice compared with vehicle-treated (**Figure 17A**). Measurement of macrophage mRNA markers such as *Emr1* and *Cd68* in the eWAT showed a similar tendency (**Figure 17D**). Of note, no differences could be established in SD-fed mice treated or not with CNIO-PI3Ki in any of the analysed parameters.

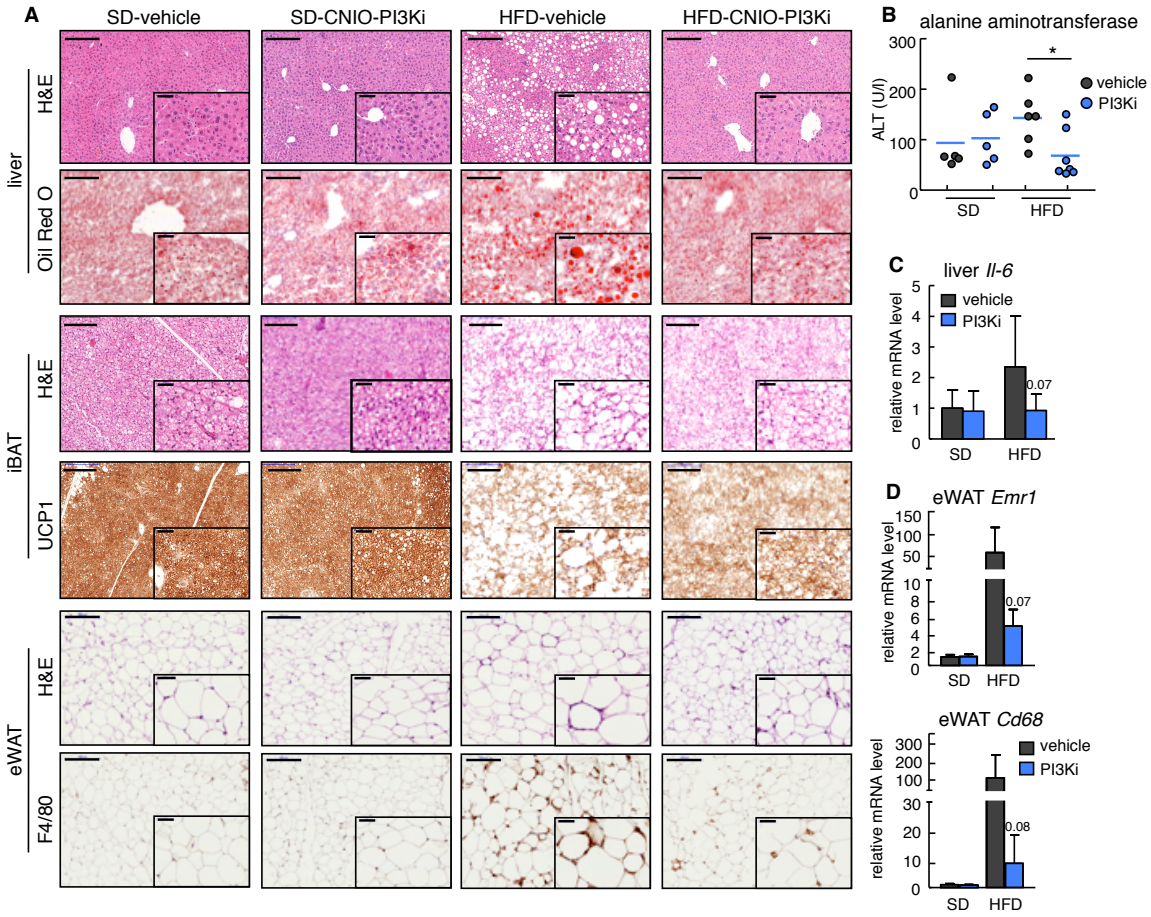

Figure 17. Reduced hepatic steatosis and inflammation after CNIO-PI3Ki treatment.
(A) Representative pictures of liver sections stained with H&E or oil red O (upper panel), interscapular BAT (iBAT) sections stained with H&E or anti-UCP1 (middle panel) and epididymal WAT (eWAT) sections stained with H&E or anti-F4/80 (lower panel). Bars in low-magnification pictures correspond to 200 µm; bars in high magnification insets correspond to 50 µm. **(B)** *Ad libitum* alanine aminotransferase (ALT) serum levels at the end of the long-term vehicle/CNIO-PI3Ki treatment. Dots correspond to individual values and blue bar to average. **(C)** *Il-6* expression relative to *β-actin* in liver. **(D)** *Emr1* and *Cd68* mRNA levels relative to *β-actin* in eWAT. Values correspond to average ± s.d. Mice in this figure are the same as in **Figure 15.**
Statistical significance was determined by the two-tailed Student's t test: *p < 0.05.

Next, we wondered whether 2.5 months CNIO-PI3Ki treatment had possibly ameliorated glucose homeostasis. However, none of the tested parameters including glucose tolerance (**Figure 18A**), insulin tolerance (**Figure 18B**), glycemia, insulinemia, and insulin resistance (quantified by the HOMA-IR index) (**Figure 18C**) showed any difference between HFD vehicle or CNIO-PI3Ki treated mice. Taking into account that the mice used for this assay had been for more than 8 months on a HFD and are presumable profoundly diabetic, we

reasoned that 2.5 months treatment would not be enough to improve glucose homeostasis. Therefore, we performed a new experiment in which diet-induced obese mice (that had been for 8 months on a HFD previously) were subjected to vehicle or 0.1 mg/ml CNIO-Pi3Ki in their drinking water and under continuous HFD conditions for 5 months. Again, obese mice treated with the CNIO-PI3K inhibitor reduced their body weight about a 20% compared to vehicle-treated mice during the first 50 days of treatment and, afterwards, stabilized their weight for the next 100 days (**Figure 18D**). This observation points out to the fact that the treatment does not cause any drug resistance, as mice do not spontaneously gain weight again. Of note, body weight is only maintained as long as the treatment is present, as PI3Ki withdrawal from the drinking water promotes rapid body weight gain (**Figure 18D**), thereby indicating that the treatment does not cause any irreversible changes in the organism and normal homeostasis can rapidly be restored. Regarding glucose homeostasis, we were able to detect normalized fasting glucose levels, comparable to those of SD fed mice, in HFD-fed mice that had been treated for 5 months with the CNIO-PI3Ki and then released from the drug for the next month (**Figure 18E**).

In conclusion, we have demonstrated that long-term low-dose CNIO-PI3Ki treatment progressively reduces body weight by decreasing fat accumulation only in the context of nutritional overload and improves hepatic steatosis, chronic inflammation and fasting glucose levels, thereby ameliorating some of the signs of the metabolic syndrome. Furthermore, CNIO-PI3Ki treatment is reversible and does not cause resistance.

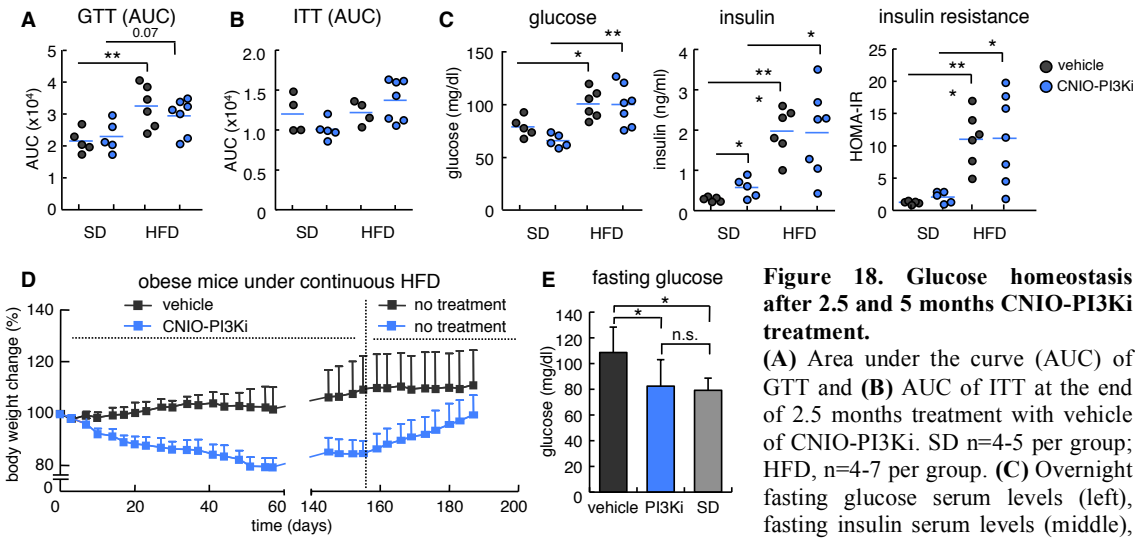

Figure 18. Glucose homeostasis after 2.5 and 5 months CNIO-PI3Ki treatment.
(A) Area under the curve (AUC) of GTT and **(B)** AUC of ITT at the end of 2.5 months treatment with vehicle of CNIO-PI3Ki. SD n=4-5 per group; HFD, n=4-7 per group. **(C)** Overnight fasting glucose serum levels (left), fasting insulin serum levels (middle), and derived insulin resistance index HOMA-IR (right) at the end of 2.5 months. **(D)** Body weight change relative to day 0. 10-month-old mice (C57BL6 male, n=9-10 per group) fed with HFD for 8 months were treated with vehicle or CNIO-PI3Ki (0.1 mg/ml) in drinking water during 5 months. At day 155, treatment was removed from the water for the rest of the experiment. Mice were fed with HFD during the entire assay. Significant weight difference between groups lasted from day 7 to day 180. **(E)** Fasting glucose levels of HFD-fed mice at the end of the procedure (5 months vehicle/CNIO-PI3Ki treatment and 48 days treatment-free) compared to SD-fed control mice.
In (A), (B) and (C) dots correspond to individual values and blue lines to average. In (E) values correspond to average ± s.d. Statistical significance was determined by the two-tailed Student's t test: *p < 0.05, **p < 0.01.

1.4 CNIO-PI3Ki protects against obesity and induces energy expenditure

We also asked whether CNIO-PI3Ki treatment would prevent obesity in lean mice subjected to *de novo* HFD. Thus, we designed two new assays in which lean SD-fed mice were switched to high fat diet together with the administration of the CNIO-PI3Ki either in the drinking water at a concentration of 0.1 mg/ml and performed at the CNIO (Madrid), or mixed with food pellets using a concentration of 0.17 g/kg and performed by the group of Dr. Rafael de Cabo at the National Institute on Aging (NIA, Baltimore). The approximate accumulated daily dose was 10 mg/kg and HFD food as well as water was available *ad libitum* in both cases. Importantly, CNIO-PI3Ki treatment clearly slowed down the rate of body weight gain despite unaffected food intake (**Figure 19A**). While vehicle treated mice increased their body weight around 50% in 80 days, CNIO-PI3Ki-treated had only gained about 25% body weight (**Figure 19A**). Moreover, mice treated with the inhibitor in their food (NIA experiment) showed improved fasting glucose levels (**Figure 19B**) suggesting that the CNIO-PI3K inhibitor treatment not only protects against obesity onset but also prevents glucose intolerance.

These observations underline the efficacy of our compound, which works in drinking water as well as mixed with food in two different and independent laboratories. On the other hand, they indicate that the beneficial effects of PI3K inhibition appear as soon as high-fat feeding starts in lean, healthy mice.

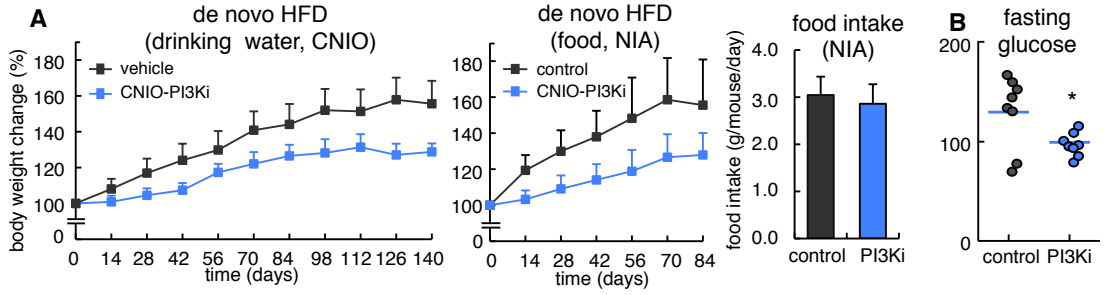

Figure 19. CNIO-PI3Ki treatment prevents obesity onset.
(A) Left, performed at the CNIO, body weight change relative to day 0. 2-months-old mice (C57BL6 male, n=8-10 per group) were put simultaneously on a HFD with CNIO-PI3Ki (0.1 mg/ml) or vehicle in drinking water for 20 weeks. Significant weight difference starts at day 3. Middle, performed at the NIA, body weight change relative to day 0. 28-weeks-old SD-fed mice (C57BL6 male, n=18-24 per group) were put on HFD or HFD supplemented with CNIO-PI3Ki (0.17 g/kg) for 12 weeks. Significant weight difference observed after first weight measurement. Right, food intake of mice fed with HFD or HFD supplemented with CNIO-PI3Ki. Intake was measured in periods of 2 days for a total of 3 periods at weeks 2, 4 and 8 of treatment. Mice are the same as in the middle panel. **(B)** Fasting glucose level of mice after 12 weeks with or without CNIO-PI3Ki treatment in their HFD food. Animals (control n=8, CNIO-PI3Ki n=8) are from assay (A) performed at the NIA.
Statistical significance was determined by the two-tailed Student's t test: *p < 0.05.

We have previously shown that CNIO-PI3Ki (15 mg/kg via oral gavage) enhances energy expenditure, at least in part, by activating thermogenesis in brown adipocytes, both *in vivo* and *in vitro* (Ortega-Molina et al., 2012). To validate whether continuous, low-dose CNIO-

PI3Ki treatment via food pellets (NIA) had a measurable impact on energy expenditure, we performed indirect calorimetry assay which revealed higher constitutive energy expenditure (**Figure 20A**), oxygen consumption and CO_2 consumption (**Figure 20B and 20C**) together with higher locomotor activity (**Figure 20D**). Still, it remains debatable to what extent increased locomotor activity translates into increased total energy expenditure (Virtue et al., 2012). In order to evaluate iBAT thermogenesis, we also measured whole-body and shoulder temperature using a thermogenic camera. Although body temperature progressively dropped due to the administered anaesthesia, only shoulder temperature was consistently higher in HFD CNIO-PI3Ki compared to both, HFD vehicle and weight-matched SD-fed control mice (**Figure 20E**).

In summary, PI3K inhibition protects against obesity and glucose resistance onset in lean mice subjected to *de novo* HFD and elevates energy expenditure at the administered low-dose.

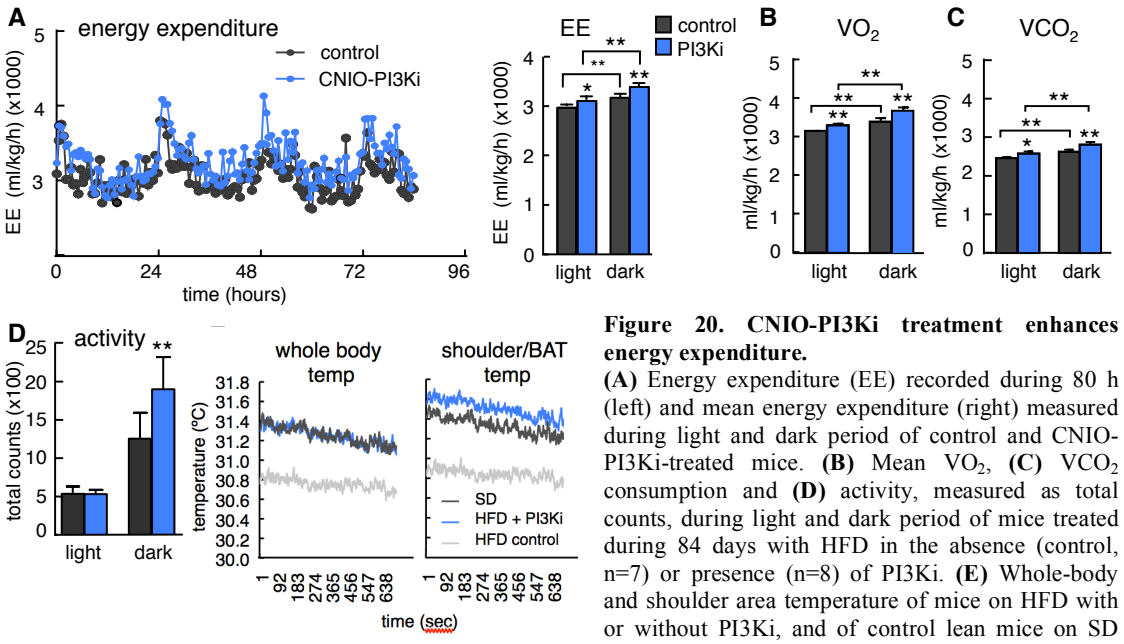

Figure 20. CNIO-PI3Ki treatment enhances energy expenditure.
(A) Energy expenditure (EE) recorded during 80 h (left) and mean energy expenditure (right) measured during light and dark period of control and CNIO-PI3Ki-treated mice. **(B)** Mean VO_2, **(C)** VCO_2 consumption and **(D)** activity, measured as total counts, during light and dark period of mice treated during 84 days with HFD in the absence (control, n=7) or presence (n=8) of PI3Ki. **(E)** Whole-body and shoulder area temperature of mice on HFD with or without PI3Ki, and of control lean mice on SD (n=6-9 per group). Temperature was recorded every second for 10 min. All these assays were performed at the NIA, and mice are the same as in **Figure 12,** middle panel (NIA). Values correspond to average ± s.d. Statistical significance was determined by the two-tailed Student's t test: *p < 0.05, **p < 0.01.

1.5 CNIO-PI3Ki treatment reduces obesity in hyperphagic mice

We next wanted to test if our inhibitor was also able to induce body weight loss in a model of obesity independent of high fat intake. Hence, we used the leptin deficient, hyperphagic, ob/ob mouse model, which constitutes a relevant model of obesity induced by a high intake of standard diet. Importantly, three months administration of CNIO-PI3Ki in the drinking water using again an accumulative daily dose of 10 mg/kg resulted in a very pronounced body weight loss compared to vehicle-treated mice (**Figure 21A**). Taking into account that CNIO-PI3Ki ob/ob mice were more hyperphagic than vehicle-treated mice (**Figure 21B**), this weight

difference is even more striking. Reaffirming our previous data, PI3Ki-treated ob/ob mice showed reduced liver damage measured by ALT levels in serum (**Figure 21C**), reduced hepatic steatosis and decreased adipocyte size in perirenal, pericardial and iBAT (**Figure 21D**). However, no differences were observed regarding glucose homeostasis (**Figure 21E**), reinforcing the idea that only longer treatments, such as 5 month treatments, are able to affect glucose tolerance.

These results prove that CNIO-PI3Ki treatment is also effective in obese hyperphagic ob/ob mice, and therefore, that CNIO-PI3Ki protects against obesity not only induced by high-fat diets but also caused from an excessive intake of a normal diet.

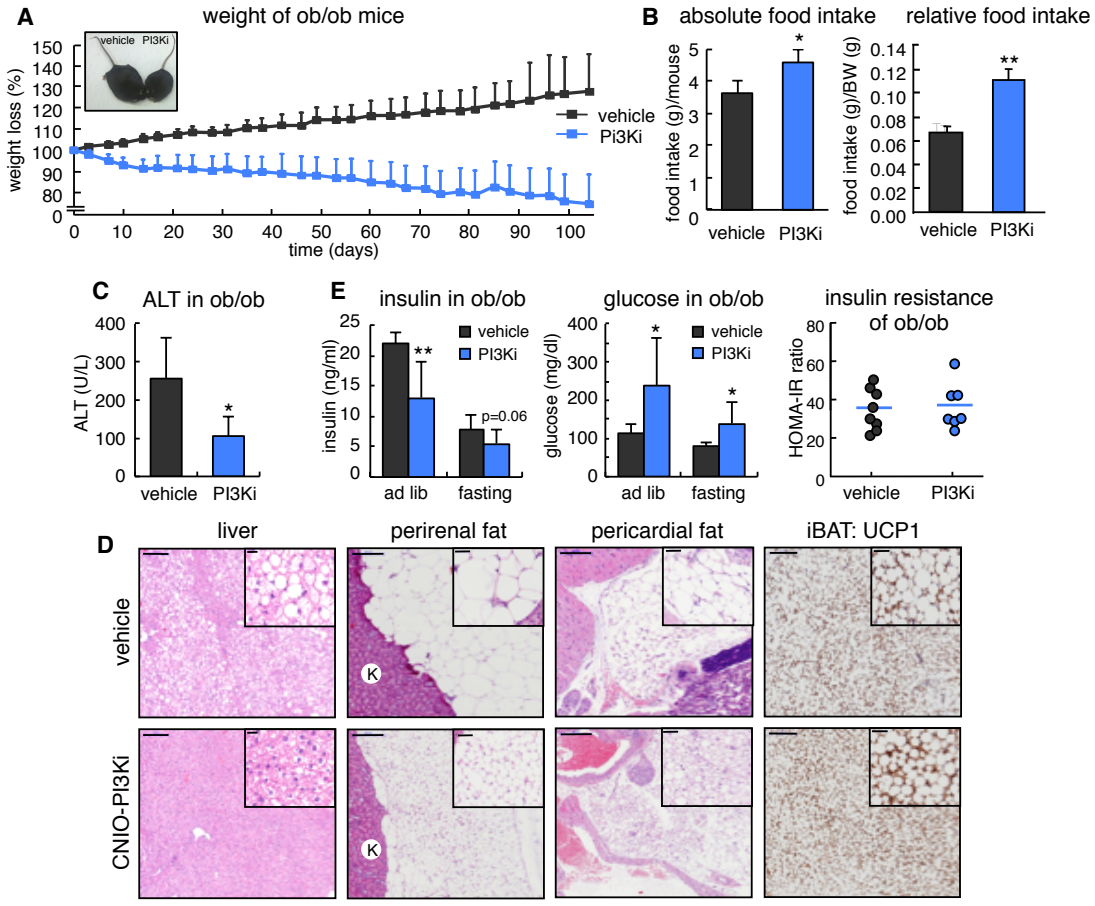

Figure 21. CNIO-PI3Ki treatment reduces obesity of hyperphagic, leptin deficient ob/ob mice.
(A) Body weight change relative to day 0, and representative picture of CNIO-PI3Ki or vehicle treated mice at the end of the treatment. Hyperphagic ob/ob male mice (12 weeks old) fed with SD and treated with vehicle or CNIO-PI3Ki (0.1 mg/ml) in drinking water during 16 weeks. C57BL6 males ob/ob mice, n=10 per group. Significant weight difference between groups starts at day 3. **(B)** Absolute (left) and relative to body weight (right) food intake of ob/ob mice treated with vehicle or CNIO-PI3Ki. Intake was measured in periods of 4 days, in a total of two periods, distributed in the middle of the treatment. **(C)** Alanine aminotransferase (ALT) levels in serum of ob/ob mice after 105 day of vehicle (n=6) or CNIO-PI3Ki (n=5) treatment. **(D)** Representative microscopic pictures of liver, perirenal and pericardial fat sections stained with H&E, and BAT stained with anti-UCP1 of ob/ob mice at the end of the treatment. Bars in low magnification pictures correspond to 200 µm, and bars in high magnification insets to 50 µm. **(E)** *Ad libitum* (ad lib) and fasting serum insulin (left) and glucose (middle) level in ob/ob mice at the end of the treatment. Right, insulin resistance of ob/ob mice measured by the HOMA-IR index. Dots correspond to individual values and blue line to average.
Values correspond to average ± s.d. Statistical significance was determined by the two-tailed Student's t test: *p < 0.05, **p<0.01.

1.6 PI3Kα inhibition promotes Ucp1 activity and causes body weight loss

The beneficial metabolic effects of overall PI3K signalling reduction have been attributed to an increase in energy expenditure (Becattini et al., 2011; Garcia-Cao et al., 2012; Ortega-Molina et al., 2012; Perino et al., 2014) and thereby to an attenuation of nutrient storage in favour of nutrient consumption. We have previously shown that GDC-0941 and CNIO-PI3Ki increase *Ucp1* expression and thermogenesis in cultured brown adipocytes (Ortega-Molina et al., 2012). Dealing with two compounds that inhibit several PI3K isoforms (in both cases principally α and δ together with γ, in a lesser extent; and β only in the case of GDC-0941), we next wanted to identify the isoform responsible for the regulation of the thermogenic activity in brown adipocytes *in vitro*. Individual inhibition of the predominantly expressed catalytic p110-α, p110-β and p110-δ subunits in brown adipocytes using shRNA revealed that only PI3Kα, but none of the other PI3Ks, resulted in enhanced *Ucp1* and *Pgc1α* expression in forskolin-stimulated brown adipocytes (**Figure 22**). This result reinforces the concept that PI3Kα inhibition is a relevant mediator of the link between PI3K and metabolism (Foukas et al., 2013; Ortega-Molina et al., 2012). Nevertheless, it does not exclude other mechanisms through which PI3Kα inhibition may induce energy expenditure nor alternative mechanisms independent of brown adipocyte thermogenesis by which inhibition of other PI3K isoforms may increase energy expenditure (Becattini et al., 2011; Perino et al., 2014).

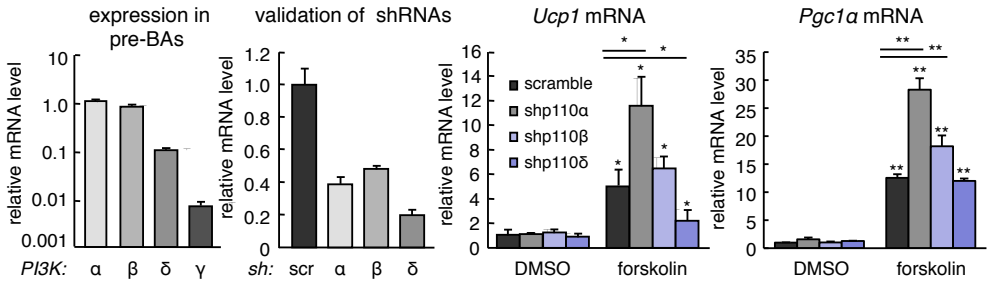

Figure 22. PI3Kα inhibition induces *Ucp1* and *Pgc1α* expression *in vitro*.
(A) Left, relative mRNA level of the different PI3K isoforms *PI3Kα*, *PI3Kβ*, *PI3Kδ* and *PI3Kγ* in pre-brown adipocytes. Middle, validation of PI3K shRNAs. *p110α*, *p110β* and *p110δ* mRNA expression in pre-brown adipocytes after sh-scramble, sh-p110α, sh-p110β and sh-p110δ lentiviral transduction. Right, relative *Ucp1* and *Pgc1α* expression in pre-brown adipocytes transduced with the indicated shRNAs and after 4h DMSO or forskolin 10 μM stimulation. mRNA levels were normalized to *β-actin*. Stimulation was performed twice with similar results and each experiment was done in triplicate. Values correspond to average ± s.d. of one experiment, n=3.
Statistical significance was determined by the two-tailed Student's t test: *p < 0.05, **p<0.01.

Furthermore, we next wanted to verify whether PI3Kα inhibition was responsible for the described body weight loss *in vivo* as well. Thus, we decided to treat 20 weeks old obese ob/ob mice daily by gavage, and during 16 days, either with vehicle or with three different PI3K inhibitors: CNIO-PI3Ki at 5 mg/kg and 1 mg/kg, BYL-719 (also called alpelisib) and acalisib,

both at 10 mg/kg and 5 mg/kg. BYL-719 (Furet et al., 2013) is a selective PI3Kα inhibitor (IC_{50} of 5 nM) currently in phase I and II clinical trials to treat various tumour types such as breast or pancreas cancer. Acalisib (Shugg et al., 2013) is mainly a δ subunit inhibitor (IC_{50} of 12.7 nM) used for mouse studies and closely related to idelalisib, which has been already approved for the treatment of chronic lymphocytic leukemia. Initially, we checked the physiological response on glucose homeostasis by following for 24 hours the glucose levels of *ad libitum* fed ob/ob mice given a single dose of the different inhibitors by gavage. A prolonged hyperglycemic peak was observed during the first 6 hours after CNIO-PI3Ki and BYL-719 treatment, while acalisib and vehicle did not have any significant effects on glucose levels (**Figure 23A**). Importantly, homeostasis was re-established after 24 hours.

Soon after daily exposure to CNIO-PI3Ki and BYL-719 (only at the dose of 10 mg/kg), ob/ob mice started losing weight (**Figure 23B**) despite maintaining their food intake constant or even more elevated than controls (**Figure 23C**). This weight loss only continued during the first 10 days of treatment and, afterwards, body weight stabilized until the end of the assay. Compared to vehicle-treated mice, CNIO-PI3Ki (1 mg/kg) and BYL-719 (5 mg/kg) treatment produced a significant 6-7% reduction in body weight, and CNIO-PI3Ki (5 mg/kg) and BYL-719 (10 mg/kg) resulted in a significant 10% body weight reduction (**Figure 23B**). Moreover, acalisib-treated mice showed a small, non-significant, body weight reduction compared to vehicle-treated animals (**Figure 23B**). Again, seven days after the beginning of the treatment, physiological glucose levels were confirmed 24 hours post-PI3Ki dosing (**Figure 23D**). Of note, PI3Ki-treated ob/ob mice, in particular those treated with BYL-719 (10 mg/kg) and CNIO-PI3Ki (5 mg/kg), showed a very important increase in water intake (**Figure 23C**), probably resulting as a mechanism to counteract the detected hyperglycaemic peak. In this context, it is relevant to mention that, at later time points (between day 9 to 16), around 20% of the mice treated with CNIO-PI3Ki and BYL-719, at both doses, had to be sacrificed due to their inability to re-establish normal glucose homeostasis.

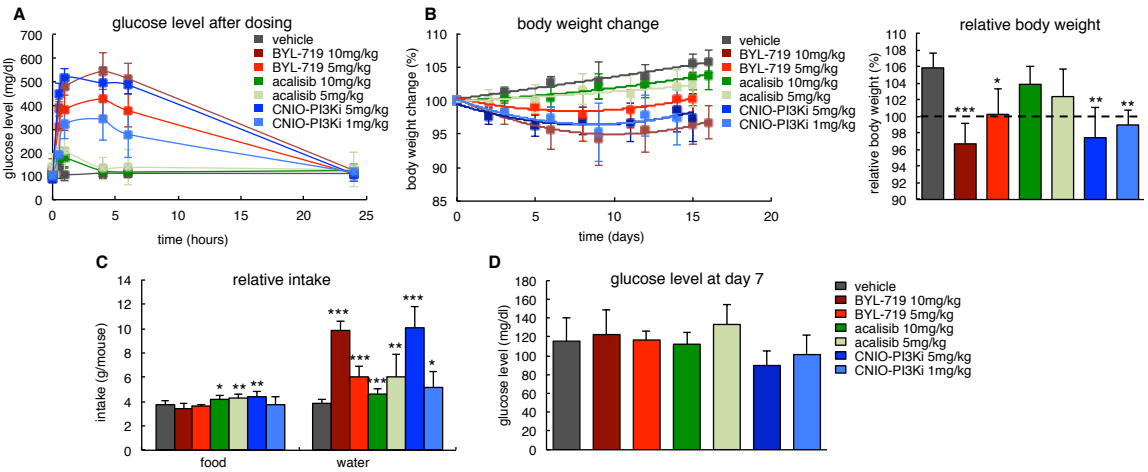

Figure 23. Effects of PI3Kα and PI3Kδ inhibition in ob/ob mice.
(A) Glucose serum levels at the indicated times after vehicle, BYL-719 (only PI3Kα-inhibitor), acalisib (mainly PI3Kδ-inhibitor) or CNIO-PI3Ki (PI3Kα and PI3Kδ inhibitor) orally administered by gavage at the specified doses. ob/ob male mice n=10 per group; 20 weeks old. **(B)** Left, body weight change relative to day 0, or right, relative to the last day of treatment (d16). For reference, the right panel includes a dotted black line corresponding to the initial weight. **(C)** Relative food and water intake during vehicle and PI3K inhibitor treatment. Intake was measured for 5 days, in the middle of the assay. **(D)** *Ad libitum* glucose serum levels, measured before new dosing, after 7 days treatment.
Values correspond to average ± s.d. Statistical significance was determined by the two-tailed Student's t test: *p < 0.05, **p<0.01, ***p<0.001.

Additionally, we analysed various metabolic parameters in serum at the end of the assay. Probably, as a sign of low fat absorption by the adipose tissue, we detected higher circulating triglycerides (**Figure 24A)** and free fatty acid levels (**Figure 24B**) in BYL-719 (10 and 5 mg/kg) and CNIO-PI3Ki-treated (5 mg/kg) ob/ob mice. Similarly, cholesterol serum levels appeared elevated in mice treated with BYL-719 (**Figure 24A**). Interestingly, CNIO-PI3Ki-treated ob/ob mice presented reduced lactate serum levels compared to vehicle-treated controls (**Figure 24A**). As previously reported in Tg-PTEN mice (Garcia-Cao et al., 2012) reduced lactate levels can be considered an indicator of increased mitochondrial activity since pyruvate, generated from glucose catabolism, can be reduced to lactic acid (anaerobic glycolysis) or further metabolized by the mitochondria (oxidative phosphorylation). Consequently, this suggests that an increased mitochondrial oxidative phosphorylation may also be contributing to the described body weight loss.

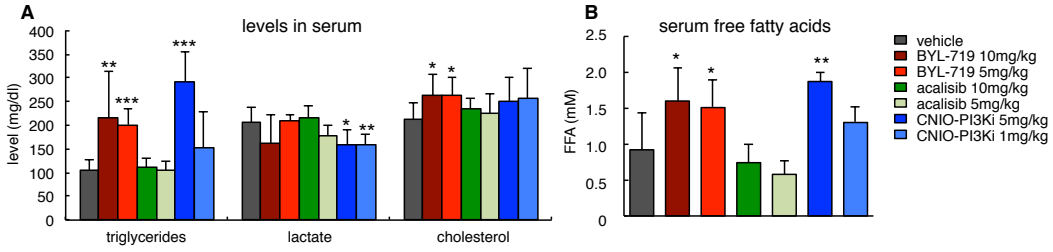

Figure 24. PI3Kα and PI3Kδ inhibition in ob/ob mice.
(A) *Ad libitum* serum triglycerides, lactate and cholesterol level; and **(B)** free fatty acids serum levels at the end of the treatment (day 16). n=6-8 per group. Values correspond to average ± s.d.
Statistical significance was determined by the two-tailed Student's t test: *p < 0.05, **p<0.01, ***p<0.001.

Aiming to determine whether the used PI3K inhibitors were having an impact on energy expenditure that could explain the different outcomes observed on body weight, we decided to perform indirect calorimetry. Therefore, we treated lean mice orally with 15 mg/kg of CNIO-PI3Ki, BYL-719 or acalisib and recorded for 6 hours (starting one hour after gavage) oxygen and CO_2 consumption. To minimize the effects of body weight on energy expenditure, we selected a cohort of mice with homogenous weights (29.5 ± 1.25 g) for this experiment. As expected, administration of CNIO-PI3Ki and BYL-719 significantly induced energy

expenditure in mice compared to controls **(Figure 25)** whereas acalisib treatment did not have any effect on energy expenditure.

Altogether, these data point out to the fact that PI3Kα inhibition, and not PI3Kδ, is the key event leading to enhanced energy expenditure and body weight reduction. Likewise, and taking into account the different concentrations used, CNIO-PI3Ki appears more potent and efficient than BYL-719 in reducing obesity.

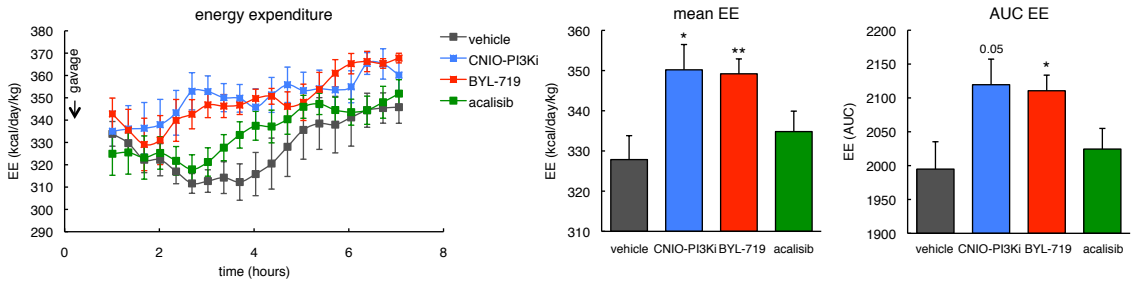

Figure 25. Energy expenditure after PI3K inhibitor administration.
Left, energy expenditure (EE) of lean mice after administration of 15 mg/kg of CNIO-PI3Ki, BYL-719 or acalisib. Animals were orally treated by gavage and EE recoded from 1 to 6 hours post-gavage. n=6-8 males, 20 weeks old. Middle, mean EE and right, area under the curve (AUC) after PI3K inhibitor treatment. Values correspond to average ± s.e.m.
Statistical significance compared to vehicle was determined by the two-tailed Student's t test: *p < 0.05, **p<0.01.

1.7 CNIO-PI3Ki treatment reduces adiposity in rhesus monkeys

Having validated that the CNIO-PI3K inhibitor treatment is able to revert obesity by reducing fat accumulation in different obesity mouse models, as well as improve some of the signs of the metabolic syndrome such hepatic steatosis and fasting glucose levels together with reduced inflammation, we next decided to examine the effects of CNIO-PI3Ki on rhesus monkeys (*Macaca mulatta*) thanks to the collaboration established with Dr. Rafael de Cabo at the National Institute on Aging (NIA, Baltimore) and performed at the Animal Centre (Poolesville).

Initially, we performed a preliminary study in which we tried to determine the best and safest CNIO-PI3Ki dose for rhesus monkeys. Therefore, we monitored the response of 6 animals (3 females and 3 males) after intravenous administration with increasing concentrations of the compound, ranging from 0.2 to 2.1 mg/kg and calculated upon allometric scaling of the mouse dosing. We confirmed that 2.1 mg/kg CNIO-PI3Ki resulted in a detectable PI3Ki serum concentration of 400 ± 224 ng/ml 2 hours post-dosing (**Figure 26A**) that was comparable to the one achieved in mice 1-6 hours post oral administration and that was well tolerated, as it did not have any harmful effects on glycemia (**Figure 26B**) or heart rate (**Figure 26C**).

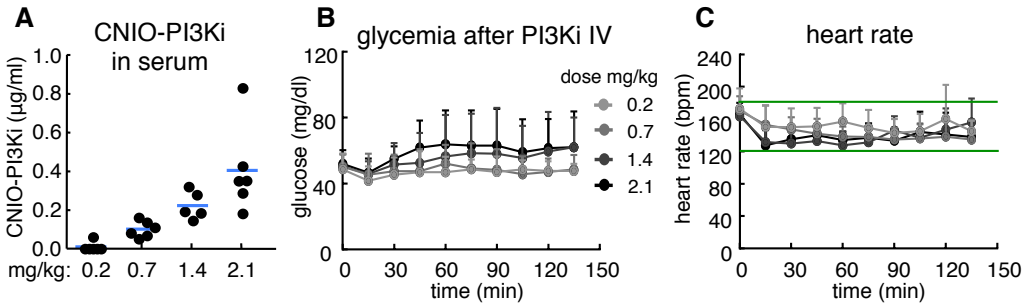

Figure 26. Preliminary dose-response study in rhesus monkeys.
(A) CNIO-PI3Ki concentration measured by mass spectrometry in serum of rhesus monkeys (n=5-6) 2h after i.v. injection of 0.2 mg/kg, 0.7 mg/kg, 1.4 mg/kg and 2.1 mg/kg CNIO-PI3Ki. Dots correspond to single individuals and blue lines to dose-specific averages. **(B)** Serum glucose values measured at specific intervals after i.v. administration of the indicated CNIO-PI3Ki doses. **(C)** Heart rate of monkeys i.v. injected with the indicated CNIO-PI3Ki doses; same colour code as (B).
All measurements performed throughout the preliminary dose-response study (n=5-6). No statistical significant differences were detected.

Once established that 2.1 mg/kg CNIO-PI3Ki was the highest and safest tolerated dose, a group of 19 naturally obese monkeys was selected for the study. Monkeys, aged between 12 to 27 years (18 ± 5.4 years) and considered naturally obese based on high body weight (11.8 ± 2.5 kg) and a body fat index ≥ 27% (Hansen et al., 2013), were randomized into control group (n=9; 5 females and 4 males) and CNIO-PI3Ki-treated group (n=10; 6 females and 4 males), and were followed during 12 weeks of treatment in a longitudinal study. Drug treatment consisted of a daily oral administration of 2.1 mg/kg CNIO-PI3Ki that led to PI3Ki serum levels of 35 ± 20 ng/ml (**Figure 27A**), around 2-fold lower than the observed in mice allowed to *ad libitum* access to 0.1 mg/ml in drinking water. During the whole assay, obese monkeys did not change their standard chow intake (**Figure 27B**) but received, however, a daily tasty treat that facilitated the dosing of the drug (control monkeys received the same treat without compound). Of note, the treat represents a 16% increase in total caloric intake (**Figure 27B).** Unfortunately, no differences were detected in total body weight in any of the two groups throughout the whole study (**Figure 27C**). Nevertheless, these additional calories from the diet resulted in a 4% trunk adiposity increase measured by DXA in the control group at the end of the 12-week experiment (**Figure 27D**). Interestingly, in contrast to the control group, CNIO-PI3Ki-treated macaques had maintained or even reduced their adiposity content (**Figure 27D**), leading to a significant 7% relative adiposity difference between both groups at the end of the 3 months treatment (**Figure 27D**).

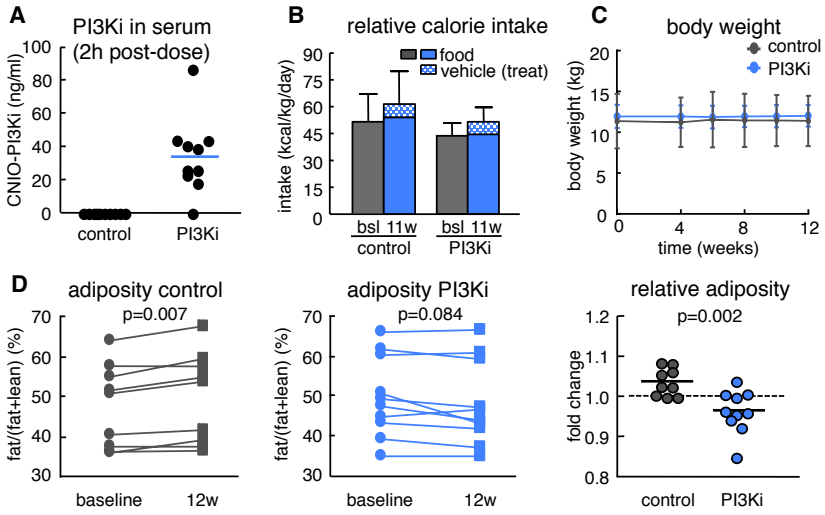

Figure 27. CNIO-PI3Ki reduces adiposity of obese rhesus monkeys.
(A) CNIO-PI3Ki concentration in serum of control (n=9) and drug-treated monkeys (n=10). Serum samples were collected 2 hours post oral administration of 2.1 mg/kg PI3Ki treatment and analyzed by mass spectrometry. Dots correspond to individual values and blue line to average. **(B)** Relative calorie intake of control (n=9) and CNIO-PI3Ki-treated (n=10) monkeys at baseline and again after 11 weeks of daily drug treatment. Values with or without vehicle (treat) are included. **(C)** Body weight of control and experimental rhesus monkeys treated with 2.1 mg/kg CNIO-PI3Ki after 4, 8 and 12 weeks treatment. Values correspond to average ± s.d. **(D)** Left, trunk adiposity evolution measured by DXA in control monkeys at baseline and after 12 weeks vehicle-treatment. Middle, progression of trunk adiposity in CNIO-PI3Ki-treated monkeys at baseline and after 12 weeks PI3Ki-treatment. Right, fold change trunk adiposity, calculated for each monkey as adiposity at week 12 relative to baseline adiposity. As a reference, dotted line represents mean adiposity at baseline.
Statistical significance was determined by the two-tailed Student's t test, except for (F), left and middle panel (longitudinal analysis) that was determined by the paired Student's t test: *p < 0.05, **p<0.01.

Metabolic and welfare parameters associated to respiration, pulse, blood pressure or temperature as well as complete blood biochemistry were measured before, during and after the trial. Importantly, a tendency towards decreased relative fasting glucose levels was observed in the CNIO-PI3Ki-treated monkeys compared to controls (**Figure 28A**). Whereas fasting glucose levels did not change after 10 weeks vehicle treatment compared to baseline in control monkeys (**Figure 28A**), CNIO-PI3Ki macaques showed significantly improved glucose levels after drug treatment (**Figure 28A**). Nevertheless, no changes were found in the intravenous glucose tolerance test (IVGTT) (**Figure 28B**), fasting insulin levels (**Figure 28C**) or in the insulin resistance index HOMA-IR (**Figure 28D**). Of note, CNIO-PI3Ki did not affect any of the other metabolic and blood chemistry parameters tested including temperature, heart rate, total proteins, ALT, bilirubin, creatinine, calcium, sodium, potassium, cholesterol, triglycerides, white and red blood cells, hemoglobin, hematocrit, MCV, MCH, lymphocytes and platelets, thereby indicating that the CNIO-PI3Ki is a safe treatment with no associated toxicities at the specified dose in monkeys.

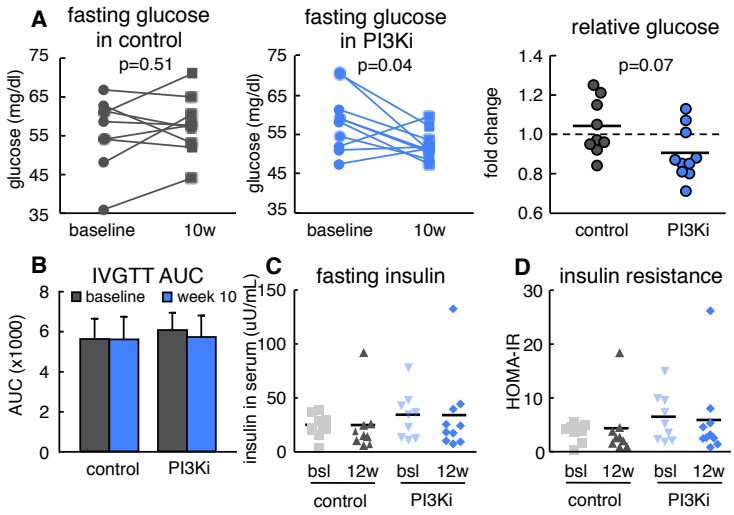

Figure 28. Effects of CNIO-PI3Ki on obese rhesus monkeys.
(A) Left, fasting glucose level evolution for each control monkey at baseline and after 10 weeks vehicle-treatment. Middle, progression of fasting glucose levels in CNIO-PI3Ki-treated monkeys at baseline and after 10 weeks PI3Ki-treatment. Right, fold change fasting glucose level for each monkey calculated as fasting glucose level at week 10 relative to baseline level. As a reference, dotted line represents mean fasting glucose level at baseline. **(B)** IVGTT performed at baseline and after 10 weeks vehicle (n=9) or 2.1 mg/kg CNIO-PI3Ki (n=10) treatment. Animals were administered glucose intravenously and blood samples collected at the indicated times. Bars represent the area under the curve (AUC) at baseline and after 10 weeks treatment (average ± s.d.). **(C)** Fasting insulin values measured at baseline and after 12 weeks vehicle or CNIO-PI3Ki treatment. **(D)** Insulin resistance, measured by the HOMA-IR index, at baseline and at the end of the treatment. In (C) and (D), dots correspond to individual values and black bar to average.
Statistical significance was determined by the two-tailed Student's t test except for (A), left and middle panel, that was determined by the paired Student's t test: *p < 0.05, **p<0.01.

In order to have a deeper look into possible genetic alterations induced by the treatment, liver, muscle and subcutaneous WAT (scWAT) biopsies taken at baseline and after 12 weeks treatment were used for gene expression analysis by Q-PCR. However, no overall significant differences could be established between CNIO-PI3Ki-treated macaques and controls: no changes were detected in markers of slow- (*Tnni1*) and fast- twitch fibers (*Myh2 and Myh4*) as well as in mitochondrial content in muscle (**Figure 29A**); no signs of altered gene expression was evident in the liver (**Figure 29B**); and, expression of markers of browning (*Ucp1, Prdm16* and *Pgc1α*) and immune related genes (*Emr1, CD68, CD11c* and *CD206*) remained stable in the white adipose tissue (**Figure 29C**). These results emphasize the fact that CNIO-PI3Ki treatment does not cause long-lasting changes, given that biopsies were performed ≈24 hours after the last CNIO-PI3Ki dosing, and thereby constitute another important safety aspect.

We conclude from this assay that CNIO-PI3Ki is able to reduce adiposity and may also decrease serum glucose levels in obese rhesus monkeys without any detectable toxic effects after 12 weeks of daily treatment.

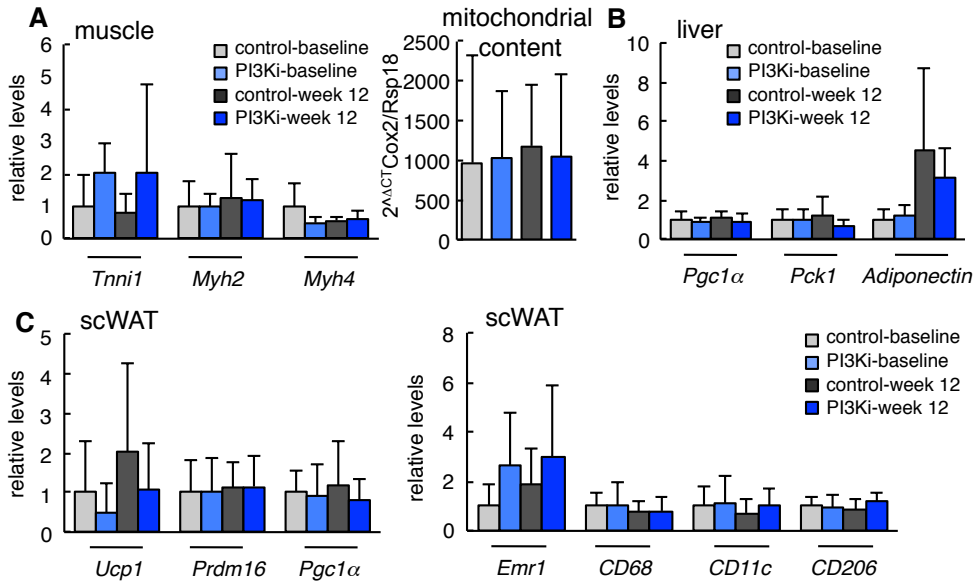

Figure 29. Effects of CNIO-PI3Ki on gene expression of obese rhesus monkeys.
(A) Left, relative mRNA levels in muscle of rhesus monkeys treated with or without the CNIO-PI3Ki at baseline (control n=4; PI3Ki n=7) and after 12 weeks (control n=6; PI3Ki n=7). Right, mitochondrial content in muscle of monkeys measured as *Cox2* expression relative to *Rsp18*. **(F)** Relative expression in liver of rhesus monkeys before (control n=5; PI3Ki n=10) and after 12 weeks (control n=8; PI3Ki n=6) treatment. **(G)** Relative mRNA levels of genes related to brown-adipocyte function (left) or inflammation (right), in subcutaneous WAT (scWAT) of rhesus monkeys at baseline (control n=7; PI3Ki n=8) and after 12 weeks (control n=8; PI3Ki n=8).
All mRNA levels were normalized with *Ipo8*. Values correspond to average ± s.d.
Statistical significance was determined by the two-tailed Student's t test:*p < 0.05, **p<0.01.

Altogether we conclude that the pharmacological inhibition of PI3K reduces body adiposity and some signs of the metabolic syndrome, such as hepatic steatosis and high fasting glucose levels, in obese mice and monkeys.

PART 2. ROLE OF THE TUMOUR SUPPRESSOR GENE p21 IN THE FASTING RESPONSE

For decades, dietary restriction has been known to protect against cancer and expand lifespan in a great variety of organisms including worms, flies and mice. Similarly, alternative fasting periods have been demonstrated to improve healthspan and delay ageing onset. The positive effects exerted by both, calorie restriction and alternative fasting periods, are thought to be partially mediated by the reduction of circulating insulin, Igf1 and cytokine levels which, among others, lead to decreased growth factor signalling and mTOR activity, improved mitochondrial function and decreased inflammation. Nevertheless, the underlying mechanisms are still poorly understood.

2.1 Characterization of fasting-induced *p21* upregulation

Previous reports have described that *p21* mRNA is induced in many tissues upon fasting through a mechanism that is independent of p53 and partly mediated by FOXO1 (Tinkum et al., 2013). Aiming to confirm and further explore the role of p21 in the fasting response, we decided to start by fasting WT mice for 48 hours and analyse the expression of a panel of different cell cycle inhibitors and tumour suppressor genes in the liver. Interestingly, only $p21^{Cip1}$ mRNA was strongly upregulated upon fasting whereas the expression of $p16^{Ink4a}$, $p19^{Arf}$, $p27^{Kip1}$, or *p53* remained unchanged (**Figure 30A**). Continuing our analysis, we detected induced *p21* levels upon fasting not only in liver, but also in a great variety of organs and tissues, such as the epididymal white adipose tissue (eWAT), brown adipose tissue (BAT), intestine, muscle, lung and spleen (**Figure 30B**). Confirming previous data (Tinkum et al., 2013), we also found that fasting-induced *p21* upregulation was independent of the $p19^{Arf}$/p53 pathway, as we found elevated *p21* mRNA levels in fasted $p19^{Arf}$ KO as well as in p53KO mice (**Figure 30C and 30D**). The sirtuin SIRT1 is involved in many responses to nutrient deprivation (Dominy et al., 2010), but, still, *p21* upregulation by fasting was not affected in Sirt1-heterozygous mice (**Figure 30D**). As a reference for comparison, the induction of *p21* mRNA in the liver was of higher magnitude (>10 fold) than that of *Pgc1α* (<5 fold) (**Figure 30D**).

Thus, we show that p21 is induced in several tissues upon fasting in a p53 independent manner.

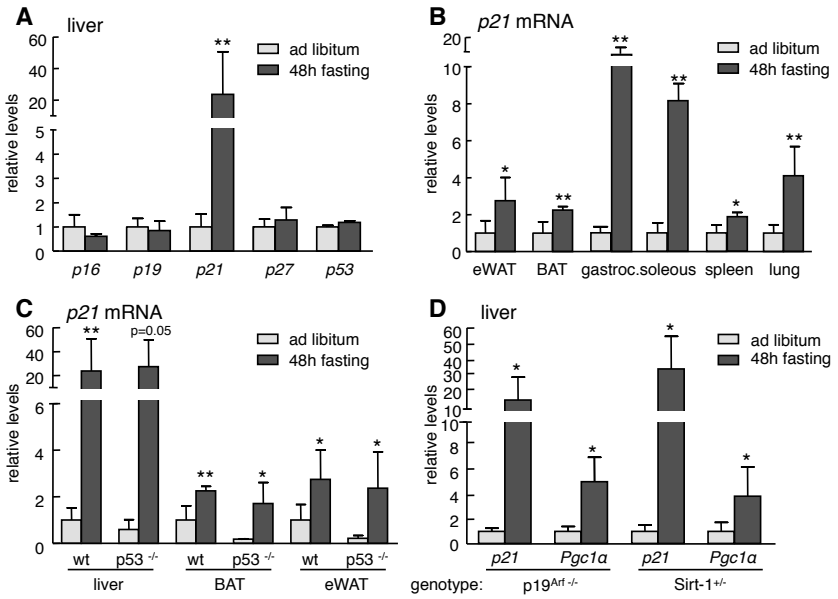

Figure 30. *p21* is highly induced after fasting. **(A)** Expression of the indicated tumour suppressors in the liver of 48 h fasted WT mice compared to *ad libitum*-fed mice. n=4, C57BL6 males, 12 weeks old. **(B)** Relative *p21* mRNA level in epididymal white adipose tissue (eWAT), brown adipose tissue (BAT), gastrocnemius, soleous, spleen and lung of 48 hours fasted mice compared to fed mice. **(C)** Relative *p21* mRNA level in liver, BAT and eWAT of *ad libitum* fed and 48 hours fasted WT and p53KO mice **(D)** Relative expression of *p21* and *Pgc1α* in the liver of 48 h fasted or *ad libitum* fed $p19^{ARF-/-}$ and SIRT-$1^{+/-}$ mice. n=4, 12 weeks old male. Data are expressed as mean ± s.d. mRNA levels are relative to *β-actin,* except for gastrocnemius and soleous that are relative to *Gapdh*. Statistical significance was determined by the two-tailed Student's t test: *p < 0.05, **p < 0.01.

The induction of *p21* by nutrient deprivation was also recapitulated in cultured cells. In particular, *p21* was significantly induced when human hepatocellular carcinoma HepG2 cells or mouse immortalized primary hepatocytes were starved in glucose- and serum-free medium for 24 hours (**Figure 31**). In general, nutrient deprivation, among many other effects, decreases PI3K activity and elevates cAMP, both being important for metabolic adaptation (Lempradl et al., 2015). To explore the contribution of these pathways to the upregulation of *p21*, cells were treated with a pharmacological inhibitor of PI3K or with forskolin, which is a compound that increases cAMP levels. Interestingly, forskolin, but not PI3K inhibition, further enhanced the upregulation of *p21* by nutrient deprivation in cells (**Figure 31**). This suggests that *p21* upregulation is positively regulated by PKA, and it is not further affected by PI3K inhibition.

Together, these observations reinforce the concept that $p21^{Cip1}$ is a sensor of nutrient deprivation both *in vivo* and *in vitro*.

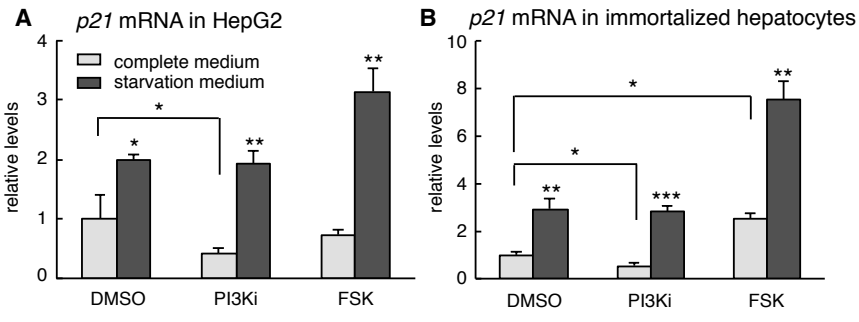

Figure 31. p21 is induced in cultured hepatocytes upon starvation. Relative *p21* expression in human hepatocellular carcinoma HepG2 cells (left) or primary large-T immortalized mouse hepatocytes (right) cultured for 24h in complete (DMEM + 10% FBS) or starvation medium (glucose free DMEM), and treated for 5 hours with DMSO, forskolin 10 μM or PI3Ki 10 μM. Experiment was performed twice with similar results and each time in triplicate. Data represent one experiment (n=3) and are expressed as mean ± s.d. mRNA levels are relative to *β-actin*. Statistical significance was determined by the two-tailed Student's t test: *p < 0.05, **p < 0.01, *** p < 0.001.

2.2 Impaired adaptation to prolonged fasting in p21^{Cip1} deficient mice

In order to address the role of p21 in the metabolic adaptation to fasting and test whether its induction upon fasting is of physiological significance, p21KO mice were starved for up to 48 hours.

Consistent with previous reports, we did not detect any obvious differences after 24 hours of fasting (Tinkum et al., 2013). However, after 48 hours fasting, p21 deficient mice presented dramatic differences compared to WT controls. From a behavioural point of view, p21KO mice were either extremely stressed or lethargic, even though their weight loss was comparable to that of WT mice (**Figure 32A**). Upon necropsy, we observed conserved white adipose tissue (WAT) and interscapular brown adipose tissue (BAT) in WT mice (**Figure 32B**), while p21KO mice had only remnants of WAT and BAT (**Figure 32B**). Additionally, histological analysis of eWAT and BAT sections confirmed a clear reduction in lipid droplet size in fasted p21 deficient mice compared to controls **(Figure 32C)**.

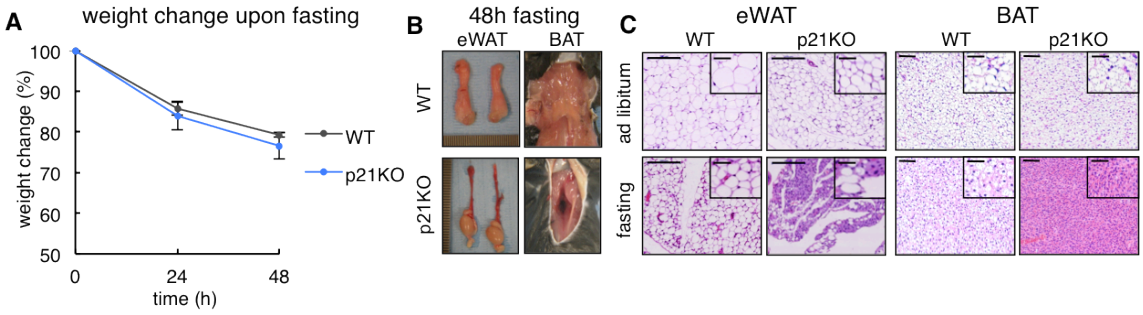

Figure 32. p21KO mice are unable to adapt to 48 hours fasting.
(A) Relative weight loss of 12 weeks old WT and p21KO mice after 24 and 48 hours fasting. **(B)** Representative pictures of epididymal white adipose tissue (eWAT) and interscapular brown adipose tissue (BAT) of WT and p21KO mice after 48 hours fasting. **(C)** Representative pictures of H&E-stained sections of eWAT and BAT of *ad libitum* fed or 48 hours fasted WT and p21KO mice. Bars correspond to 0.2 mm. High magnification insets correspond to 50 µm.

To further characterize the phenotype of 48 hours fasted p21KO mice, we continued by measuring a subset of parameters that highlighted their misadaptation to fasting. Mice deficient in p21 showed a dramatic drop in body temperature (rectal) that reached 25ºC upon fasting (**Figure 33A**). Moreover, a number of metabolic adaptations were significantly altered in fasted p21KO mice (**Figure 33B, 33C, 33D and 33E**). In particular, circulating serum free fatty acids (FFA), triglycerides (TG) and ketone bodies (KB) were strongly reduced compared to WT mice, which suggests that p21KO mice exhaust lipid stores prematurely compared to WT mice. Similarly, metabolic related hormones such as insulin, IGF1 and leptin were also significantly decreased in 48h fasted p21KO mice compared to controls, indicating a severe state of energy depletion. In contrast, no differences were detected in adiponectin serum levels. Serum glucose

levels were highly variable among fasted p21KO mice, as some individual p21KO mice had relatively high levels of glucose, which could reflect their profound decrease in insulin and IGF1 levels. Regarding serum amino acids, fasted p21KO mice presented significantly higher levels of phenylalanine, tyrosine, alanine, leucine and valine (**Figure 33E**), indicative of an enhanced proteolytic adaptation that may partially compensate for the loss of lipid stores.

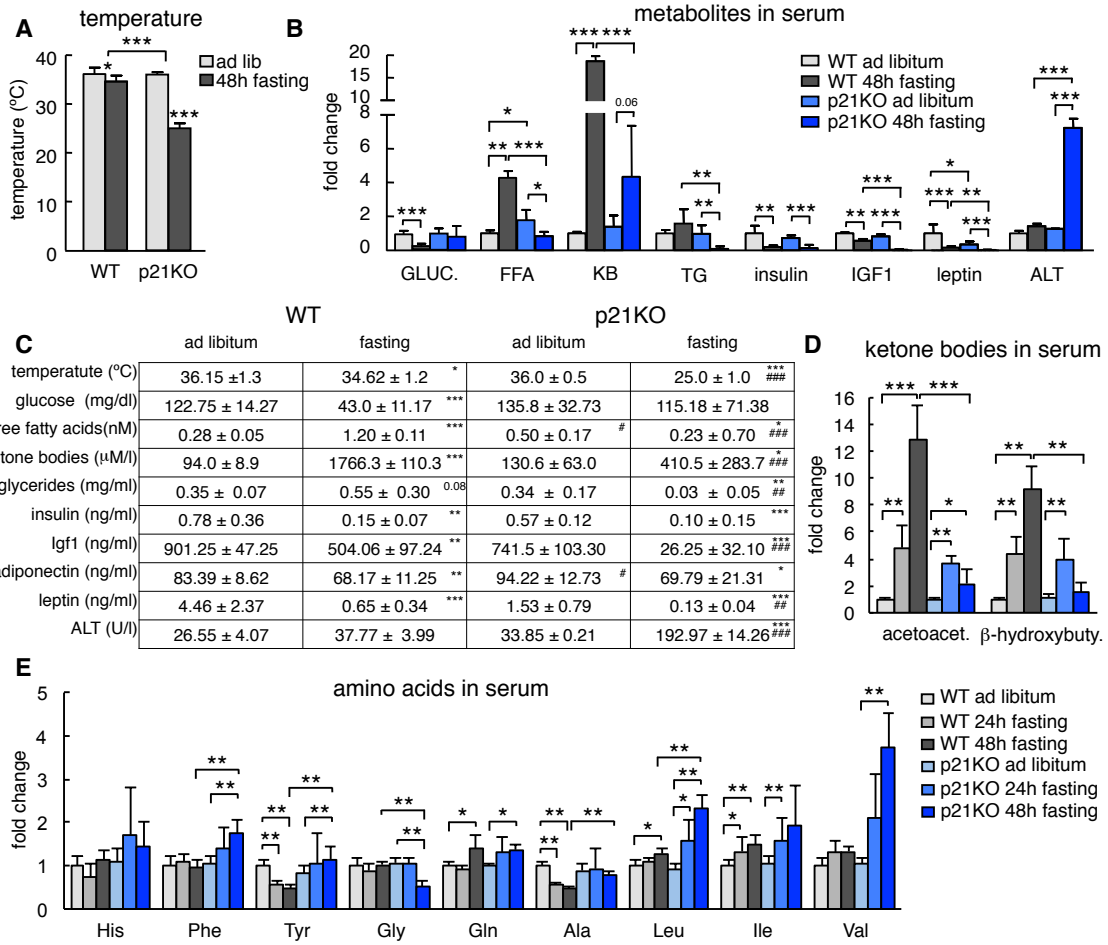

Figure 33. Altered metabolic profile in 48h fasted p21-deficient mice.
(A) Temperature of fed and 48 hours fasted WT and p21KO mice. Temperature was measured with a rectal thermometer. n=4-6 males, 12 weeks old. Values correspond to average ± s.d. **(B)** Relative glucose (GLUC.), free fatty acids (FFA), ketone bodies (KB), triglycerides (TG), insulin, IGF1, leptin and alanine aminotransferase (ALT) serum levels in WT and p21KO mice after 48 hours fasting or *ad libitum* feeding. Values correspond to average ± s.d **(C)** Temperature and level of the indicated metabolites in serum. *represents significant difference with *ad libitum* controls and # represents significant difference with WT controls **(D)** Relative level of ketones bodies (acetoacetate and β-hydroxybutyrate) and **(E)** of the indicated amino acids in the serum of WT and p21KO mice after *ad libitum* feeding, or after 24 hours or 48 hours fasting. Measurement performed by NMR. Values correspond to average ± s.d. n=4-5 male mice, 12 weeks old.
Data are expressed as mean ± s.d. Statistical significance was determined by the two-tailed Student's t test: *p < 0.05, **p < 0.01, ***p<0.001.

Finally, all the above alterations were accompanied by hepatic damage, as reflected, by increased serum alanine aminotransferase (ALT) levels (**Figure 33B**) and apoptosis measured

by active-caspase3 staining in the liver (**Figure 34A**). Of note, proliferation levels, measured by Ki67 immunohistochemistry, were moderately, but significantly, higher in 48 hours fasted p21KO livers compared to WT controls (**Figure 34B**).

Altogether, these data demonstrate that in the absence of p21, nutrient and energy stores are prematurely exhausted upon fasting. They also support a relevant role for p21 in the adaptation to nutrient starvation, as p21KO mice are unable to efficiently adapt to prolonged fasting periods of 48 hours.

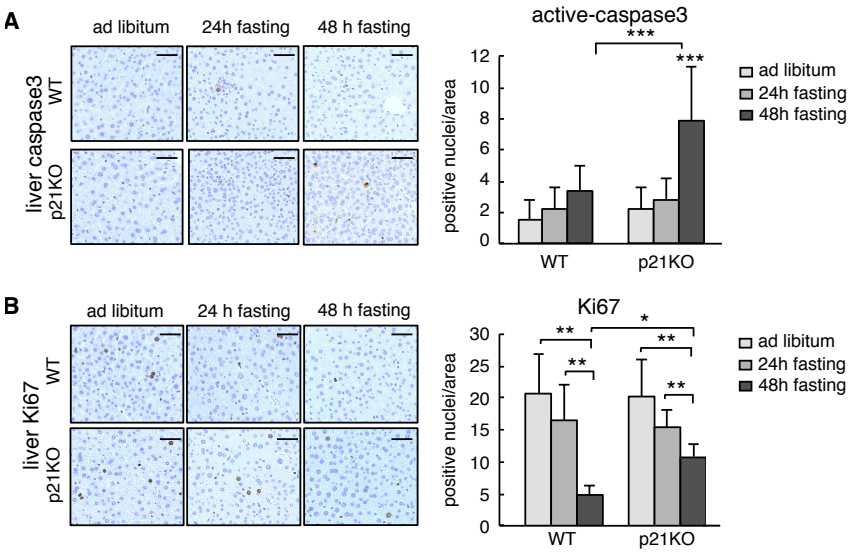

Figure 34. Increased apoptosis in the liver of fasted 21KO mice. **(A)** Left, representative pictures of active caspase-3 stained liver sections of WT and p21KO mice under feeding conditions, and after 24 hours or 48 hours fasting. Bars correspond to 25 μm. Right, quantification of positive active-caspase 3 nuclei per area. **(B)** Left, representative pictures of Ki67 stained liver sections of WT and p21KO mice under feeding conditions, and after 24 or 48 hours fasting. Bars correspond to 25 μm. Right, quantification of positive Ki67 nuclei per area. In (A) and (B) 10-15 similar areas were selected per animal in a total of 3 representative mice per group. Values correspond to average ± s.d. Statistical significance was determined by the two-tailed Student's t test: *p < 0.05, **p < 0.01, ***p<0.001.

2.3 Enhanced energy expenditure and activity in p21KO mice during fasting

All the previous observations suggest that p21KO mice suffer a premature exhaustion of energetic reserves during fasting.

To directly evaluate this, we measured energy expenditure (EE), performing indirect calorimetry, in WT and p21KO mice during 48 hours of fasting as well as under standard feeding conditions (**Figure 35A**). Of note, p21KO mice presented higher EE levels during the first dark and second light fasting periods, resulting in an overall increased EE during the total fasting period. In contrast, no significant differences in EE were observed under normal *ad libitum* feeding conditions (**Figure 35B**).

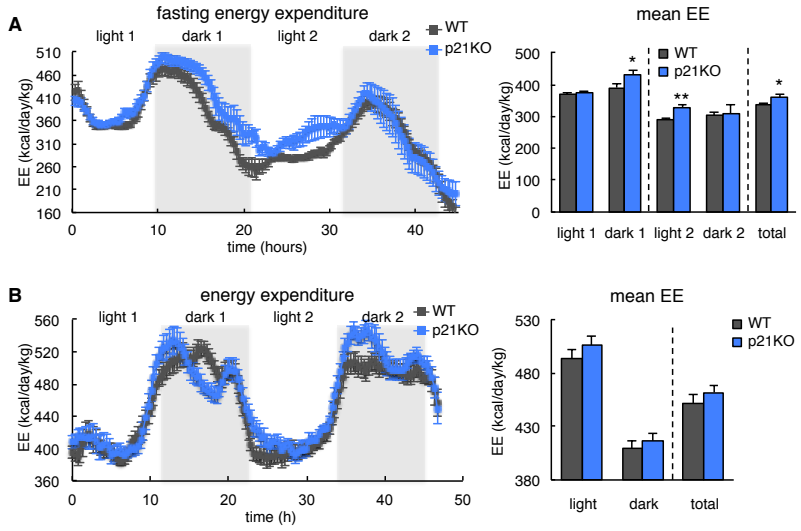

Figure 35. Enhanced energy expenditure in p21KO mice during fasting.
(A) Left, energy expenditure (EE) of WT and p21KO mice during 48 hours of fasting. Right, mean EE of WT and p21KO at the indicated period during fasting. **(B)** Left, Energy Expenditure (EE) of WT and p21KO mice *under ad libitum* feeding conditions. Right, mean EE of WT and p21KO at the indicated period. n=8 C57BL6 males, 12 weeks old. Data are expressed as mean ± s.e.m.
Statistical significance was determined by the two-tailed Student's t test: *p < 0.05, **p < 0.01.

Fasting induces stress and behavioural changes that reflect in elevated locomotor activity (Chen et al., 2005). Interestingly, p21KO mice showed a significant increase in activity during the entire 48 hours of fasting (**Figure 36A**), while no significant differences could be established under feeding conditions (**Figure 36B**).

Together, we conclude that in the absence of p21, mice do not adapt efficiently to energy deprivation and nutrient stores are prematurely exhausted.

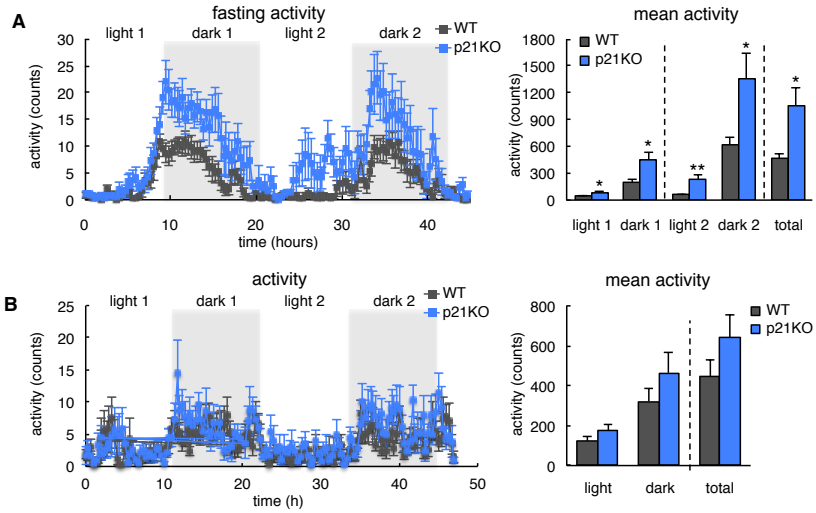

Figure 36. Enhanced activity in p21KO mice during fasting.
(A) Left, activity of WT and p21KO mice during 48 hours of fasting. Right, mean activity of WT and p21KO at the indicated period during fasting. **(B)** Left, activity of WT and p21KO mice under *ad libitum* feeding conditions. Right, mean activity of WT and p21KO at the indicated period. n=8 C57BL6 males, 12 weeks old. Data are expressed as mean ± s.e.m. Statistical significance was determined by the two-tailed Student's t test: *p < 0.05, **p < 0.01.

2.4 Global transcriptome changes in p21^{Cip1} deficient mice

Aiming to gain insight into the mechanisms responsible for the defective adaptation of p21KO mice to prolonged fasting, we obtained the liver RNA-seq profiles of WT and p21KO mice under standard feeding conditions and after 24 hours fasting (n=2-3 per condition and genotype). We chose 24 hours of fasting to capture early defects in p21KO mice, prior to the severe phenotype observed at 48 hours.

A total of 451 genes (128 UP and 323 DOWN) were differentially expressed (FDR q< 0.05) between p21KO and WT livers after 24 hours fasting; 96 of these genes (8 UP and 88 DOWN) were already differentially expressed under *ad libitum* feeding conditions (**Figure 37A and Supplementary Figure S1**). Gene-set enrichment analysis (GSEA) of KEGG pathways indicated a reduced number of altered pathways in p21KO livers compared to WT under *ad libitum* feeding conditions (**Figure 37B**). In contrast, fasted p21KO livers presented a great number of downregulated pathways, mostly related to inflammation and metabolism, compared to controls (**Figure 37B and Supplementary Figure S2**). Of note, no upregulated pathway was found in the liver of fasted p21KO mice.

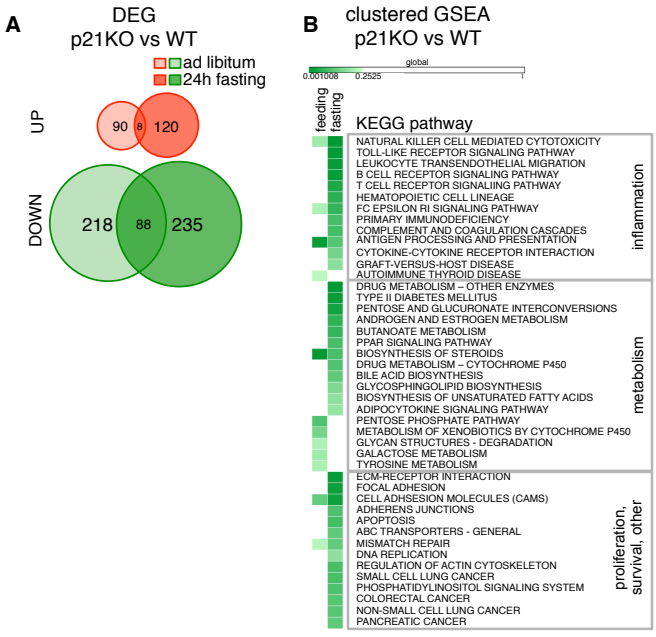

Figure 37. Global transcription changes in p21^{Cip1} deficient mice. **(A)** Venn diagram of differentially expressed genes (DEG) in the liver of p21KO compared to WT mice under *ad libitum* feeding conditions and upon 24 hours fasting. Data were obtained from RNA-seq analysis of 2-3 male mice per group. Red circles correspond to upregulated and green circles to downregulated genes. Values were considered significant when FRD value was q<0.05. **(B)** Heat map of significantly altered pathways (KEGG) in the liver of p21KO mice compared to WT controls under feeding conditions or upon 24 hours fasting. Results were considered significant when FDR<0.25.

2.5 Decreased immune response in 24 hours fasted p21 deficient mice

One of the major consequences of starvation and dietary restriction is a general decrease in the number of infiltrating leukocytes and markers of inflammation (Mitchell et al., 2010; Robertson and Mitchell, 2013; Sokolović et al., 2013). The reduction in gene sets related to immune function and inflammation observed in 24 h fasted p21KO mice (**Figure 38A**) suggests that the

effects of fasting appear prematurely in p21KO mice compared to WT controls. We supported the GSEA data by first confirming a general reduction in the mRNA levels of genes related to the immune system in the liver of p21KO fasted mice compared to controls (**Figure 38B**).

Moreover, this was further substantiated by quantifying infiltrating leukocytes (CD45+ cells) in the liver, which showed a significant reduction in fasted p21KO livers compared to fasted WT controls (**Figure 38C**). Consequently, this was translated into a reduction of all the analysed immune system populations, without affecting their relative distribution within the tissue (**Figure 38D**). Finally, F4/80 staining revealed reduced macrophage infiltration in the liver of p21KO fasted mice compared to controls (**Figure 38E**).

We interpret this reduction in leukocyte population and transcriptional level of markers related to immune function as indicative of the accelerated physiological effects of fasting in p21KO mice.

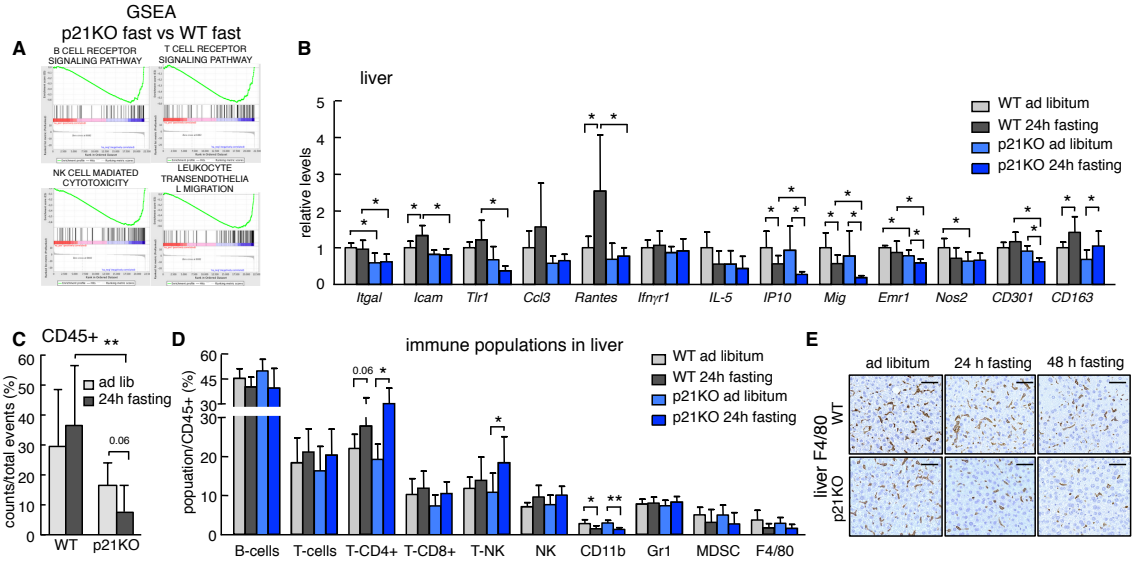

Figure 38. Decreased immune response in fasted p21KO mice.
(A) Representative GSEA plots of immune-related pathways downregulated in 24 hours fasted p21KO mice compared to 24 hours fasted controls. FDR<0.25 **(B)** Relative expression of the indicated genes related to inflammation in the liver of WT and p21KO mice under *ad libitum* feeding conditions or 24 hours fasting. mRNA levels were normalized to *β-actin*. n=6, C57BL6 males, 12 weeks old. **(C)** CD45+ immune cells relative to total events and **(D)** percentage of the indicated immune cell populations relative to CD45+ leukocytes in the liver of *ad libitum* fed or 24 hours fasted WT and p21KO mice. n=6 males, 12-16 weeks. **(E)** Representative pictures of F4/80 stained liver sections of WT and p21KO mice under feeding conditions, 24 hours and 48 hours fasting. Bars correspond to 50 μm.
Values correspond to average ± s.d. Statistical significance was determined by the two-tailed Student's t test: *p < 0.05, **p < 0.01.

2.6 Decreased PPARα activity in the liver of p21KO mice

We took note of the fact that "PPAR signalling" was one of the pathways downregulated in fasted p21KO mice compared to WT mice (**Figure 39A**). PPARα is a critical hepatic

transcription factor activated by fatty acids in response to nutrient deprivation that plays a key role in promoting fatty acid β-oxidation and ketogenesis. Notably, PPARα is required for the adaptation to fasting as shown in PPARα-KO mice (Kersten et al., 1999; Leone et al., 1999).

We first validated RNA-seq data by directly measuring the mRNA of *PPARα*, *-γ* and *-δ* isoforms together with some well-established PPARα transcriptional targets in the liver of fed and fasted p21KO and WT mice. Interestingly, PPARγ and some of the PPARα target genes such as *Cd36*, *Abcd2, Saa3*, *Gyk*, *Acot1* and *Acot3* were significantly downregulated in 24h fasted p21KO livers (**Figure 39B**). One of the main characteristics of PPARα-KO mice is the accumulation of fatty acids in the liver upon fasting due to their inability to undergo ketogenesis (Kersten et al., 1999; Leone et al., 1999). Even though we could not establish significant differences after 24 or 28 hours fasting, we were able to observe a tendency towards increased FFAs in the liver of p21KO mice compared to controls after 48 hours fasting (**Figure 39C**).

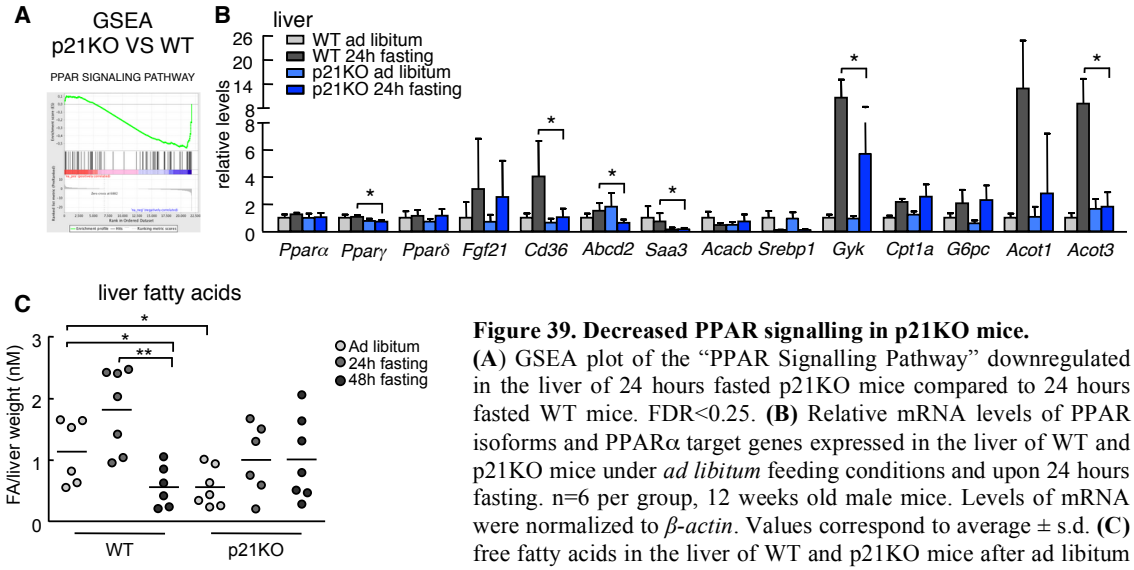

Figure 39. Decreased PPAR signalling in p21KO mice.
(A) GSEA plot of the "PPAR Signalling Pathway" downregulated in the liver of 24 hours fasted p21KO mice compared to 24 hours fasted WT mice. FDR<0.25. **(B)** Relative mRNA levels of PPAR isoforms and PPARα target genes expressed in the liver of WT and p21KO mice under *ad libitum* feeding conditions and upon 24 hours fasting. n=6 per group, 12 weeks old male mice. Levels of mRNA were normalized to *β-actin*. Values correspond to average ± s.d. **(C)** free fatty acids in the liver of WT and p21KO mice after ad libitum feeding, 24 and 48 hours fasting. n=6-7 male mice, 12 weeks old. Statistical significance was determined by the two-tailed Student's t test: *p < 0.05, **p<0.01, ***p<0.001. Only significant differences between WT and p21KO fasted samples are represented.

To explore a possible mechanistic link between p21 and PPARα, we first tested if p21 plays a cell-autonomous role in hepatocytes upon nutrient deprivation. Interestingly, after 48 hours of serum and glucose starvation, cultured immortalized p21KO primary hepatocytes underwent massive cell death, whereas WT control hepatocytes remained largely viable (**Figure 40A**). Afterwards, we compared the induction of PPARα target genes in WT and p21KO hepatocytes. Remarkably, the induction of PPARα targets after 24 hours nutrient starvation (**Figure 40B)** or with PPARα agonist WY-14,643 treatment (**Figure 40C**) was completely blunted or significantly reduced in p21KO hepatocytes. These data indicate that p21 is an important positive regulator of PPARα.

Altogether, our data demonstrate that p21 is a fasting-induced factor necessary for the efficient adaptation to fasting. Mice deficient in p21 present severe adaptational abnormalities to fasting including premature energy exhaustion, and molecular analysis indicate that p21 is a positive regulator of the activity of PPARα, a master regulator of fasting adaptation.

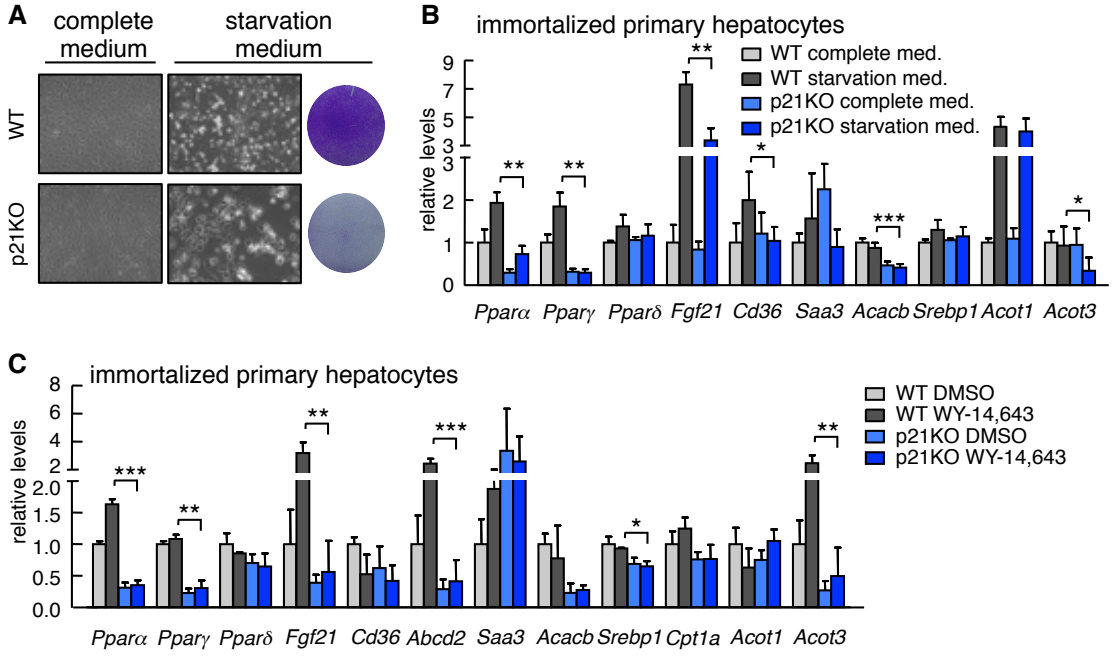

Figure 40. Decreased PPARα activity in p21KO mice.
(A) Left panel, representative pictures of WT and p21KO large-T immortalized primary hepatocytes cultured for 48 hours in complete medium (DMEM + 10% FBS) or starvation medium (glucose-free DMEM). Right, representative pictures of WT and p21KO immortalized primary hepatocytes stained with crystal violet after 48 hours culturing in starvation medium. Experiment was repeated three times in triplicate. **(B)** Relative mRNA levels of PPARα target genes expressed in WT and p21KO immortalized primary hepatocytes after culturing in complete (DMEM + 10% FBS) or starvation medium (glucose-free DMEM) for 24 hours. Experiment was performed twice with similar results in duplicate or triplicate. n=5-6. **(C)** Relative expression of PPARα target genes in WT and p21KO immortalized primary hepatocytes cultured in complete medium and treated with DMSO or 10 μM of the PPARα agonist WY-14,643 for 24 hours. Experiment was performed twice in triplicate with similar results. One experiment is represented, n=3. mRNA levels were normalized to *β-actin*. Values correspond to average ± s.d.
Statistical significance was determined by the two-tailed Student's t test: *p < 0.05, **p<0.01, ***p<0.001. Only significant differences between WT and p21KO samples are represented.

2.7 Fasting induces senescence in combination with a low oncogenic stress

Activated oncogenes induce compensatory tumour-suppressive mechanisms, such as cellular senescence and apoptosis. In particular, senescence leads to a persistent growth arrest that is principally characterized by a complex pro-inflammatory response, known as senescence-associated secretory phenotype (SASP); the activation of the CDKN2A locus, which encodes p16 and ARF; and the activation of the p53-pathway, together with the induction of p15, p21, p27 and Rb (Campisi and d'Adda di Fagagna, 2007; Collado et al., 2007; Muñoz-Espín and Serrano, 2014).

Importantly, oncogene-induced senescence has been shown to diminish cancer development *in vivo* by inducing a stable growth arrest (Collado et al., 2005; Michaloglou et al., 2005). Initially, it was thought that cells could only undergo senescence under high oncogenic stress conditions. However, a low oncogenic stress in combination with CDK2 (Campaner et al., 2010) or CDK4 (Puyol et al., 2010) deletion can also induce a full senescence response. Given the fact that fasting greatly upregulates *p21* levels, and, consequently, inhibits CDK2 activity, we hypothesized that fasting could also induce a senescence response in the context of low oncogenic stress.

Therefore, we decided to fast Eμ-Myc mice for 48 hours at 10 weeks of age, when moderate oncogenic c-Myc activity is present and mice do not exhibit yet signs of lymphoma or other associated malignancies (pre-tumoural stage). Interestingly, senescence associated-β galactosidase (SA-β gal) staining revealed positively stained areas in the pre-tumoural spleen of 48h fasted Eμ-Myc mice, but not in fed Eμ-Myc mice (**Figure 41A**). However, the degree of senescence was highly variable between individuals. Quantification of SA-β gal positive areas allowed us to distinguish highly, medium and low senescent spleens. In contrast, standard fed Eμ-Myc or WT littermate controls barely presented any SA-β gal staining (**Figure 41A**). Besides SA-β gal activity, senescent cells present important gene expression alterations. In particular, we confirmed induced expression of the senescence markers *p16*, *p19* and *p21* in fasted Eμ-Myc spleens compared to controls (**Figure 41B**), which further supports a senescence response. Remarkably, higher *p16*, *p19* and *p21* mRNA levels positively correlate with high SA-β gal staining.

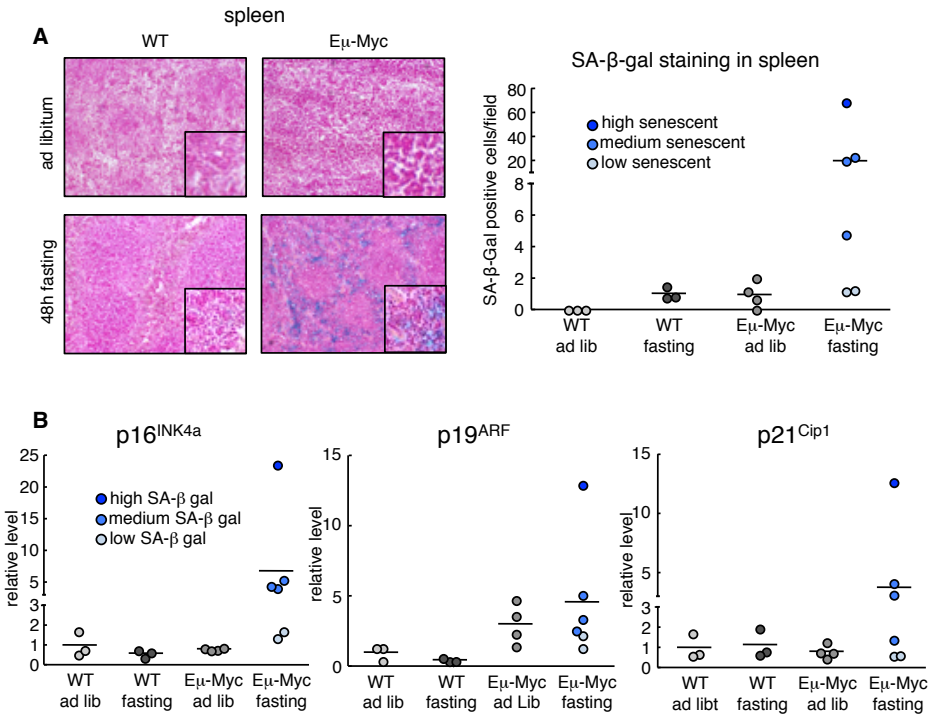

Figure 41. Fasting-induced senescence in pre-tumoural Eμ-Myc spleens.
(A) Left, SA-β Gal staining in spleen OCT sections of *ad libitum* fed or 48 hours fasted WT and Eμ-Myc mice at 10 weeks of age. Right, quantification of positive SA-β Gal cells per field. 10-15 similar areas were selected per animal. According to the number of positive cells, animals were divided into high, medium and low senescent. Picture of fasted Eμ-Myc spleen corresponds to a high senescent case. **(B)** Relative expression of $p16^{INK4A}$, $p19^{ARF}$ and $p21^{Cip1}$ in the spleen of *ad libitum* fed or 48h fasted WT and Eμ-Myc mice. Mice were adjudged to high, medium and low SA-βGal positive staining. mRNA levels were normalized to *β-actin*. Dots correspond to individual mice and black line to averages. In (A) and (B) n=3-6 male mice, 10 weeks old, mixed background.

Senescence is a tumour-suppressive response that prevents the proliferation of cancerous cells by inducing a stable cell cycle arrest. Therefore, we next wanted to address if the observed fasting-induced senescence response would be translated into an improved tumour-free survival of Eμ-Myc mice. Unfortunately, a single 48 hours fasting period at 10 weeks of age did not significantly affect overall survival of fasted Eμ-Myc mice compared to controls (**Figure 42A**). Nevertheless, we observed a non-significant trend towards extended maximal survival that suggests that repeated fasting periods could possibly delay tumorigenesis (**Figure 42B**).

Figure 42. Survival of Eμ-Myc mice upon 48h fasting.
(A) *Kaplan-Meier* survival curve of control Eμ-Myc mice or Eμ-Myc mice fasted for 48 hours at 10 weeks of age. n=11-13, males. Statistical significance was determined by the log-rank (Mantel Cox) test. **(B)** Maximal survival of control or 48h fasted (at the age of 10 w) Eμ-Myc mice. Values correspond to average ± s.d. n=11-13, males. Statistical significance was determined by the two-tailed Student's t test.

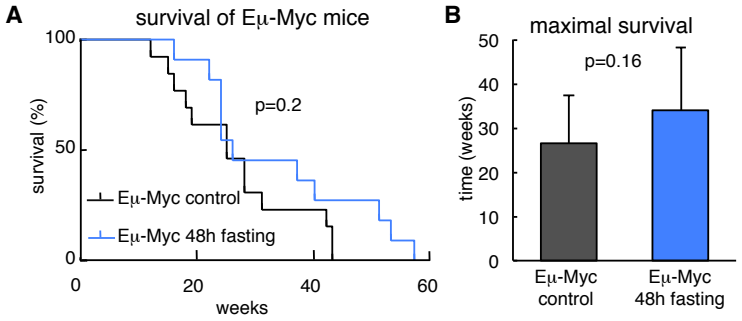

Altogether, these results show that, in the context of a low oncogenic stress, fasting is able to promote senescence in the pre-tumoural spleen of Eμ-Myc mice.

DISCUSSION

PART1. EFFECT OF PHARMACOLOGICAL PI3K INHIBITION ON METABOLIC SYNDROME AND OBESITY

The PI3K/AKT signalling pathway is one of the main regulators of proliferation, growth, survival and metabolism. In particular, PI3K activity has been shown to play an important role in insulin sensitivity and glucose homeostasis (Carracedo and Pandolfi, 2008) and PI3K downregulation, either by genetic PTEN overexpression or treatment with a synthetic PI3K inhibitor (CNIO-PI3Ki), enhances energy expenditure and thermogenesis (Ortega-Molina et al., 2012). Importantly, boosting energy expenditure is considered a promising therapeutic strategy to fight obesity; an increasing public health problem and a major risk factor for the development of type II diabetes and metabolic syndrome, as well as of cancer and cardiovascular diseases (Haslam and James, 2005). Despite great efforts to develop efficient and safe anti-obesity drugs, there are currently a reduced number of pharmacological treatments available, as most of them show limited efficacy or have been withdrawn from the market due to substantial adverse side effects that included cardiovascular effects, central nervous system toxicity, hypertension, memory impairment and psychiatric effects (Giordano et al., 2016). Therefore, it is of great importance to develop new therapeutic options. Numerous independent studies have reported the beneficial effects of PI3K signalling pathway downregulation, including PTEN upregulation (Garcia-Cao et al., 2012; Ortega-Molina et al., 2012), deletion of single PI3K isoforms (Becattini et al., 2011; Chattopadhyay et al., 2011; Foukas et al., 2013) and deletion of the PI3K-downstream substrate AKT1 (Wan et al., 2012). Based on these evidences, we hypothesized that the pharmacological inhibition of PI3K could be an effective treatment against obesity and the metabolic syndrome.

1.1 PI3K inhibitors as anti-obesity treatment in obese mice

As a first step to assess the possible use of PI3K inhibitors in the treatment against obesity, we began by determining whether the pharmacological inhibition of PI3K produced evident changes *in vivo*. Given the relevant role of PI3K in insulin signal transduction and glucose homeostasis, we decided to evaluate the effects of a single oral dose of PI3K inhibitor treatment. We therefore measured the acute effects of CNIO-PI3Ki treatment on fasting glycemia, initially. As expected, oral CNIO-PI3Ki administration (15 mg/kg) resulted in a high, but transient, serum glucose peak that was maintained within physiological ranges and that was comparable to a normal post-prandial glycemia. Importantly, this glucose peak was rapidly reversed 6 hours post-PI3Ki administration, reflecting a quick glucose homeostasis recovery. Supporting this fast homeostatic readjustment, CNIO-PI3Ki administration led to detectable serum drug levels only

1 to 6 hours after dosing, being completely eliminated after 24 hours. As a consequence of the inhibition of PI3K, we detected reduced AKT and FOXO1 phosphorylation in the liver and BAT of treated mice. The liver is responsible for the production of glucose during fasting through the transcriptional activation of genes involved in gluconeogenesis upon PI3K/AKT downregulation and consequent FOXO activity. Indeed, after PI3Ki treatment, we observed elevated expression of the gluconeogenic gene *G6Pc* in the liver of treated mice. In turn, the adipose tissue is another relevant target of PI3K inhibition (Ortega-Molina et al., 2012) and, accordingly, CNIO-PI3Ki and GDC-0941 treatment led to enhanced expression of UCP1, both at a protein level in the BAT and at a transcriptional level in white adipose depots. Together, this suggests an increased thermogenic activity in the BAT as well as in the brown adipocytes (known as brite or beige adipocytes) interspersed within the WAT (Wu et al., 2013). Thus, pharmacological PI3K inhibition produces a transient glycemic peak, within physiological range, together with increased UCP1 expression.

In order to test the anti-obesity capacity of pharmacological PI3K inhibition, we have compared in parallel the activity of two PI3K inhibitors, CNIO-PI3Ki (developed at the CNIO) and GDC-0941, in diet-induced obese mice. Both PI3K inhibitors are highly specific class IA PI3Ks p110α and p110δ inhibitors, show similar inhibitory capacity *in vitro*, and do not cross the blood-brain barrier (Ortega-Molina et al., 2012; Workman et al., 2010). Additionally, we have demonstrated that they do not affect the arcuate nucleus of the hypothalamus; a master regulator of metabolism that is exposed to peripheral circulation and releases, among others, important orexigenic and anorexigenic hormones (Sohn et al., 2013; Yeo and Heisler, 2012). The lack of hypothalamic effects of these PI3K inhibitors constitutes a relevant safety feature to take into account for a future anti-obesity use. Importantly, treatment with both PI3K inhibitors reduced the weight of obese mice in a short period of 10 days, despite maintaining their high-fat food intake constant. Even though the weight loss of mice happened in a dose-depend manner, it is worth mentioning that GDC-0941 treatment had to be administered at a higher dose (75 mg/kg) than CNIO-PI3Ki (10 mg/kg) to achieve similar results. Notably, the reduction in body weight was entirely due to the loss of adiposity, without affecting lean mass content. This was particularly striking in the pericardial fat, as well as reflected by a reduction in liver steatosis. Moreover, in the case of the highest dose of CNIO-PI3Ki (15 mg/kg), there were evident browning areas in the epididymal, pericardial, and perirenal fat depots.

To simulate a hypothetical clinical application, we tested the effects of long-term treatment with a low dose of CNIO-PI3Ki administered through the drinking water that resulted in 40-fold lower serum drug levels compared to the peak of drug achieved 1-6 hours post-oral gavage. Nonetheless, the daily accumulative dose of the drug was calculated for 10 mg/kg, which is sufficient to partially inhibit the pathway. As expected, dietary-induced obese mice

treated with CNIO-PI3Ki through the drinking water lost weight while maintaining their average high-fat food intake unaltered. Notably, this weight loss happened in a progressive manner and only during a period of 50 days. Afterwards, treated mice stabilized their body weight at a set point 20% below non-treated obese mice and as long as the treatment was administered. This effect can be explained by the fact that mice under chronic CNIO-PI3Ki treatment present enhanced energy expenditure, which may lead to a resetting of energy balance at a lower body weight. The long-lasting stability of this new energetic balance also suggests that chronic PI3Ki treatment does not elicit compensatory changes to defend body weight, nor causes drug resistance. The body weight loss was due to a reduction in adiposity, as lean mass content remained stable throughout the entire treatment. Together, these are desirable features for an anti-obesity treatment in humans because a slow, progressive and controlled weight loss would allow better medical supervision.

Long-term treatment with CNIO-PI3Ki produced a range of beneficial effects beyond body weight and adiposity loss. In particular, the liver of treated mice presented decreased steatosis and reduced hepatic damage measured by serum ALT levels. Also, expression of the pro-inflammatory cytokine *Il6* in the liver as well as the infiltration of macrophages and expression of inflammation-related genes in the eWAT was reduced in treated mice, thereby confirming a decrease in obesity-associated inflammation. In contrast to the previous short-term, high-dose assay, and despite reduced adipocyte size and fat accumulation, we could not observe browning areas in the WAT of low-dose treated mice. To explain this difference we could argue that either the browning of the WAT or the induction of UCP1 are below detection level; that the activation of UCP1 may be happening in a transient manner; or that the administered dose is too low to have a detectable impact on UCP1 expression. While glucose homeostasis and insulin resistance did not improve after 2.5 months treatment, mice treated for 5 months showed normalized serum fasting glucose levels. We reason that dealing with extremely insulin resistant mice after 8 months under continuous high-fat feeding, 2.5 months treatment may not be sufficient to improve glucose homeostasis. In general, these data demonstrate that long-term CNIO-PI3Ki treatment improves some of the symptoms associated with the metabolic syndrome such as fat accumulation and hyperglycemia.

Interestingly, the effects of CNIO-PI3Ki on body weight were reversible upon withdrawal of the treatment, as mice rapidly readjusted their body weight to the same level as control high-fat fed mice in the absence of drug. This reversibility indicates that long-term exposure to CNIO-PI3Ki does not cause irreversible metabolic alterations that may compromise tissue functioning. In line with this, we did not detect any evidence of toxic effects in mice even after 5 months of continuous treatment with CNIO-PI3Ki.

Besides reducing body weight and adiposity in obese high-fat fed mice, CNIO-PI3Ki treatment was also effective in hyperphagic, standard-diet fed ob/ob mice, suggesting that the treatment is active against obesity produced by nutritional overload, independently of the fat content of the diet. In contrast, CNIO-PI3Ki treatment did not have any effect on healthy, lean mice under standard diet. Nevertheless, when healthy lean mice were put *de novo* on a high-fat diet, CNIO-PI3Ki treatment significantly delayed body weight gain as well as glucose intolerance onset, indicating that the treatment is effective as soon as high-fat food is present, even without a pre-existing context of obesity or high-fat food intake. It is well known that in response to overnutrition, the WAT can expand via both an increase in adipocyte size (hypertrophy) and adipocyte number (hyperplasia), thereby leading to obesity (Steinberg et al., 1962; Peckham et al., 1962). Importantly, newly published reports demonstrate that *de novo* adult adipogenesis (only in the visceral eWAT) and adipocyte hypertrophy (in both, visceral eWAT and subcutaneous iWAT) induced by high-fat diet depends on PI3K/AKT2 activity (Jeffery et al., 2015). This is consistent with our data and suggests that PI3K inhibition may be limiting both processes, and thereby delaying obesity onset. Altogether, these scenarios (efficacy on ob/ob mice, lack of effect on mice with standard diet, and efficacy upon *de novo* high-fat feeding) point to nutritional overload as a key requisite for the anti-obesity activity of PI3K inhibition. This constitutes another important and attractive safety feature for a hypothetical use in humans because PI3Ki would presumably be effective only on people under nutritional overload, but not on lean people with an energetically balanced diet.

In summary, we have demonstrated that CNIO-PI3Ki treatment is an efficient and safe anti-obesity intervention in obese mice that improves some of the signs of the metabolic syndrome such as adiposity and hyperglycemia, and reduces obesity-associated symptoms including liver steatosis and inflammation.

1.2 p110α in the regulation of energy homeostasis

CNIO-PI3Ki is a specific class IA PI3Kα (catalytic subunit p110α) and PI3Kδ (catalytic subunit p110δ) inhibitor that induces *Ucp1* expression and thermogenesis *in vivo*, as well as in cultured brown adipocytes (Ortega-Molina et al., 2012). Whereas p110α is ubiquitously expressed, p110δ is principally expressed in leukocytes and plays a key role in antigen receptor and cytokine-mediated B and T cell development, differentiation and function (Hawkins and Stephens, 2015). Reinforcing the idea that p110α, but not p110δ, is the key mediator of the metabolic responses of PI3K (Foukas et al., 2013; Vanhaesebroeck et al., 2010), we first confirmed that p110α downregulation in brown adipocytes led to significantly increased levels of the thermogenic-related genes *Ucp1* and *Pgc1α* compared to controls upon forskolin

stimulation. In contrast, p110β and p110δ downregulation did not elicit transcriptional changes in thermogenic genes, further supporting a specific role of PI3Kα in the regulation of thermogenesis.

Additionally, we validated the metabolic role of p110α *in vivo* by treating obese, hyperphagic ob/ob mice with three different PI3K inhibitors: CNIO-PI3Ki (α and δ inhibitor), BYL-719 (selective α inhibitor) and acalisib (selective δ inhibitor). With the intention to imitate the intake of a pill, treatments were administered daily by oral gavage and during 15-16 days. Interestingly, while acalisib treatment did not affect body weight, CNIO-PI3Ki and BYL-719 significantly reduced body weight of mice throughout the assay. In particular, ob/ob mice showed a body weight reduction of 7% and 10% compared to vehicle controls after treatment with 1 mg/kg and 5 mg/kg CNIO-PI3Ki, respectively. In the case of BYL-719, treatment with 10 mg/kg resulted in 10% body weight reduction. Treatment with CNIO-PI3Ki and BYL-719 produced an important, dose-dependent hyperglycemic peak that was cleared after 24 hours. Presumably, the detected increase in water intake contributes to the normalization of glycemia. Nevertheless, it is important to bear in mind that, starting at day 9, some mice had to be sacrificed due to their inability to re-establish normal glucose homeostasis. This difference with previous assays can be explained, at least in part, by the aggressive model that we are using (ob/ob mice are profoundly insulin resistant) combined with the treatment dosing (one single, full-concentration dose). Therefore, this is a critical fact to consider when designing a hypothetical use in humans, as dosing and timing of the treatment should be tightly supervised. As a result, we have confirmed that the inhibition of PI3Kα alone (BYL-719) or in combination with PI3Kδ (CNIO-PI3Ki) reduces body weight in obese mice and causes an increase in glucose levels upon administration, while single PI3Kδ downregulation (acalisib) does not have major effects on weight or glycemia.

Finally, we have demonstrated that CNIO-PI3Ki and BYL-719, but not acalisib (all of them administered at a dose of 15 mg/kg), lead to increased energy expenditure in lean, WT mice during the next 7 hours after drug administration. This result further emphasizes the role of PI3Kα in thermogenesis and energy expenditure control. Nevertheless, and even though all our data indicate that PI3Kα inhibition is responsible for the increased thermogenic program, and consequently, of the elevated energy expenditure and body weight reduction, we cannot exclude that PI3Kδ may be also contributing to the improvement of obesity or some of its associated-symptoms. During obesity, the adipose tissue exhibits an altered immune infiltration profile characterized by abundant pro-inflammatory M1 macrophages (McNelis and Olefsky, 2014) and deregulated IKK-NFκB and JNK-AP1 signalling pathways (Solinas et al., 2007) that give rise to elevated IL6 and TNF serum levels (Weisberg et al., 2003). In fact, pharmacological

inhibition of the TBK1 and IKKε kinases has been shown to produce body weight loss due to enhanced energy expenditure, together with improved insulin sensitivity and decreased hepatic steatosis in obese mice (Reilly et al., 2012). Taking this into account, the predominant role of PI3Kδ in hematopoietic cells and the fact that PI3Kδ is a main target of CNIO-PI3Ki, it is conceivable that inhibition of PI3Kδ could also explain some of the beneficial effects of PI3K inhibition by reducing obesity-related inflammatory responses.

Therefore, we conclude that p110α is the critical mediator of the positive effects on body weight, thermogenesis and energy expenditure of PI3K inhibition, and that inhibition of p110δ alone does not impact on weight, thermogenesis or energy regulation.

1.3 PI3K, energy expenditure and obesity

In this thesis, we have demonstrated that PI3Kα inhibition elevates thermogenesis, energy expenditure (EE) and, thereby, reduces obesity in mice. Typically, thermogenesis is induced through the activation of the uncoupling protein UCP1 in the BAT, in a process driven by the release of epinephrine by the sympathetic nervous system (SNS) in response to cold or overfeeding (Lowell and Spiegelman, 2000). In turn, UCP1 is able to dissociate oxidative phosphorylation from ATP synthesis, thereby dissipating energy as heat and increasing EE (Cannon and Nedergaard, 2004). However, this main switch commanded by the SNS can be modulated via PI3K, as reduced PI3K levels, and increased FOXO1 and PGC1α activity, additionally stimulate thermogenesis by inducing *Ucp1* expression (Ortega-Molina et al., 2012). Although the presence and relevance of BAT in human thermogenesis was controversial, physiologically active BAT was clearly identified in adult humans 7 years ago (Cypess et al., 2009; van Marken Lichtenbelt et al., 2009; Virtanen et al., 2009). These findings have generated a growing interest in BAT activation as a promising target for the treatment of obesity and offer a potential translational use of the CNIO-PI3Ki treatment for human obesity treatment. Supporting the idea that suppressed PI3K activity positively regulates thermogenesis, CNIO-PI3Ki treatment by oral gavage led to elevated UCP1 levels in the brown and white adipose tissue of obese mice; higher temperature around the BAT and shoulder area and to enhanced EE. However, we could not detect an increase in browning or *Ucp1* expression neither in the long-term CNIO-PI3Ki treatment nor in the ob/ob mice assay, thereby suggesting that other mechanisms may be stimulating EE as well.

In general, EE results from the sum of the resting metabolic rate (obligatory and stable EE required to perform cellular and organ functions), physical activity and adaptive thermogenesis. As already discussed, adaptive thermogenesis can be increased by, first, activating the BAT, for example through the inhibition of PI3K (Ortega-Molina et al., 2012) or

through the use of β3-adrenergic signalling mimetics (Clapham and Arch, 2007); or, secondly, by stimulating the differentiation of brown adipocytes. Similarly, resting metabolic rate and EE can be boosted by inhibiting anaerobic glycolysis in favour of oxidative phosphorylation (García-Cao et al., 2012). Providing evidence for this possible mechanism, we detected lower lactate levels, indicative of increased oxidative phosphorylation, in ob/ob mice treated by gavage with CNIO-PI3Ki. Finally, alternative strategies to induce energy expenditure consider the use of physical activity mimetics that provide similar benefits for those individuals with physical or time limitations (Himms-Hagen, 2004; Goodyear, 2008); compounds that increase thermogenic activity in the skeletal muscle; or drugs that stimulate mitochondrial uncoupling. In this regard, various drugs including resveratrol, which activates SIRT1 (Lagouge et al., 2006), the AMPK activator AICAR (5-aminoimidazole-4-carboxamide ribonucleotide) (Koh et al., 2008) or DNP (2,4-dinitrophenol) (Colman, 2007) have been extensively studied, although, in general, they have shown limited efficacy or toxic side effects.

Besides the induction of energy expenditure, other potential anti-obesity approaches primarily focus on either reducing appetite and food intake by amplifying inhibitory effects of anorexigenic signals or by blocking orexigenic factors, or on blocking nutrient absorption in the gut (Bray and Tartaglia, 2000). Similarly, several methods that promote nutrient turnover, stimulate adipocyte apoptosis, or that inhibit lipid synthesis could be effective strategies to reduce fat and protein storage (Bray and Tartaglia, 2000). In this context, PI3K inhibition could also be preventing fat storage by limiting adipocyte hypertrophy and hyperplasia since PI3K/AKT2 signalling has been demonstrated to be essential for both processes under high-fat diet conditions (Jeffery et al., 2015).

Thus, our data suggest that PI3K inhibition reduces obesity by promoting energy expenditure through various mechanisms that include the induction of thermogenesis, the stimulation of oxidative phosphorylation and, possibly, the prevention of adipogenesis and adipocyte hypertrophy.

1.4 CNIO-PI3Ki treatment in obese rhesus monkeys

We have extended the use of the CNIO-PI3Ki treatment to rhesus monkeys. For this purpose, we treated naturally obese monkeys for 3 months with a single daily oral dose of CNIO-PI3Ki. Of note, the administered dose resulted in relatively low serum drug concentrations, considering that the levels achieved 2 hours post-dosing (35 ng/ml) are about two times lower than the levels reached in the long-term assay in mice (63 ng/ml). Interestingly, treatment with CNIO-PI3Ki caused a modest, but significant, decrease in adiposity (7.6% reduction) and a trend towards reduced fasting glucose in monkeys. Although food intake was similar between the

CNIO-PI3Ki treated and control group, it is necessary to point out that both groups received a daily extra-treat in which the drug was administered. This treat represents a 16% increase in the total caloric intake and can be considered as a high-fat diet mimetic. The fact that CNIO-PI3Ki treatment reduces adiposity in the presence of a greater caloric intake further supports the idea that CNIO-PI3Ki works in the context of nutritional overload. Although the observed adiposity reduction was not translated into a reduction in body weight, we believe that either a longer treatment or a higher dose of the CNIO-PI3Ki could conceivably produce an eventual decrease in body weight.

Remarkably, no toxic secondary side effects associated to respiration, blood pressure, pulse, temperature or complete blood biochemistry were detected in any of the treated animals, indicating that the CNIO-PI3Ki is a safety treatment at the specified dose in rhesus monkeys as well. Moreover, transcriptional analysis of the liver and adipose tissue revealed no long-lasting gene expression changes after 3 months CNIO-PI3Ki treatment, demonstrating that the drug does not cause major or irreversible metabolic alterations.

1.5 Concluding remarks

Based on the evidence presented here, we propose that moderate pharmacological inhibition of PI3K could be an effective and safe therapeutic strategy against human obesity and metabolic syndrome in the future. Furthermore, we propose a model in which PI3K promotes anabolism and nutrient storage in the context of nutritional overload, which eventually promotes obesity, liver steatosis and hyperglycemia. Nevertheless, a partial reduction of PI3K activity (specifically of p110α) by CNIO-PI3Ki treatment induces energy expenditure through several mechanisms that may include the stimulation of thermogenesis in the brown and white adipose tissue, the induction of oxidative phosphorylation, and the reduction of adipocyte hyperthrophy and adipogenesis. In this manner, CNIO-PI3Ki treatment reduces adiposity, liver steatosis and inflammation, as well as promotes normoglycemia in obese mice, thereby improving some symptoms of the metabolic syndrome (**Figure 41**). Likewise, CNIO-PI3Ki treatment reduces adiposity and glucose levels in obese monkeys, thereby highlighting a translational potential use in humans.

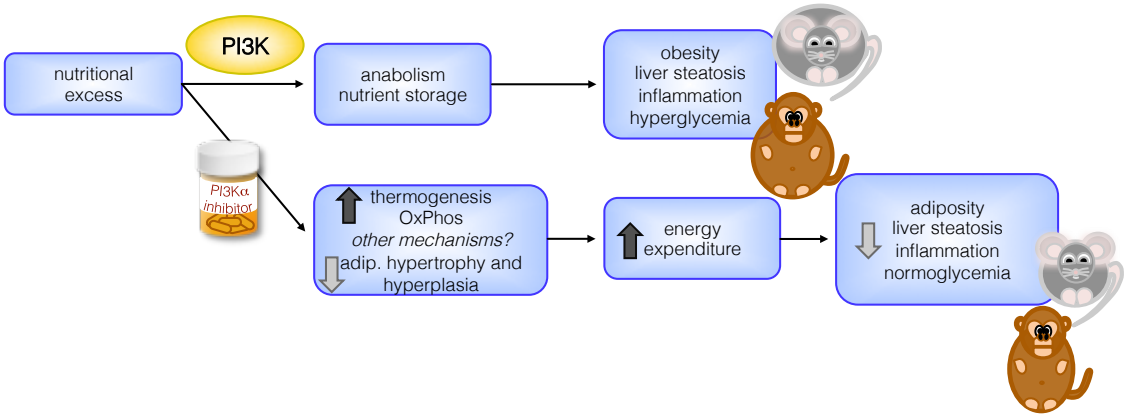

Figure 41: Positive effects of pharmacological PI3K inhibition.
Under nutritional excess, PI3K activity promotes obesity, liver steatosis and hyperglycemia by stimulating anabolism and nutrient storage. However, the pharmacological inhibition of PI3Kα leads to induced energy and thereby, to reduced adiposity, liver steatosis, inflammation and normoglycemia in obese mice and, partly, in obese monkeys.

PART 2. ROLE OF p21 IN THE FASTING RESPONSE

Fasting is the most extreme form of dietary restriction because it requires complete abstinence from food, but not from water. Although long-term fasting periods are only sustainable and advantageous in lower organisms such as yeast and worms, mammals can also benefit from alternative fasting cycles. Indeed, intermittent fasting cycles have been shown to promote healthy lifespan and delay the onset of age-associated diseases such as type II diabetes, metabolic syndrome, cardiovascular disease and cancer (Longo and Mattson, 2014). Some of the mechanisms responsible for these positive effects include improved mitochondrial function, insulin sensitivity and glucose homeostasis; increased stress and cancer resistance; enhanced autophagy, regenerative capacity and DNA repair; and reduced inflammation, proliferation and oxidative damage. However, the underlying molecular pathways are still poorly understood.

Here, we have addressed a general question regarding the involvement of tumour suppressor genes in the response to fasting with the idea that they could be mediating some of the reported beneficial effects of starvation. Some of the most important tumour suppressors are activated in response to cellular stresses such as DNA damage and oxidative or oncogenic stress, and participate in signalling pathways that prevent proliferation as well as stimulate DNA repair under these stressful conditions (Sherr, 2004; Vogelstein et al., 2000; Vurusaner et al., 2012). At the same time, fasting is a physiological stress that triggers complex metabolic, cellular and molecular adaptations (Cahill, 2006; Lempradl et al., 2015; Wang et al., 2006). But still,

nothing is known about the possible role that stress-responsive tumour suppressors may play during fasting.

2.1 p21 is a fasting-inducible factor

In order to investigate whether tumour suppressor genes play a role in the adaptation to fasting, we began by asking if their expression was affected in response to starvation. Interestingly, *p21* was highly induced in multiple tissues including liver, adipose depots, muscle, and lung upon 48 hours fasting, whereas none of the other tested tumour suppressors including *p16*, *p19*, *p27* and *p53* altered their expression. This observation confirms previous reports that demonstrate an important upregulation of *p21* mRNA levels, in a process that is independent of the p53 activity and is partly mediated through the activation of FOXO1 (Tinkum et al., 2013). Confirming this result, we extended these observations by ruling out the participation of p53, which is the main activator of p21 transcription in response to DNA damage and oncogenic stress (Abbas and Dutta, 2009), and of p19 and Sirt1. Besides FOXO1 (Seoane et al., 2004; Tinkum et al., 2013), whose activity is enhanced by reduced insulin levels, CREB is activated by glucagon in response to fasting and it is another transcriptional activator of *p21* upon nutrient shortage (Everett et al., 2013).

p21 is an important tumour suppressor gene involved in cell cycle regulation, senescence, apoptosis, DNA repair and transcriptional control (Abbas and Dutta, 2009). However, the role of p21 in metabolism has remained largely unexplored and controversial since p21 loss has been associated with both, adipose tissue hyperplasia and obesity (Naaz et al., 2004) as well as with reduced adipocyte size and impaired adipocyte differentiation (Inoue et al., 2008). Given the reduced number of studies linking p21 to metabolism, and the important p21 induction observed after 48 hours of fasting in various tissues, we decided to further analyze the role of p21 in the fasting response.

2.2 p21 enables efficient adaptation to fasting

To study whether the upregulation of p21 is of physiological significance, we decided to fast mice lacking p21. As already reported (Tinkum et al., 2013), p21KO mice did not present any obvious differences regarding appearance, fat accumulation or metabolic adaptation markers after 24 hours fasting. However, after 48 hours of fasting, p21KO mice manifested profound defects in the adaptation to fasting and became severely morbid showing clear signs of energy exhaustion as reflected by the almost complete lack of adipose tissue upon necropsy. One of the main adaptations to fasting consists in the release of triglycerides and free fatty acids as well as

fat-derived ketone bodies to the bloodstream by the adipose tissue and liver, respectively, that meet the energy-demanding needs of tissues, especially the brain (Wang et al., 2006). Interestingly, 48 hours fasted p21KO mice presented low serum triglycerides, free fatty acids, and ketone bodies levels compared to fasted WT mice. This was accompanied by a greater reduction of IGF1, insulin and leptin levels compared to WT controls. Together with these deficiencies, p21KO mice showed a dramatic body temperature drop, probably as a consequence of the absence of BAT. In an advanced stage of the metabolic adaptations to fasting, proteins are rapidly degraded in the muscle and released to the bloodstream in order to boost gluconeogenesis in the liver. In the case of p21KO mice, we detected increased circulating amino acids in the serum indicative of an enhanced proteolytic adaptation that may partially compensate the premature loss of lipid stores. In addition, there was evidence of hepatic damage, based on the elevated serum alanine aminotransferase (ALT) levels and apoptotic hepatocytes.

To detect energetic adaptive differences, we performed calorimetry analyses during a period of 48 hours under *ad libitum* feeding conditions followed by 48 hours fasting. Importantly, we observed that p21KO mice presented higher energy expenditure than WT controls during the first 36 hours of fasting, which could explain the premature exhaustion of nutrient stores. Also, this was accompanied by an increase in locomotor activity that can be interpreted as an enhanced foraging. At the same time, it may also constitute an additional expense of energy that aggravates the observed premature energy depletion (Westerterp, 2013). As a reference, no differences were observed in energy expenditure and activity under standard feeding conditions.

Additionally, *in vitro* studies also pointed to a role of p21 in the fasting response. First, cultured human hepatocellular carcinoma HepG2 cells and immortalized hepatocytes presented upregulated *p21* expression upon nutrient starvation. Remarkably, recapitulating the *in vivo* effects of p21-deficiency, p21KO hepatocytes underwent massive cell death after 48 hours of nutrient starvation, unlike WT hepatocytes that remained largely viable.

Thus, we show that p21 deficiency leads to enhanced energy expenditure, premature energy depletion and inability to efficiently adapt to long fasting periods.

2.3 p21 deficiency and transcriptional changes

To get a better insight into the mechanisms that could explain the inability of p21KO mice to properly adapt to fasting, we performed unbiased examination of the liver transcriptome by RNA-seq of WT and p21KO mice upon 24 hours fasting, when the severe defects of fasting have not been manifested yet. This analysis revealed important differences between WT and

p21KO mice. Of note, gene set enrichment analysis (GSEA) revealed a great number of downregulated pathways associated to metabolism or related to different immune-related responses in the liver of fasted p21KO mice.

Regarding the involvement of immune-related pathways, we confirmed by diverse techniques that fasting produces a greater and more profound decrease of immune-related responses in p21KO livers compared to controls. Fasting consistently reduces the number of tissue infiltrating leukocytes and inflammatory-associated processes in the liver of normal mice (Mitchell et al., 2010; Robertson and Mitchell, 2013; Sokolović et al., 2013). In the case of p21KO, this reduction was significantly more pronounced than in WT mice, which we interpret as a further indication that the absence of p21 results in an accelerated onset of the effects of fasting.

Furthermore, within the metabolic-related group, RNA-seq analysis also pointed out to a defective activation of the "PPAR signalling pathway" in fasted p21KO livers. This is particularly interesting because PPARα is known to be a critical factor expressed in hepatocytes and necessary for the correct adaptation to fasting (Contreras et al., 2013). PPARα is a member of the nuclear hormone receptor superfamily of transcription factors and it is involved in the regulation of a variety of processes, ranging from inflammation to glucose, lipid and amino acid metabolism, energy homeostasis and hepatocyte proliferation (Rakhshandehroo et al., 2010). Under fasting conditions, PPARα is activated by fatty acids and stimulates fatty acid β-oxidation as well as ketogenesis in the liver. In fact, PPARα-deficient mice present an abnormal response to fasting that renders them unable to efficiently adapt, thereby demonstrating the relevance of PPARα activity during nutrient deprivation.

Therefore, we decided to study the PPARα response in depth and focused first on the regulation of PPARα transcriptional targets. Interestingly, the liver of p21KO fasted mice showed impaired upregulation of a subset of PPARα transcriptional targets. Moreover, p21KO hepatocytes showed a blunted or reduced activation of some of the transcriptional PPARα target genes upon 24 hours nutrient starvation or treatment with the PPARα agonist WY-14,643, further supporting a cell-autonomous function of p21 in the fasting response. The mechanistic basis for the regulation of PPARα by p21 remains to be established. One possible mechanistic link could be provided by the histone acetyltransferase coactivators p300/CBP, since the interaction of p21 with p300/CBP (Snowden et al., 2000) and p300/CBP with PPARα (Dowell et al., 1997) have already been described. In fact, we have been able to reproduce the interaction of p21 with CBP. Still, and most likely due to various technical problems associated with the lack of an adequate cellular model (expressing high p21 and PPARα levels) and of a good PPARα antibody available in the lab, we have not been able to detect CBP-PPARα and p21-

PPARα interactions. Another possible mechanism linking p21 with PPARα could be mediated through cyclin-dependent kinases (CDKs). In this regard, it is known that CDK4 directly binds and activates PPARγ, a related peroxisome proliferator-activated receptor that is mainly expressed in adipocytes, and, thereby, stimulates lipid uptake and adipogenesis in the adipose tissue (Abella et al., 2005). Even though our data indicate an effect over PPARα, it is conceivable that other CDKs could be binding different members of the PPAR family.

Similar to p21KO mice, PPARα-deficient mice present low body temperature as well as reduced serum glucose and ketone bodies after 48 hours fasting, although no major differences regarding plasma free fatty acids and triglycerides (Kersten et al., 1999; Leone et al., 1999). Of note, they are also characterized by the accumulation of triglycerides and fatty acids in the liver upon fasting due to their inability to undergo ketogenesis. In the case of p21KO mice, it seems clear that, in the WAT, lipolysis and the release of free fatty acids to the bloodstream is correctly working. However, when fatty acids reach the liver, they may not be efficiently converted into ketone bodies. This could explain that the WAT is required to foster lipolysis and that, therefore, lipid stores are prematurely exhausted. An open remaining question would be: what is then happening to the released fatty acids? One possible explanation could be that, as in the case of PPARα-KO mice, fasted p21KO animals accumulate them in the liver. Nevertheless, quantification of hepatic free fatty acids showed no significant differences between p21KO livers and controls (although a tendency towards higher levels in p21KO mice after 48 hours fasting). Other potential explanations could be that ketogenesis and ketone body formation is diminished, but not absolutely blocked, as a consequence of the impaired PPARα activation, or finally, that fatty acids may be excreted without entering the liver.

Altogether, we conclude that the tumour suppressor p21 is a fasting-induced factor that contributes to fasting adaptation (**Figure 42**). Mechanistically, our data suggest that p21 is a positive regulator of PPARα, which, in turn, is a critical mediator of the metabolic responses to fasting.

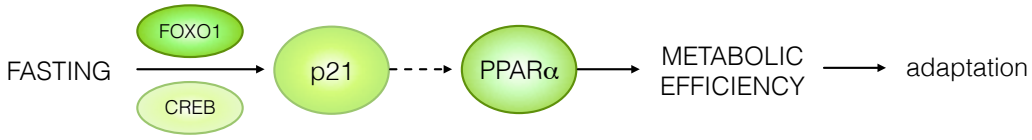

Figure 42: p21 is necessary for the efficient adaptation to fasting.
p21 is highly upregulated upon fasting in a p53-independent process that is partly mediated by FOXO1 and CREB. In turn, p21 acts as a positive regulator of PPARα, which promotes fatty acid β-oxidation and, thereby, metabolic efficiency and adaptation to fasting.

2.4 Fasting-induced senescence

Senescence is a compensatory tumour-suppressive response, characterized by a persistent growth arrest (Hayflick and Moorhead, 1961) that is induced in response to several stimuli such as telomere shortening (Harley et al., 1990), oxidative stress (Lee et al., 1999; Parrinello et al., 2003), active chromatin (euchromatin) inducers (Ogryzko et al., 1996), oncogenic activation (Serrano et al., 1997), and tumour suppressor loss (Alimonti et al., 2010). These stimuli are signalled through various pathways, many of which activate p53, and converge in the activation of the cyclin-dependent kinase inhibitors p16, p15, p21 and p27, as well as the tumour suppressor Rb. Furthermore, senescent cells present derepression of the CDKN2A locus, which encodes p16 and ARF, and elicit a complex pro-inflammatory response known as senescence-associated secretory phenotype (SASP) that is principally mediated by NF-κB and CEBPβ (Campisi and d'Adda di Fagagna, 2007; Collado et al., 2007; Muñoz-Espín and Serrano, 2014).

Importantly, oncogene-induced senescence has been shown to diminish cancer development *in vivo* by inducing a stable growth arrest (Collado et al., 2005; Michaloglou et al., 2005). This response was initially thought to depend on a high oncogenic stress. However, combination of a mild oncogenic stress together with the deletion of CDK2 (Campaner et al., 2010) or CDK4 (Puyol et al., 2010) was shown to promote a full senescence response in mice thereby lowering the threshold that allows cells to senesce. Taking into account that fasting highly induces p21 expression in multiple tissues and that, in turn, p21 is a strong CDK inhibitor (principally of CDK2), we hypothesised that a low oncogenic stress combined with fasting may promote senescence, as well. One of the best-studied oncogenes is Myc, a transcription factor whose overexpression directly contributes to malignant transformation and is frequently present in human cancers (Kress et al., 2015). In fact, Eμ-Myc transgenic mice, carrying a c-Myc oncogene driven by the immunoglobulin μ or κ enhancer, are widely used as spontaneous high-incidence lymphoma and early B cells leukemia models (Adams et al., 1985). To ensure moderate oncogenic c-Myc stress, 10 weeks old male Eμ-Myc mice in pre-tumoural stage (free of lymphoma or other associated malignancies) were selected. Interestingly, 48 hours fasting induced a senescent response only in the pre-tumoural spleen of Eμ-Myc mice, as measured by staining with the senescence associated-β galactosidase (SA-β gal) marker and the increased expression of the senescence markers *p16*, *p19* and *p21*. In contrast, standard fed Eμ-Myc or WT littermate controls (fed or fasted) did barely show SA-β gal positive staining or altered *p16*, *p19* and *p21* expression in the spleen. Of note, fasted Eμ-Myc spleens presented highly variable senescence degrees, ranging from highly senescent to medium or low senescent.

In fact, elevated SA-β gal staining positively correlated with a higher *p16*, *p19* and *p21* expression in pre-tumoural spleens of fasted Eμ-Myc mice.

Senescence is a tumour-suppressive response that, among others, avoids proliferation of cancerous cells by inducing a stable cell cycle arrest (Campisi and d'Adda di Fagagna, 2007; Collado et al., 2007; Muñoz-Espín and Serrano, 2014). Given that 48 hours of fasting induces a senescent response in the pre-tumoural spleen of Eμ-Myc mice, and this presumably limits the proliferative capacity of tumour cells, we were next wondering whether this would be translated into an extended tumour-free survival of mice. Unfortunately, neither overall mice survival nor maximal survival was significantly extended in Eμ-Myc mice that had been subjected to a single event of 48 hours of fasting at 10 weeks of age. One possible reason for this lack of effect could be that a single fasting event may not be strong enough to halt proliferation in the spleen in the long-term. Therefore, we propose that the effects of alternative fasting periods on tumour-free survival should further be assessed.

Altogether, our data indicate that fasting can lower the threshold that allows a senescent response in the cells as a low oncogenic stress induces senescence in the pre-tumoural spleen of Eμ-Myc mice (**Figure 43**).

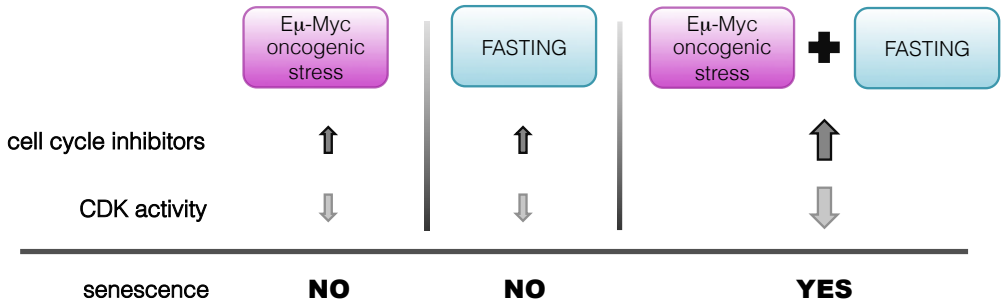

Figure 43. Fasting lowers the senescence threshold.
Oncogenic Eμ-Myc stress or fasting alone are not able to promote a full senescence response in cells, because they partially induce cell cycle inhibitors and retain moderate CDK activity. However, the combination of both conditions highly induces cell cycle inhibitors and inhibits CDKs, thereby stimulating senescence.

CONCLUSIONS

1. The pharmacological inhibition of PI3K is an efficient and safe anti-obesity treatment in obese mice.

1.3 CNIO-PI3Ki treatment produces a progressive weight loss in obese mice until reaching a new balance that is 20% below the original weight. This body weight reduction is selectively restricted to the loss of adiposity and is caused by an increase in energy expenditure.

1.4 CNIO-PI3Ki treatment reduces glycemia, hepatic steatosis and inflammation, thereby improving some of the pathologies associated to the metabolic syndrome.

1.5 CNIO-PI3Ki treatment is reversible, does not lead to resistance and does not cause secondary toxic side effects in obese mice. Moreover, CNIO-PI3Ki only manifests its anti-obesity activity under conditions of nutritional overload.

1.6 Selective inhibition of PI3K isoforms, both *in vitro* and *in vivo*, indicates that inhibition of PI3K-p110α is critical for the beneficial effects on obesity and metabolic syndrome.

1.7 CNIO-PI3Ki treatment reduces adiposity and improves glycemia in obese rhesus monkeys in the absence of detectable toxic effects.

2. The tumour suppressor gene p21 is an important mediator of the fasting response.

2.3 *p21*, but not other tumour suppressors, is highly induced in numerous tissues upon fasting and in a p53-independent manner.

2.4 p21-deficient mice cannot efficiently adapt to long-term, 48-hours fasting periods and show signs of premature energy exhaustion as well as accelerated physiological adaptations.

2.5 p21-null mice show impaired PPARα signalling activation in the liver upon fasting.

2.6 p21-deficient hepatocytes cannot survive prolonged nutrient starvation periods and present reduced PPARα activity after both, nutrient starvation and PPARα agonist WY-14,643 treatment.

2.7 Fasting can induce senescence in oncogenically-stressed cells *in vivo*, as shown in the case of the pre-tumoural spleen of Eμ-Myc mice.

CONCLUSIONES

1. **La inhibición farmacológica de PI3K es un método eficiente y seguro para tratar la obesidad en ratones obesos.**
   1.1 El tratamiento con CNIO-PI3Ki produce una pérdida progresiva de peso en ratones obesos hasta alcanzar un nuevo equilibrio, un 20% por debajo del peso original. Esta pérdida de peso se debe a una reducción de la adiposidad, exclusivamente, y tiene como causa el aumento del gasto energético.
   1.2 El tratamiento con CNIO-PI3Ki reduce los niveles de glucosa, la esteatosis hepática y la inflamación, mejorando así algunas de las patologías asociadas al síndrome metabólico.
   1.3 El tratamiento con CNIO-PI3Ki es reversible, no causa resistencia y no presenta efectos secundarios tóxicos en ratones obesos. Además, sólo exhibe actividad anti-obesidad en un contexto de exceso nutricional
   1.4 La inhibición selectiva de las isoformas de PI3K, tanto *in vitro* como *in vivo*, indica que la inhibición de PI3K-p110α es clave para los efectos beneficiosos sobre la obesidad y el síndrome metabólico.
   1.5 El tratamiento con CNIO-PI3Ki reduce la adiposidad y mejora la glicemia, en ausencia de toxicidad, de macacos obesos.

2. **El gen supresor de tumores p21 es un importante mediador en la respuesta a ayuno.**
   2.1 La expresión de *p21*, pero no de otros supresores de tumores, se induce tras un periodo de ayuno en numerosos tejidos y de manera independiente de p53.
   2.2 Ratones deficientes en p21 no pueden adaptarse eficientemente a periodos prolongados de ayuno (48 horas), ya que muestran una pérdida prematura de energía y adaptaciones fisiológicas prematuras.
   2.3 Tras un periodo de ayuno, los ratones deficientes en p21 presentan una menor activación de la señalización de PPARα en el hígado.
   2.4 Hepatocitos deficientes en p21 no pueden sobrevivir en medio sin nutrientes y muestran una activación reducida de PPARα tras su cultivo en medio de ayuno o tras su estimulación con el agonista de PPARα WY-14,643.
   2.5 El ayuno es capaz de inducir una respuesta senescente en células bajo estrés oncogénico *in vivo,* tal y como sucede en el caso del bazo pretumoral de ratones Eμ-Myc.

BIBLIOGRAPHY

Abbas, T., and Dutta, A. (2009). p21 in cancer: intricate networks and multiple activities. Nat. Rev. Cancer *9*, 400–414.

Abella, A., Dubus, P., Malumbres, M., Rane, S.G., Kiyokawa, H., Sicard, A., Vignon, F., Langin, D., Barbacid, M., and Fajas, L. (2005). Cdk4 promotes adipogenesis through PPARgamma activation. Cell Metab. *2*, 239–249.

Adams, J.M., Harris, A.W., Pinkert, C.A., Corcoran, L.M., Alexander, W.S., Cory, S., Palmiter, R.D., and Brinster, R.L. (1985). The c-myc oncogene driven by immunoglobulin enhancers induces lymphoid malignancy in transgenic mice. Nature *318*, 533–538.

Albanes, D. (1987). Total calories, body weight, and tumor incidence in mice. Cancer Res. *47*, 1987–1992.

Alessi, D.R., James, S.R., Downes, C.P., Holmes, A.B., Gaffney, P.R., Reese, C.B., and Cohen, P. (1997). Characterization of a 3-phosphoinositide-dependent protein kinase which phosphorylates and activates protein kinase B alpha. Curr. Biol. *7*, 261–269.

Alimonti, A., Nardella, C., Chen, Z., Clohessy, J.G., Carracedo, A., Trotman, L.C., Cheng, K., Varmeh, S., Kozma, S.C., Thomas, G., et al. (2010). A novel type of cellular senescence that can be enhanced in mouse models and human tumor xenografts to suppress prostate tumorigenesis. J. Clin. Invest. *120*, 681–693.

Altarejos, J.Y., and Montminy, M. (2011). CREB and the CRTC co-activators: sensors for hormonal and metabolic signals. Nat. Rev. Mol. Cell Biol. *12*, 141–151.

Backer, J.M. (2008). The regulation and function of Class III PI3Ks: novel roles for Vps34. Biochem. J. *410*, 1–17.

Bai, X., Ma, D., Liu, A., Shen, X., Wang, Q.J., Liu, Y., and Jiang, Y. (2007). Rheb activates mTOR by antagonizing its endogenous inhibitor, FKBP38. Science *318*, 977–980.

Bartke, A. (2005). Role of the growth hormone/insulin-like growth factor system in mammalian aging. Endocrinology *146*, 3718–3723.

Becattini, B., Marone, R., Zani, F., Arsenijevic, D., Seydoux, J., Montani, J.P., Dulloo, A.G., Thorens, B., Preitner, F., Wymann, M.P., and Solinas, G. (2011). PI3K within a nonhematopoietic cell type negatively regulates diet-induced thermogenesis and promotes obesity and insulin resistance. Proc. Natl. Acad. Sci. *108*, 854–863.

Beckonert, O., Keun, H.C., Ebbels, T.M., Bundy, J., Holmes, E., Lindon, J.C., and Nicholson, J.K. (2007). Metabolic profiling, metabolomic and metabonomic procedures for NMR spectroscopy of urine, plasma, serum and tissue extracts. Nat. Protoc. *2*, 2692–2703.

Benjamin, D., Colombi, M., Moroni, C,. and Hall, M.N. (2011). Rapamycin passes the torch: a new generation of mTOR inhibitors. Nat. Rev. Drug Discov. *10*, 868–880.

Bensaad, K., Tsuruta, A., Selak, M.A., Vidal, M.N., Nakano, K., Bartrons, R., Gottlieb, E., and Vousden, K.H. (2006). TIGAR, a p53-inducible regulator of glycolysis and apoptosis. Cell *126*, 107–120.

Beyaz, S., Mana, M.D., Roper, J., Kedrin, D., Saadatpour, A., Hong, S.J., Bauer-Rowe, K.E., Xifaras, M.E., Akkad, A., Arias, E., et al. (2016). High-fat diet enhances stemness and tumorigenicity of intestinal progenitors. Nature *531*, 53–58.

Biggs, W.H., Meisenhelder, J., Hunter, T., Cavenee, W.K., and Arden, K.C. (1999). Protein kinase B/Akt-mediated phosphorylation promotes nuclear exclusion of the winged helix transcription factor FKHR1. Proc. Natl. Acad. Sci. USA *96*, 7421–7426.

Bjedov, I. , Toivonen, J.M., Kerr, F., Slack, C., Jacobson, J., Foley, A., and Partridge, L. (2010). Mechanisms of life span extension by Rapamycin in the fruit fly drosophila melanogaster. Cell Metab. *11*, 35–46.

Bornstein, G., Bloom, J., Sitry-Shevah, D., Nakayama, K., Pagano, M., and Hershko, A. (2003). Role of the SCFSkp2 ubiquitin ligase in the degradation of p21Cip1 in S Phase. J. Biol. Chem. *278* , 25752–25757.

Bray, G.A., and Tartaglia, L.A. (2000). Medicinal strategies in the treatment of obesity. Nature *404*, 672–677.

Brown, E.J., Beal, P.A., Keith, C.T., Chen, J., Shin, T.B., and Schreiber, S.L. (1995). Control of p70 S6 kinase by kinase activity of FRAP in vivo. Nature *377*, 441–446.

Brugarolas, J., Chandrasekaran, C., Gordon, J.I., Beach, D., Jacks, T., and Hannon, G.J. (1995). Radiation-induced cell cycle arrest compromised by p21 deficiency. Nature *377*, 552–557.

Brugge, J., Hung, M.C., and Mills, G.B. (2007). A new mutational AKTivation in the PI3K pathway. Cancer Cell *12*, 104–107.

Brunet, A., Bonni, A., Zigmond, M.J., Lin, M.Z., Juo, P., Hu, L.S., Anderson, M.J., Arden, K.C., Blenis, J., and Greenberg, M.E. (1999). Akt promotes cell survival by phosphorylating and inhibiting a Forkhead transcription factor. Cell *96*, 857–868.

Burkewitz, K., Zhang, Y., and Mair, W.B. (2014). AMPK at the nexus of energetics and aging. Cell Metab. *20*, 10–25.

Caballero, B. (2007). The global epidemic of obesity: An overview. Epidemiol. Rev. *29*, 1–5.

Cahill, G.F. (2006). Fuel metabolism in starvation. Annu. Rev. Nutr. *26*, 1–22.

Calle, E.E., and Kaaks, R. (2004). Overweight, obesity and cancer: epidemiological evidence and proposed mechanisms. Nat. Rev. Cancer *4*, 579–591.

Campaner, S., Doni, M., Hydbring, P., Verrecchia, A., Bianchi, L., Sardella, D., Schleker, T., Perna, D., Tronnersjö, S., Murga, M., et al. (2010). Cdk2 suppresses cellular senescence induced by the c-myc oncogene. Nat. Cell Biol. *12*, 54–59.

Campisi, J., and d'Adda di Fagagna, F. (2007). Cellular senescence: when bad things happen to good cells. Nat. Rev. Mol. Cell Biol. *8*, 729–740.

Cannon, B., and Nedergaard, J. (2004). Brown adipose tissue: function and physiological significance. Physiol. Rev. *1*, 277–359.

Cantley, L.C. (2002). The phosphoinositide 3-kinase pathway. Science *296*, 1655–1657.

Carracedo, A., and Pandolfi, P.P. (2008). The PTEN-PI3K pathway: of feedbacks and cross-talks. Oncogene *27*, 5527–5541.

Catrina, S.B., Okamoto, K., Pereira, T., Brismar, K., and Poellinger, L. (2004). Hyperglycemia regulates hypoxia-inducible factor-1alpha protein stability and function. Diabetes *53*, 3226–3232.

Cava, E., and Fontana, L. (2013). Will calorie restriction work in humans? Aging (Albany. NY). *5*, 507–514.

Chakravarthy, M.V, Lodhi, I.J., Yin, L., Malapaka, R.R., Xu, H.E., Turk, J., and Semenkovich, C.F. (2009). Identification of a physiologically relevant endogenous ligand for PPARalpha in liver. Cell *138*, 476–488.

Chandarlapaty, S., Sawai, A., Scaltriti, M., Rodrik-Outmezguine, V., Grbovic-Huezo, O., Serra, V., Majumder, P.K., Baselga, J., and Rosen, N. (2011). AKT inhibition relieves feedback suppression of receptor tyrosine kinase expression and activity. Cancer Cell *19*, 58–71.

Chattopadhyay, M., Selinger, E.S., Ballou, L.M., and Lin, R.Z. (2011). Ablation of PI3K p110-α prevents high-fat diet-induced liver steatosis. Diabetes *60*, 1483–1492.

Chen, D., Steele, A.D., Lindquist, S., and Guarente, L. (2005). Increase in activity during calorie restriction requires Sirt1. Science *310*, 1641.

Chen, J., Jackson, P.K., Kirschner, M.W., and Dutta, A. (1995). Separate domains of p21 involved in the inhibition of Cdk kinase and PCNA. Nature *374*, 386–388.

Cheng, Y., and Prusoff, W.H. (1973). Relationship between the inhibition constant (K1) and the concentration of inhibitor which causes 50 per cent inhibition (I50) of an enzymatic reaction. Biochem. Pharmacol. *22*, 3099–3108.

Chung, J., Kuo, C.J., Crabtree, G.R., and Blenis, J. (1992). Rapamycin-FKBP specifically blocks growth-dependent activation of and signaling by the 70 kd S6 protein kinases. Cell *69*, 1227–1236.

Clancy, D.J., Gems, D., Harshman, L.G., Oldham, S., Stocker, H., Hafen, E., Leevers, S.J., and Partridge, L. (2001). Extension of life-span by loss of CHICO, a Drosophila insulin receptor substrate protein. Science *292*, 104–106.

Clapham, J.C., and Arch, J.R. (2007). Thermogenic and metabolic antiobesity drugs: rationale and opportunities. Diabetes Obes. Metab. *9*, 259–75.

Collado, M., Gil, J., Efeyan, A., Guerra, C., Schuhmacher, A.J., Barradas, M., Benguría, A., Zaballos, A., Flores, J.M., Barbacid, M., et al. (2005). Tumour biology: senescence in premalignant tumours. Nature *436*, 642.

Collado, M., Blasco, M.A., and Serrano, M. (2007). Cellular senescence in cancer and aging. Cell *130*, 223–233.

Colman, E. (2007). Dinitrophenol and obesity: an early twentieth-century regulatory dilemma. Regul Toxicol Pharmacol. *115*, 115–117.

Colman, R.J., Beasley, T.M., Kemnitz, J.W., Johnson, S.C., Weindruch, R., and Anderson, R.M. (2014). Caloric restriction reduces age-related and all-cause mortality in rhesus monkeys. Nat. Commun. *5*, 3557.

Cone, R.D., Cowley, M.A, Butler, A.A., Fan, W., Marks, D.L., and Low, M.J. (2001). The arcuate nucleus as a conduit for diverse signals relevant to energy homeostasis. Int. J. Obes. Relat. Metab. Disord. *25*, S63–S67.

Contreras, A.V., Torres, N., and Tovar, A.R. (2013). PPAR-α as a key nutritional and environmental sensor for metabolic adaptation. Adv. Nutr. *4*, 439–452.

Coqueret, O., and Gascan, H. (2000). Functional interaction of STAT3 transcription factor with the cell cycle inhibitor p21(WAF1/CIP1/SDI1). J. Biol. Chem. *275*, 18794–18800.

Cross, D.A., Alessi, D.R., Cohen, P., Andjelkovic, M., and Hemmings, B.A. (1995). Inhibition of glycogen synthase kinase-3 by insulin mediated by protein kinase B. Nature *378*, 785–789.

Crouthamel, M.C., Kahana, J.A., Korenchuk, S., Zhang, S.Y., Sundaresan, G., Eberwein, D.J., Brown, K.K., and Kumar, R. (2009). Mechanism and management of AKT inhibitor-induced hyperglycemia. Clin. Cancer Res. *15*, 217–225.

Currie, R.A., Walker, K.S., Gray, A., Deak, M., Casamayor, A., Downes, C.P., Cohen, P., Alessi, D.R., and Lucocq, J. (1999) Role of phosphatidylinositol 3,4,5-trisphosphate in regulating the activity and localization of 3-phosphoinositide-dependent protein kinase-1. Biochem. J. *337,* 575–583.

Cypess, A.M., Lehman, S., Williams, G., Tal, I., Rodman, D., Goldfine, A.B., Kuo, F.C., Palmer, E.L., Tseng, Y.H., Doria, A., et al. (2009). Identification and importance of brown adipose tissue in adult humans. N. Engl. J. Med. *360*, 1509–1517.

Daitoku, H., Yamagata, K., Matsuzaki, H., Hatta, M., and Fukamizu, A. (2003). Regulation of PGC-1 promoter activity by protein kinase B and the forkhead transcription factor FKHR. Diabetes *52*, 642–649.

Dalamaga, M., Diakopoulos, K.N., and Mantzoros, C.S. (2012). The role of adiponectin in cancer: a review of current evidence. Endocr. Rev. *33*, 547–594.

Delavaine, L., and La Thangue, N.B. (1999). Control of E2F activity by p21Waf1/Cip1. Oncogene *18*, 5381–5392

Després, J.P., and Lemieux, I. (2006). Abdominal obesity and metabolic syndrome. Nature *444*, 881–887.

Dijkers, P.F., Medema, R.H., Pals, C., Banerji, L., Thomas, N.S., Lam, E.W., Burgering, B.M., Raaijmakers, J.A., Lammers, J.W., Koenderman, L., and Coffer, P.J. (2000). Forkhead transcription factor FKHR-L1 modulates cytokine-dependent transcriptional regulation of $p27^{(KIP1)}$. Mol. Cell. Biol. *20*, 9138–9148.

Dominy, J.E., Lee, Y., Gerhart-Hines, Z., and Puigserver, P. (2010). Nutrient-dependent regulation of PGC-1α's acetylation state and metabolic function through the enzymatic activities of Sirt1/GCN5. Biochim. Biophys. Acta *1804*, 1676–1683.

Dorrello, N.V., Peschiaroli, A., Guardavaccaro, D., Colburn, N.H., Sherman, N.E., and Pagano, M. (2006). S6K1- and betaTRCP-mediated degradation of PDCD4 promotes protein translation and cell growth. Science *314*, 467–471.

Dos, D.S., Ali, S.M., Kim, D.H., Guertin, D.A., Latek, R.R., Erdjument-Bromage, H., Tempst, P., and Sabatini, D.M. (2004). Rictor, a novel binding partner of mTOR, defines a rapamycin-insensitive and raptor-independent pathway that regulates the cytoskeleton. Curr. Biol. *14*, 1296–1302.

Dowell, P., Ishmael, J.E., Avram, D., Peterson, V.J., Nevrivy, D.J., and Leid, M. (1997). p300 functions as a coactivator for the peroxisome proliferator-activated receptor alpha. J. Biol. Chem. *272*, 33435–33443.

Du, K., Herzig, S., Kulkarni, R.N., and Montminy, M. (2003). TRB3: a tribbles homolog that inhibits Akt/PKB activation by insulin in liver. Science *300*, 1574–1577.

Dutto, I., Tillhon, M., Cazzalini, O., Stivala, L.A., and Prosperi, E. (2014). Biology of the cell cycle inhibitor p21 CDKN1A: molecular mechanisms and relevance in chemical toxicology. Arch. Toxicol. *89*, 155–178.

Eickholt, B.J., Ahmed, A.I., Davies, M., Papakonstanti, E.A., Pearce, W., Starkey, M.L., Bilancio, A., Need, A.C., Smith, A.J., Hall, S.M., et al. (2007). Control of axonal growth and regeneration of sensory neurons by the p110delta PI 3-kinase. Plos One *2*, e869.

El-Deiry, W.S., Tokino, T., Velculescu, V.E., Levy, D.B., Parsons, R., Trent, J.M., Lin, D., Mercer, W.E., Kinzler, K.W., and Vogelstein, B. (1993). WAF1, a potential mediator of p53 tumor suppression. Cell *75*, 817–825.

Ellulu, M., Abed, Y., Rahmat, A., Ranneh, Y., and Ali, F. (2014). Epidemiology of obesity in developing countries: challenges and prevention. Glob. Epidemic Obes. *2*, 2.

Eng, C. (2003). PTEN: one gene, many syndromes. Hum. Mutat. *22*, 183–198.

Engelman, J.A., Luo, J., and Cantley, L.C. (2006). The evolution of phosphatidylinositol 3-kinases as regulators of growth and metabolism. Nat. Rev. Genet. *7*, 606–619.

Everett, L.J., Le Lay, J., Lukovac, S., Bernstein, D., Steger, D.J., Lazar, M.A., and Kaestner, K.H. (2013). Integrative genomic analysis of CREB defines a critical role for transcription factor networks in mediating the fed/fasted switch in liver. BMC Genomics *14*, 337.

Fabrizio, P., Pozza, F., Pletcher, S.D., Gendron, C.M., and Longo, V.D. (2001). Regulation of longevity and stress resistance by Sch9 in yeast. Science *292*, 288–290.

Faivre, S., Kroemer, G., and Raymond, E. (2006). Current development of mTOR inhibitors as anticancer agents. Nat. Rev. Drug Discov. *5*, 671–688.

Falasca, M., and Maffucci, T. (2012). Regulation and cellular functions of class II phosphoinositide 3-kinases. Biochem. J. *443*, 587–601.

Fasshauer, M., Klein, J., Ueki, K., Kriauciunas, K.M., Benito, M., White, M.F., and Kahn, C.R. (2000). Essential role of insulin receptor substrate-2 in insulin stimulation of Glut4 translocation and glucose uptake in brown adipocytes. J. Biol. Chem. *275*, 25494–25501.

Finck, B.N., and Kelly, D.P. (2006). PGC-1 coactivators: inducible regulators of energy metabolism in health and disease. J. Clin. Invest. *116*, 615–622.

Fisher, J.S., Gao, J., Han, D.H., Holloszy, J.O., and Nolte, L.A. (2002). Activation of AMP kinase enhances sensitivity of muscle glucose transport to insulin. Am. J. Physiol. Endocrinol. Metab. *282*, E18–E23.

Fontana, L., and Partridge, L. (2015). Promoting health and longevity through diet: from model organisms to humans. Cell *161*, 106–118.

Fontana, L., Partridge, L., and Longo, V.D. (2010). Extending healthy life span-from yeast to humans. Science *328*, 321–326.

Font-Burgada, J., Sun, B., and Karin, M. (2016). Obesity and Cancer: The oil that feeds the flame. Cell Metab. *23*, 48–62.

Foukas, L.C., Bilanges, B., Bettedi, L., Pearce, W., Ali, K., Sancho, S., Withers, D.J., and Vanhaesebroeck, B. (2013). Long-term p110α PI3K inactivation exerts a beneficial effect on metabolism. EMBO Mol. Med. *5*, 563–571.

Franke, T.F., Kaplan, D.R., Cantley, L.C., and Toker, A. (1997). Direct regulation of the Akt proto-oncogene product by phosphatidylinositol-3,4-bisphosphate. Science *275*, 665–668.

Friedman, D.B., and Johnson, T.E. (1988). A mutation in the age-1 gene in caenorhabditis elegans lengthens life and reduces hermaphrodite fertility. Genetics *118*, 75–86.

Fulco, M., and Sartorelli, V. (2008). Comparing and contrasting the roles of AMPK and SIRT1 in metabolic tissues. Cell Cycle *7*, 3669–3679.

Furet, P., Guagnano, V., Fairhurst, R.A., Imbach-Weese, P., Bruce, I., Knapp, M., Fritsch, C., Blasco, F., Blanz, J., Aichholz, R., et al. (2013). Discovery of NVP-BYL719 a potent and selective phosphatidylinositol-3 kinase alpha inhibitor selected for clinical evaluation. Bioorganic Med. Chem. Lett. *23*, 3741–3748.

Gao, T., Furnari, F., and Newton, A.C. (2005). PHLPP: A phosphatase that directly dephosphorylates Akt, promotes apoptosis, and suppresses tumor growth. Mol. Cell *18*, 13–24.

Gao, X., Zhang, Y., Arrazola, P., Hino, O., Kobayashi, T., Yeung, R.S., Ru, B., and Pan, D. (2002). Tsc tumour suppressor proteins antagonize amino-acid-TOR signalling. Nat. Cell Biol. *4*, 699–704.

Garcia-Cao, I., Song, M.S., Hobbs, R.M., Laurent, G., Giorgi, C., De Boer, V.C.J., Anastasiou, D., Ito, K., Sasaki, A.T., Rameh, L., et al. (2012). Systemic elevation of PTEN induces a tumor-suppressive metabolic state. Cell *149*, 49–62.

Gartel, A.L., and Tyner, A.L. (2002). The role of the cyclin-dependent kinase inhibitor p21 in apoptosis. Mol. Cancer Ther. *1*, 639–649.

Giordano, A., Frontini, A., and Cinti, S. (2016). Convertible visceral fat as a therapeutic target to curb obesity. Nat Rev Drug Discov. *advance online.*

Gonidakis, S., Finkel, S.E., and Longo, V.D. (2010). Genome-wide screen identifies Escherichia coli TCA-cycle-related mutants with extended chronological lifespan dependent on acetate metabolism and the hypoxia-inducible transcription factor ArcA. Aging Cell *9*, 868–881.

Gonzalez-Rodriguez, A., Clampit, J.E., Escribano, O., Benito, M., Rondinone, C.M., and Valverde, A.M. (2007). Developmental switch from prolonged insulin action to increased insulin sensitivity in protein tyrosine phosphatase 1B-deficient hepatocytes. Endocrinology *148*, 594–608.

Goodrick, C.L., Ingram, D.K., Reynolds, M.A., Freeman, J.R., and Cider, N. (1990). Effects of intermittent feeding upon body weight and lifespan in inbred mice: interaction of genotype and age. Mech. Ageing Dev. *55*, 69–87.

Goodyear , L.J. (2008). The exercise pill-too good to be true? N. Engl. J. Med. *359*, 1842–1844.

Gronke, S., Clarke, D.F., Broughton, S., Andrews, T.D., and Partridge, L. (2010). Molecular evolution and functional characterization of drosophila insulin-like peptides. PLoS Genet *6*, e1000857.

Guarente, L. (2013). Calorie restriction and sirtuins revisited. Genes Dev. *27*, 2072–2085.

Guevara-Aguirre, J., Balasubramanian, P., Guevara-Aguirre, M., Wei, M., Madia, F., Cheng, C.W., Hwang, D., Martin-Montalvo, A., Saavedra, J., Ingles, S., et al. (2011). Growth hormone receptor deficiency is associated with a major reduction in pro-aging signaling, cancer, and diabetes in humans. Sci. Transl. Med. *3*, 70ra13.

Haeusler, R.A., Kaestner, K.H., and Accili, D. (2010). FoxOs function synergistically to promote glucose production. J. Biol. Chem. *285*, 35245–35248.

Hall, R.K., Yamasaki, T., Kucera, T., Waltner-Law, M., O'Brien, R., and Granner, D.K. (2000). Regulation of phosphoenolpyruvate carboxykinase and insulin-like growth factor-binding protein-1 gene expression by insulin. The role of winged helix/forkhead proteins. J. Biol. Chem. *275*, 30169–30175.

Hansen, B.C., Newcomb, J.D., Chen, R., and Linden, E.H. (2013). Longitudinal dynamics of body weight change in the development of type 2 diabetes. Obesity *21*, 1643–1649.

Harley, C.B., Futcher, A.B., and Greider, C.W. (1990). Telomeres shorten during ageing of human fibroblasts. Nature *345*, 458–460.

Harper, J.W., Adami, G.R., Wei, N., Keyomarsi, K., and Elledge, S.J. (1993). The p21 Cdk-interacting protein Cipl is a potent inhibitor of Gl cyclin-dependent kinases. Cell *75*, 805–816.

Harrington, L.S., Findlay, G.M., Gray, A., Tolkacheva, T., Wigfield, S., Rebholz, H., Barnett, J., Leslie, N.R., Cheng, S., Shepherd, P.R., et al. (2004). The TSC1-2 tumor suppressor controls insulin-PI3K signaling via regulation of IRS proteins. J. Cell Biol. *166*, 213–223.

Harrison, D.E., Strong, R., Sharp, Z.D., Nelson, J.F., Astle, C.M., Flurkey, K., Nadon, N.L., Wilkinson, J.E., Frenkel, K., Carter, C.S., et al. (2009). Rapamycin fed late in life extends lifespan in genetically heterogeneous mice. Nature *460*, 392–395.

Haruta, T., Uno, T., Kawahara, J., Takano, A., Egawa, K., Sharma, P.M., Olefsky, J.M., and Kobayashi, M. (2000). A rapamycin-sensitive pathway down-regulates insulin signaling via phosphorylation and proteasomal degradation of insulin receptor substrate-1. Mol. Endocrinol. *14*, 783–794.

Harvie, M.N., Pegington, M., Mattson, M.P., Frystyk, J., Dillon, B., Evans, G., Cuzick, J., Jebb, S.A., Martin, B., Cutler, R.G., et al. (2011). The effects of intermittent or continuous energy restriction on weight loss and metabolic disease risk markers: a randomized trial in young overweight women. Int. J. Obes. (Lond). *35*, 714–727.

Haslam, D.W., and James, W.P.T. (2005). Obesity. Lancet *366*, 1197–1209.

Hayflick, L., and Moorhead, P.S. (1961). The serial cultivation of human diploid cell strains. Exp. Cell Res. *25*, 585–621.

Hawkins, P.T., and Stephens, L.R. (1015). PI3K signalling in inflammation. Biochim. Biophys. Acta. *1851*, 882–897.

Herzig, S., Long, F., Jhala, U.S., Hedrick, S., Quinn, R., Bauer, A., Rudolph, D., Schutz, G., Yoon, C., Puigserver, P., et al. (2001). CREB regulates hepatic gluconeogenesis through the coactivator PGC-1. Nature *413*, 179–183.

Houtkooper, R.H., Williams, R.W., and Auwerx, J. (2010). Metabolic networks of longevity. Cell *142*, 9–14.

Iizuka, K., Bruick, R.K., Liang, G., Horton, J.D., and Uyeda, K. (2004). Deficiency of carbohydrate response element-binding protein (ChREBP) reduces lipogenesis as well as glycolysis. Proc. Natl. Acad. Sci. USA *101*, 7281–7286.

Inoki, K., Li, Y., Xu, T., and Guan, K.L. (2003a). Rheb GTpase is a direct target of TSC2 GAP activity and regulates mTOR signaling. Genes Dev. *17*, 1829–1834.

Inoki, K., Zhu, T., and Guan, K.-L. (2003b). TSC2 mediates cellular energy response to control cell growth and survival. Cell *115*, 577–590.

Inoue, N., Yahagi, N., Yamamoto, T., Ishikawa, M., Watanabe, K., Matsuzaka, T., Nakagawa, Y., Takeuchi, Y., Kobayashi, K., Takahashi, A., et al. (2008). Cyclin-dependent kinase inhibitor, p21WAF1/CIP1, is involved in adipocyte differentiation and hypertrophy, linking to obesity, and insulin resistance. J. Biol. Chem. *283*, 21220–21229.

Jacks, T., Remington, L., Williams, B.O., Schmitt, E.M., Halachmi, S., Bronson, R.T., and Weinberg, R.A. (1994). Tumor spectrum analysis in p53-mutant mice. Curr. Biol. *4*, 1–7.

Jeffery, E., Church, C.D., Holtrup, B., Colman, L., and Rodeheffer, M.S. (2015). Rapid depot-specific activation of adipocyte precursor cells at the onset of obesity. Nat. Cell Biol. *4*, 376–385.

Jeong, J.Y., Jeoung, N.H., Park, K.G., and Lee, I.K. (2012). Transcriptional regulation of pyruvate dehydrogenase kinase. Diabetes Metab. J. *36*, 328–335.

Jia, K., Chen, D., and Riddle, D.L. (2004). The TOR pathway interacts with the insulin signaling pathway to regulate C. elegans larval development, metabolism and life span. Development *131*, 3897–3906.

Johnson, J.B., Summer, W., Cutler, R.G., Martin, B., Hyun, D.H., Dixit, V.D., Pearson, M., Nassar, M., Tellejohan, R., Maudsley, S., et al. (2007). Alternate day calorie restriction improves clinical findings and reduces markers of oxidative stress and inflammation in overweight adults with moderate asthma. Free Radic. Biol. Med. *42*, 665–674.

Johnson, S.C., Rabinovitch, P.S., and Kaeberlein, M. (2013). mTOR is a key modulator of ageing and age-related disease. Nature *493*, 338–345.

Jones, R.G., Plas, D.R., Kubek, S., Buzzai, M., Mu, J., Xu, Y., Birnbaum, M.J., and Thompson, C.B. (2005). AMP-activated protein kinase induces a p53-dependent metabolic checkpoint. Mol. Cell *18*, 283–293.

Jozwiak, J., Jozwiak, S., and Wlodarski, P. (2008). Possible mechanisms of disease development in tuberous sclerosis. Lancet Oncol. *9*, 73–79.

Junnila, R.K., List, E.O., Berryman, D.E., Murrey, J.W., and Kopchick, J.J. (2013). The GH/IGF-1 axis in ageing and longevity. Nat. Rev. Endocrinol. *9*, 366–376.

Kaeberlein, M., Powers, R.W., Steffen, K.K., Westman, E.A., Hu, D., Dang, N., Kerr, E.O., Kirkland, K.T., Fields, S., and Kennedy, B.K. (2005). Regulation of yeast replicative life span by TOR and Sch9 in response to nutrients. Science *310*, 1193–1196.

Kaeberlein, T.L., Smith, E.D., Tsuchiya, M., Welton, K.L., Thomas, J.H., Fields, S., Kennedy, B.K., and Kaeberlein, M. (2006). Lifespan extension in caenorhabditis elegans by complete removal of food. Aging Cell *5*, 487–494.

Kahn, S.E., Hull, R.L., and Utzschneider, K.M. (2006). Mechanisms linking obesity to insulin resistance and type 2 diabetes. Nature *444*, 840–846.

Kamijo, T., Zindy, F., Roussel, M.F., Quelle, D.E., Downing, J.R., Ashmun, R.A, Grosveld, G., and Sherr, C.J. (1997). Tumor suppression at the mouse INK4a locus mediated by the alternative reading frame product p19ARF. Cell *91*, 649–659.

Kamijo, T., Bodner, S., Van De Kamp, E., Randle, D.H., and Sherr, C.J. (1999). Tumor spectrum in ARF-deficient mice. Cancer Res. *59*, 2217–2222.

Kapahi, P., Zid, B.M., Harper, T., Koslover, D., Sapin, V., and Benzer, S. (2004). Regulation of lifespan in Drosophila by modulation of genes in the TOR signaling pathway. Curr. Biol. *14*, 885–890.

Katso, R., Okkenhaug, K., Ahmadi, K., White, S., Timms, J., and Waterfield, M.D. (2001). Cellular function of phosphoinositide 3-kinases: implications for development, homeostasis, and cancer. Annu. Rev. Cell Dev. Biol. *17*, 615–675.

Kawaguchi, T., Takenoshita, M., Kabashima, T., and Uyeda, K. (2001). Glucose and cAMP regulate the L-type pyruvate kinase gene by phosphorylation/dephosphorylation of the carbohydrate response element binding protein. Proc. Natl. Acad. Sci. USA *98*, 13710–13715.

Kenyon, C.J. (2010). The genetics of ageing. Nature *464*, 504–512.

Kenyon, C., Chang, J., Gensch, E., Rudner, A., and Tabtiang, R. (1993). A C. elegans mutant that lives twice as long as wild type. Nature *366*, 461–464.

Kersten, S., Seydoux, J., Peters, J.M., Gonzalez, F.J., Desvergne, B., and Wahli, W. (1999). Peroxisome proliferator-activated receptor alpha mediates the adaptive response to fasting. J. Clin. Invest. *103*, 1489–1498.

Kippin, T.E., Martens, D.J., and Van Der Kooy, D. (2005). p21 loss compromises the relative quiescence of forebrain stem cell proliferation leading to exhaustion of their proliferation capacity. Genes Dev. *19*, 756–767.

Kitaura, H., Shinshi, M., Uchikoshi, Y., Ono, T., Tsurimoto, T., Yoshikawa, H., Iguchi-Ariga, S.M., and Ariga, H. (2000). Reciprocal regulation via protein-protein interaction between c-myc and p21(cip1/waf1/sdi1) in DNA replication and transcription. J. Biol. Chem. *275*, 10477–10483.

Van Der Klaauw, A.A., and Farooqi, I.S. (2015). The hunger genes: pathways to obesity. Cell *161*, 119–132.

Knight, Z.A, and Shokat, K.M. (2007). Chemically targeting the PI3K family. Biochem. Soc. Trans. *35*, 245–249.

Knowles, B.B., Howe, C.C., and Aden, D.P. (1980). Human hepatocellular carcinoma cell lines secrete the major plasma proteins and hepatitis B surface antigen. Science *209*, 497–499.

Kobayashi, N., Ueki, K., Okazaki, Y., Iwane, A., Kubota, N., Ohsugi, M., Awazawa, M., Kobayashi, M., Sasako, T., Kaneko, K., et al. (2011). Blockade of class IB phosphoinositide-3 kinase ameliorates obesity-induced inflammation and insulin resistance. Proc. Natl. Acad. Sci. USA *108*, 5753–5758.

Koh, H.J., Brandauer, J., and Goodyear, L.J. (2008). LKB1 and AMPK and the regulation of skeletal muscle metabolism. Curr. Opin. Clin. Nutr. Metab. Care *11*, 227–232.

Kondoh, H., Lleonart, M.E., Gil, J., Wang, J., Degan, P., Peters, G., Martinez, D., Carnero, A., and Beach, D. (2005). Glycolytic enzymes can modulate cellular life span. Cancer Res. *65*, 177–185.

Kops, G.J., de Ruiter, N.D., de Vries-Smits, A.M., Powell, D.R., Bos, J.L., and Burgering, B.M. (1999). Direct control of the Forkhead transcription factor AFX by protein kinase B. Nature *398*, 630–634.

Kops, G.J., Dansen, T.B., Polderman, P.E., Saarloos, I., Wirtz, K.W., Coffer, P.J., Huang, T.T., Bos, J.L., Medema, R.H., and Burgering, B.M. (2002). Forkhead transcription factor FOXO3a protects quiescent cells from oxidative stress. Nature *419*, 316–321.

Kress, T.R., Sabò, A., and Amati, B. (2015). MYC: connecting selective transcriptional control to global RNA production. Nat. Rev. Cancer *15*, 593–607.

Kruiswijk, F., Labuschagne, C.F., and Vousden, K.H. (2015). p53 in survival, death and metabolic health: a lifeguard with a licence to kill. Nat. Rev. Mol. Cell Biol. *16*, 393–405.

De la Cueva, E., García-Cao, I., Herranz, M., López, P., García-Palencia, P., Flores, J.M., Serrano, M., Fernández-Piqueras, J., and Martín-Caballero, J. (2006). Tumorigenic activity of p21Waf1/Cip1 in thymic lymphoma. Oncogene *25*, 4128–4132.

Labaer, J., Garrett, M.D., Stevenson, L.F., Slingerland, J.M., Sandhu, C., Chou, H.S., Fattaey, A., and Harlow, E. (1997). New functional activities for the p21 family of CDK inhibitors. Genes Dev. *11*, 847–862.

Lagouge, M., Argmann, C., Gerhart-Hines, Z., Meziane, H., Lerin, C., Daussin ,F., Messadeq, N., Milne, J., Lambert, P., Elliott, P., et al. (2006). Resveratrol improves mitochondrial function and protects against metabolic disease by activating SIRT1 and PGC-1alpha. Cell *127*, 1109–22.

Langmead, B., Trapnell, C., Pop, M., and Salzberg, S.L. (2009). Ultrafast and memory-efficient alignment of short DNA sequences to the human genome. Genome Biol. *10*, 1–10.

Laplante, M., and Sabatini, D.M. (2013). Regulation of mTORC1 and its impact on gene expression at a glance. J. Cell Sci. *126*, 1713–1719.

Laron, Z. (2008). The GH-IGF1 axis and longevity. The paradigm of IGF1 deficiency. Hormones *7*, 24–27.

Lee, S., and Helfman, D.M. (2004). Cytoplasmic p21Cip1 is involved in ras-induced inhibition of the ROCK/LIMK/Cofilin pathway. J. Biol. Chem. *279*, 1885–1891.

Lee, A.C., Fenster, B.E., Ito, H., Takeda, K., Bae, N.S., Hirai, T., Yu, Z.X., Ferrans, V.J., Howard, B.H., and Finkel, T. (1999). Ras proteins induce senescence by altering the intracellular levels of reactive oxygen species. J. Biol. Chem. *274*, 7936–7940.

Lee, C., Raffaghello, L., Brandhorst, S., Safdie, F.M., Bianchi, G., Martin-Montalvo, A., Pistoia, V., Wei, M., Hwang, S., Merlino, A., et al. (2012). Fasting cycles retard growth of tumors and sensitize a range of cancer cell types to chemotherapy. Sci. Transl. Med. *4*, 124ra27.

Lempradl, A., Pospisilik, J.A., and Penninger, J.M. (2015). Exploring the emerging complexity in transcriptional regulation of energy homeostasis. Nat. Rev. Genet. *16*, 665–681.

Leone, T.C., Weinheimer, C.J., and Kelly, D.P. (1999). A critical role for the peroxisome proliferator-activated receptor alpha (PPARalpha) in the cellular fasting response: the PPARalpha-null mouse as a model of fatty acid oxidation disorders. Proc. Natl. Acad. Sci. USA *96*, 7473–7478.

Li, D.M., and Sun, H. (1997). TEP1, encoded by a candidate tumor suppressor locus, is a novel protein tyrosine phosphatase regulated by transforming growth factor-beta. Cancer Res. *57*, 2124–2129.

Li, H., Handsaker, B., Wysoker, A., Fennell, T., Ruan, J., Homer, N., Marth, G., Abecasis, G., Durbin, R., and 1000 Genome Project Data Processing Subgroup (2009). The sequence alignment/map format and SAMtools. Bioinformatics *25*, 2078–2079.

Li, J., Yen, C., Liaw, D., Podsypanina, K., Bose, S., Wang, S.I., Puc, J., Miliaresis, C., Rodgers, L., McCombie, R., et al. (1997). PTEN, a putative protein tyrosine phosphatase gene mutated in human brain, breast, and prostate cancer. Science *275*, 1943–1947.

Li, X., Monks, B., Ge, Q., and Birnbaum, M.J. (2007). Akt/PKB regulates hepatic metabolism by directly inhibiting PGC-1alpha transcription coactivator. Nature *447*, 1012–1016.

Li, Y., Dowbenko, D., and Lasky, L.A. (2002). AKT/PKB phosphorylation of p21Cip/WAF1 enhances protein stability of p21Cip/WAF1 and promotes cell survival. J. Biol. Chem. *277*, 11352–11361.

Li, Y., Xu, S., Mihaylova, M.M., Zheng, B., Hou, X., Jiang, B., Park, O., Luo, Z., Lefai, E., Shyy, J.Y., et al. (2011). AMPK phosphorylates and inhibits SREBP activity to attenuate hepatic steatosis and atherosclerosis in diet-induced insulin-resistant mice. Cell Metab. *13*, 376–388.

Libina, N., Berman, J.R., and Kenyon, C. (2003). Tissue-specific activities of C. elegans DAF-16 in the regulation of lifespan. Cell *115*, 489–502.

Liu, P., Cheng, H., Roberts, T.M., and Zhao, J.J. (2009). Targeting the phosphoinositide 3-kinase pathway in cancer. Nat. Rev. Drug Discov. *8*, 627–644.

Liu, P., Gan, W., Chin, Y.R., Ogura, K., Guo, J., Zhang, J., Wang, B., Blenis, J., Cantley, L.C., Toker, A., et al. (2015). PtdIns(3,4,5)P3-Dependent Activation of the mTORC2 Kinase Complex. Cancer Discov. *5*, 1194–1209.

Liu, Y., Dentin, R., Chen, D., Hedrick, S., Ravnskjaer, K., Schenk, S., Milne, J., Meyers, D.J., Cole, P., Yates, J., et al. (2008). A fasting inducible switch modulates gluconeogenesis via activator/coactivator exchange. Nature *456*, 269–273.

Long, X., Lin, Y., Ortiz-Vega, S., Yonezawa, K., and Avruch, J. (2005). Rheb binds and regulates the mTOR kinase. Curr. Biol. *15*, 702–713.

Longo, V.D., and Mattson, M.P. (2014). Fasting: molecular mechanisms and clinical applications. Cell Metab. *19*, 181–192.

Longuet, C., Sinclair, E.M., Maida, A., Baggio, L.L., Maziarz, M., Charron, M.J., and Drucker, D.J. (2008). The glucagon receptor is required for the adaptive metabolic response to fasting. Cell Metab. *8*, 359–371.

López, M., Lage, R., Saha, A.K., Pérez-Tilve, D., Vázquez, M.J., Varela, L., Sangiao-Alvarellos, S., Tovar, S., Raghay, K., Rodríguez-Cuenca, S., et al. (2008). Hypothalamic fatty acid metabolism mediates the orexigenic action of ghrelin. Cell Metab. *7*, 389–399.

López, M., Varela, L., Vázquez, M.J., Rodríguez-Cuenca, S., González, C.R., Velagapudi, V.R., Morgan, D. a, Schoenmakers, E., Agassandian, K., Lage, R., et al. (2010). Hypothalamic AMPK and fatty acid metabolism mediate thyroid regulation of energy balance. Nat. Med. *16*, 1001–1008.

Lorenzo, M., Valverde, A.M., Teruel, T., and Benito, M. (1993). IGF-I is a mitogen involved in differentiation-related gene expression in fetal rat brown adipocytes. J. Cell Biol. *123*, 1567–1575.

Lowell, B.B., and Spiegelman, B.M. (2000). Towards a molecular understanding of adaptive thermogensis. Nature *404*, 652–660.

Luo, J., Field, S.J., Lee, J.Y., Engelman, J.A., and Cantley, L.C. (2005). The p85 regulatory subunit of phosphoinositide 3-kinase down-regulates IRS-1 signaling via the formation of a sequestration complex. J. Cell Biol. *170*, 455–464.

Maehama, T., and Dixon, J.E. (1998). The tumor suppressor, PTEN/MMAC1, dephosphorylates the lipid second messenger, phosphatidylinositol 3,4,5-trisphosphate. J. Biol. Chem. *273*, 13375–13378.

Manning, B.D., and Cantley, L.C. (2007). AKT/PKB signaling: navigating downstream. cell *129*, 1261–1274.

van Marken Lichtenbelt, W.D., Vanhommerig, J.W., Smulders, N.M., Drossaerts, J.M., Kemerink, G.J., Bouvy, N.D., Schrauwen, P., and Teule, G.J. (2009). Cold-activated brown adipose tissue in healthy men. N. Engl. J. Med. *360*, 1500–1508.

Martín-Caballero, J., Flores, J.M., García-Palencia, P., and Serrano, M. (2001). Tumor susceptibility of p21waf1/cip1-deficient mice. Cancer Res. *61*, 6234–6238.

Martínez de Morentin, P.B., González-García, I., Martins, L., Lage, R., Fernández-Mallo, D., Martínez-Sánchez, N., Ruíz-Pino, F., Liu, J., Morgan, D.A., Pinilla, L., et al. (2014). Estradiol regulates brown adipose tissue thermogenesis via hypothalamic AMPK. Cell Metab. *20*, 41–53.

Matoba, S., Kang, J.G., Patino, W.D., Wragg, A., Boehm, M., Gavrilova, O., Hurley, P.J., Bunz, F., and Hwang, P.M. (2006). p53 regulates mitochondrial respiration. Science *312*, 1650–1653.

Mattison, J.A., Roth, G.S., Beasley, T.M., Tilmont, E.M., Handy, A.M., Herbert, R.L., Longo, D.L., Allison, D.B., Young, J.E., Bryant, M., et al. (2012). Impact of caloric restriction on health and survival in rhesus monkeys from the NIA study. Nature *489*, 318–321.

Mattson, M.P. (2012). Energy intake and exercise as determinants of brain health and vulnerability to injury and disease. Cell Metab. *16*, 706–722.

Mayo, L.D., and Donner, D.B. (2001). A phosphatidylinositol 3-kinase/Akt pathway promotes translocation of Mdm2 from the cytoplasm to the nucleus. Proc. Natl. Acad. Sci. USA *98*, 11598–11603.

McNelis, J., and Olefsky, J. (2014). Macrophages, immunity, and metabolic disease. Immunity *41*, 36–48.

Michaloglou, C., Vredeveld, L.C., Soengas, M.S., Denoyelle, C., Kuilman, T., van der Horst, C.M., Majoor, D.M., Shay, J.W., Mooi, W.J., and Peeper, D.S. (2005). BRAFE600-associated senescence-like cell cycle arrest of human naevi. Nature *436*, 720–724.

Mihaylova, M.M., Vasquez, D.S., Ravnskjaer, K., Denechaud, P.D., Yu, R.T., Alvarez, J.G., Downes, M., Evans, R.M., Montminy, M., and Shaw, R.J. (2011). Class IIa histone deacetylases are hormone-activated regulators of FOXO and mammalian glucose homeostasis. Cell *145*, 607–621.

Minamino, T., Orimo, M., Shimizu, I., Kunieda, T., Yokoyama, M., Ito, T., Nojima, A., Nabetani, A., Oike, Y., Matsubara, et al. (2009). A crucial role for adipose tissue p53 in the regulation of insulin resistance. Nat. Med. *15*, 1082–1087.

Mitchell, J.R., Verweij, M., Brand, K., van de Ven, M., Goemaere, N., van den Engel, S., Chu, T., Forrer, F., Müller, C., de Jong, M., et al. (2010). Short-term dietary restriction and fasting precondition against ischemia reperfusion injury in mice. Aging Cell *9*, 40–53.

Mitchell, S.J., Martin-Montalvo, A., Mercken, E.M., Palacios, H.H., Ward, T.M., Abulwerdi, G., Minor, R.K., Vlasuk, G.P., Ellis, J.L., Sinclair, D.A., et al. (2014). The SIRT1 activator SRT1720 extends lifespan and improves health of mice fed a standard diet. Cell Rep. *6*, 836–843.

Moldovan, G.L., Pfander, B., and Jentsch, S. (2007). PCNA, the maestro of the replication fork. Cell *129*, 665–679.

Müller, H., de Toledo, F.W., and Resch, K.L. (2001). Fasting followed by vegetarian diet in patients with rheumatoid arthritis: a systematic review. Scand. J. Rheumatol. *30*, 1–10.

Muñoz-Espín, D., and Serrano, M. (2014). Cellular senescence: from physiology to pathology. Nat. Rev. Mol. Cell Biol. *15*, 482–496.

Naaz, A., Holsberger, D.R., Iwamoto, G.A., Nelson, A., Kiyokawa, H., and Cooke, P.S. (2004). Loss of cyclin-dependent kinase inhibitors produces adipocyte hyperplasia and obesity. FASEB J. *18*, 1925–1927.

Nemoto, S., Fergusson, M.M., and Finkel, T. (2005). SIRT1 functionally interacts with the metabolic regulator and transcriptional coactivator PGC-1α. J. Biol. Chem. *280*, 16456–16460.

Ni, Y.G., Wang, N., Cao, D.J., Sachan, N., Morris, D.J., Gerard, R.D., Kuro-O, M., Rothermel, B.A., and Hill, J.A.(2007). FoxO transcription factors activate Akt and attenuate insulin signaling in heart by inhibiting protein phosphatases. Proc. Natl. Acad. Sci. USA *104*, 20517–20522.

Nobukuni, T., Joaquin, M., Roccio, M., Dann, S.G., Kim, S.Y., Gulati, P., Byfield, M.P., Backer, J.M., Natt, F., Bos, J.L., et al. (2005). Amino acids mediate mTOR/raptor signaling through activation of class 3 phosphatidylinositol 3OH-kinase. Proc. Natl. Acad. Sci. USA *102*, 14238–14243.

Ogden, C.L., Carroll, M.D., Kit, B.K., and Flegal, K.M. (2014). Prevalence of childhood and adult obesity in the United States, 2011-2012. JAMA *311*, 806–814.

Ogryzko, V.V., Hirai, T.H., Russanova, V.R., Barbie, D.A., and Howard, B.H. (1996). Human fibroblast commitment to a senescence-like state in response to histone deacetylase inhibitors is cell cycle dependent. Mol. Cell. Biol. *16*, 5210–5218.

Okar, D.A., Lange, A.J., Manzano, À., Navarro-Sabatè, A., Riera, L., and Bartrons, R. (2001). PFK-2/FBPase-2: maker and breaker of the essential biofactor fructose-2,6-bisphosphate. Trends Biochem. Sci. *26*, 30–35.

Ortega-Molina, A., Efeyan, A., Lopez-Guadamillas, E., Muñoz-Martin, M., Gómez-López, G., Cañamero, M., Mulero, F., Pastor, J., Martinez, S., Romanos, E., et al. (2012). Pten positively regulates brown adipose function, energy expenditure, and longevity. Cell Metab. *15*, 382–394.

Padmanabhan, S., Mukhopadhyay, A., Narasimhan, S.D., Tesz, G., Czech, M.P., and Tissenbaum, H.A. (2009). A PP2A regulatory subunit regulates C. elegans insulin/igf-1 signaling by modulating AKT-1 phosphorylation. Cell *136*, 939–951.

Pal, A., Barber, T.M., Van de Bunt, M., Rudge, S.A., Zhang, Q., Lachlan, K.L., Cooper, N.S., Linden, H., Levy, J.C., Wakelam, M.J., et al. (2012). Mutations as a cause of constitutive insulin sensitivity and obesity. N. Engl. J. Med. *367*, 1002–1011.

Parrinello, S., Samper, E., Krtolica, A., Goldstein, J., Melov, S., and Campisi, J. (2003). Oxygen sensitivity severely limits the replicative lifespan of murine fibroblasts. Nat. Cell Biol. *5*, 741–747.

Pawlak, M., Lefebvre, P., and Staels, B. (2015). Molecular mechanism of PPARα action and its impact on lipid metabolism, inflammation and fibrosis in non-alcoholic fatty liver disease. J. Hepatol. *62*, 720–733.

Peckham, S.C., Entenman, C. and Carroll, H.W. (1962). The influence of a hypercaloric diet on gross body and adipose tissue composition in the rat. J. Nutr. *77*, 187–197.

Perino, A., Beretta, M., Kilić, A., Ghigo, A., Carnevale, D., Repetto, I.E., Braccini, L., Longo, D., Liebig-Gonglach, M., Zaglia, T., et al. (2014). Combined inhibition of PI3Kβ and PI3Kγ reduces fat mass by enhancing α-MSH-dependent sympathetic drive. Sci. Signal. *7*, ra110.

del Peso, L., González-García, M., Page, C., Herrera, R., and Nuñez, G. (1997). Interleukin-3-induced phosphorylation of BAD through the protein kinase Akt. Science *278*, 687–689.

Philipp, J., Vo, K., Gurley, K.E., Seidel, K., and Kemp, C.J. (1999). Tumor suppression by p27Kip1 and p21Cip1 during chemically induced skin carcinogenesis. Oncogene *18*, 4689–4698.

Ponugoti, B., Kim, D.H., Xiao, Z., Smith, Z., Miao, J., Zang, M., Wu, S.Y., Chiang, C.M., Veenstra, T.D., and Kemper, J.K. (2010). SIRT1 deacetylates and inhibits SREBP-1C activity in regulation of hepatic lipid metabolism. J. Biol. Chem. *285*, 33959–33970.

Potter, C.J., Pedraza, L.G., and Xu, T. (2002). Akt regulates growth by directly phosphorylating Tsc2. Nat. Cell Biol. *4*, 658–665.

Powers, R.W., Kaeberlein, M., Caldwell, S.D., Kennedy, B.K., and Fields, S. (2006). Extension of chronological life span in yeast by decreased TOR pathways. Genes Dev. *20*, 174–184.

Puigserver, P., Rhee, J., Donovan, J., Walkey, C.J., Yoon, J.C., Oriente, F., Kitamura, Y., Altomonte, J., Dong, H., Accili, D., and Spiegelman, B.M. (2003). Insulin-regulated hepatic gluconeogenesis through FOXO1-PGC-1alpha interaction. Nature *423*, 550–555.

Puyol, M., Martín, A., Dubus, P., Mulero, F., Pizcueta, P., Khan, G., Guerra, C., Santamaría, D., and Barbacid, M. (2010). A synthetic lethal interaction between k-ras oncogenes and cdk4 unveils a therapeutic strategy for non-small cell lung carcinoma. Cancer Cell *18*, 63–73.

Puzio-Kuter, A.M. (2011). The role of p53 in metabolic regulation. Genes Cancer *2*, 385–391.

Qiao, L.Y., Zhande, R., Jetton, T.L., Zhou, G., and Sun, X.J. (2002). In vivo phosphorylation of insulin receptor substrate 1 at serine 789 by a novel serine kinase in insulin-resistant rodents. J. Biol. Chem. *277*, 26530–26539.

Raffaghello, L., Lee, C., Safdie, F.M., Wei, M., Madia, F., Bianchi, G., and Longo, V.D. (2008). Starvation-dependent differential stress resistance protects normal but not cancer cells against high-dose chemotherapy. Proc. Natl. Acad. Sci. USA *105*, 8215–8220.

Raffaghello, L., Safdie, F., Bianchi, G., Dorff, T., Fontana, L., and Longo, V.D. (2010). Fasting and differential chemotherapy protection in patients. Cell Cycle *9*, 4474–4476.

Rakhshandehroo,M., Knoch, B., Müller, M., and Kersten, S. (2010). Peroxisome proliferator-activated receptor alpha target genes. PPAR Res. *2010*.

Randle, P.J. (1998). Regulatory interactions between lipids and carbohydrates: the glucose fatty acid cycle after 35 years. Diabetes Metab. Rev. *14*, 263–283.

Raught, B., Peiretti, F., Gingras, A.C., Livingstone, M., Shahbazian, D., Mayeur, G.L., Polakiewicz, R.D., Sonenberg, N., and Hershey, J.W. (2004). Phosphorylation of eucaryotic translation initiation factor 4B Ser422 is modulated by S6 kinases. EMBO J. *23*, 1761–1769.

Reilly, S.M., Chiang, S.H., Decker, S.J., Chang, L., Uhm, M., Larsen, M.J., Rubin, J.R., Mowers, J., White, N.M., Hochberg, I., et al. (2013). An inhibitor of the protein kinases TBK1 and IKK-ε improves obesity-related metabolic dysfunctions in mice. Nat. Med. *19*, 313–21.

Rena, G., Shaodong, G., Cichy, S.C., Unterman, T.G., and Cohen, P. (1999). Phosphorylation of the transcription factor forkhead family member FKHR by protein kinase B. J. Biol. Chem. *274*, 17179–17183.

Robertson, L.T., and Mitchell, J.R. (2013). Benefits of short-term dietary restriction in mammals. Exp. Gerontol. *48*, 1043–1048.

Rubinsztein, D.C., Mariño, G., and Kroemer, G. (2011). Autophagy and aging. Cell *146*, 682–695.

Rui, L. (2014). Energy metabolism in the liver. Compr. Physiol. *4*, 177–197.

Sabatini, D.M. (2006). mTOR and cancer: insights into a complex relationship. Nat. Rev. Cancer *6*, 10–15.

Safdie, F.M., Dorff, T., Quinn, D., Fontana, L., Wei, M., Lee, C., Cohen, P., and Longo, V.D. (2009). Fasting and cancer treatment in humans: a case series report. Aging (Albany. NY). *1*, 988–1007.

Salphati, L., Heffron, T.P., Alicke, B., Nishimura, M., Barck, K., Carano, R.A., Cheong, J., Edgar, K.A., Greve, J., Kharbanda, S., et al. (2012). Targeting the PI3K pathway in the brain-efficacy of a PI3K inhibitor optimized to cross the blood-brain barrier. Clin. Cancer Res. *18*, 6239–6248.

Samuels, Y., Wang, Z., Bardelli, A., Silliman, N., Ptak, J., Szabo, S., Yan, H., Gazdar, A., Powell, S.M., Riggins, G.J., et al. (2004). High frequency of mutations of the PIK3CA gene in human cancers. Science *304*, 554.

Sancak, Y., Thoreen, C.C., Peterson, T.R., Lindquist, R.A., Kang, S.A., Spooner, E., Carr, S.A., and Sabatini, D.M. (2007). PRAS40 is an insulin-regulated inhibitor of the mTORC1 protein kinase. Mol. Cell *25*, 903–915.

Sano, H., Kane, S., Sano, E., Mîinea, C.P., Asara, J.M., Lane, W.S., Garner, C.W., and Lienhard, G.E. (2003). Insulin-stimualted phosphorylation of a rab GTPase-activiating protein regulates GLUT4 translocation. J. Biol. Chem. *278*, 14599–14602.

Sansal, I., and Sellers, W.R. (2004). The biology and clinical relevance of the PTEN tumor suppressor pathway. J. Clin. Oncol. *22*, 2954–2963.

Sarbassov, D.D., Guertin, D.A., Ali, S.M., and Sabatini, D.M. (2005). Phosphorylation and regulation of AKT/PKB by the rictor-mTOR complex. Science *307*, 1098–1101.

Schmoll, D., Walker, K.S., Alessi, D.R., Grempler, R., Burchell, A., Guo, S., Walther, R., and Unterman, T.G. (2000). Regulation of glucose-6-phosphatase gene expression by protein kinase B-alpha and the forkhead transcription factor FKHR. Evidence for insulin response unit-dependent and -independent effects of insulin on promoter activity. J. Biol. Chem. *275*, 36324–36333.

Schu, P.V, Takegawa, K., Fry, M.J., Stack, J.H., Waterfield, M.D., and Emr, S.D. (1993). Phosphatidylinositol 3-kinase encoded by yeast VPS34 gene essential for protein sorting. Science *260*, 88–91.

Selman, C., Tullet, J.M., Wieser, D., Irvine, E., Lingard, S.J., Choudhury, A.I., Claret, M., Al-Qassab, H., Carmignac, D., Ramadani, F., et al. (2009). Ribosomal protein S6 kinase 1 signaling regulates mammalian life span. Science *326*, 140–144.

Sengupta, S., Peterson, T.R., and Sabatini, D.M. (2010). Regulation of the mTOR complex 1 pathway by nutrients, growth factors, and stress. Mol. Cell *40*, 310–322.

Seoane, J., Le, H. Van, Shen, L., Anderson, S.A., and Massagué, J. (2004). Integration of smad and forkhead pathways in the control of neuroepithelial and glioblastoma cell proliferation. Cell *117*, 211–223.

Serrano, M., Lee, H.W., Chin, L., Cordon-Cardo, C., Beach, D., and DePinho, R.A. (1996). Role of the INK4a locus in tumor suppression and cell mortality. Cell *85*, 27–37.

Serrano, M., Lin, A.W., McCurrach, M.E., Beach, D., and Lowe, S.W. (1997). Oncogenic ras provokes premature cell senescence associated with accumulation of p53 and p16(INK4a). Cell *88*, 593–602.

Sherr, C.J. (2004). Principles of tumor suppression. Cell *116*, 235–246.

Shiohara, M., El-Deiry, W.S., Wada, M., Nakamaki, T., Takeuchi, S., Yang, R., Chen, D.L., Vogelstein, B., and Koeffler, H.P. (1994). Absence of WAF1 mutations in a variety of human malignancies. Blood *84*, 3781–3784.

Shugg, R.P, Thomson, A., Tanabe, N., Kashishian, A., Steiner, B.H., Puri, K.D., Pereverzev, A., Lannutti, B.J., Jirik, F.R., Dixon, S.J., and Sims, S.M. (2013). Effects of isoform-selective phosphatidylinositol 3-kinase inhibitors on osteoclasts: actions on cytoskeletal organization, survival, and resorption. J. Biol. Chem. *288*, 35346–35357.

Snowden, A.W., Anderson, L.A., Webster, G.A., and Perkins, N.D. (2000). A novel transcriptional repression domain mediates p21(WAF1/CIP1) induction of p300 transactivation. Mol. Cell. Biol. *20*, 2676–2686.

Sohn, J.W., Elmquist, J.K., and Williams, K.W. (2013). Neuronal circuits that regulate feeding behavior and metabolism. Trends Neurosci. *36*, 504–512.

Sokolović, A., van Roomen, C.P., Ottenhoff, R., Scheij, S., Hiralall, J.K., Claessen, N., Aten, J., Oude Elferink, R.P., Groen, A.K., and Sokolović, M. (2013). Fasting reduces liver fibrosis in a mouse model for chronic cholangiopathies. Biochim. Biophys. Acta *1832*, 1482–1491.

Solinas, G., Naugler, W., Galimi, F., Lee, M.S., and Karin, M. (2006). Saturated fatty acids inhibit induction of insulin gene transcription by JNK-mediated phosphorylation of insulin-receptor substrates. Proc. Natl. Acad. Sci. USA *103*, 16454–16459.

Solinas, G., Vilcu, C., Neels, J.G., Bandyopadhyay, G.K., Luo, J.L., Naugler, W., Grivennikov, S., Wynshaw-Boris, A., Scadeng, M., Olefsky, J.M., and Karin, M. (2007). JNK1 in hematopoietically derived cells contributes to diet-induced inflammation and insulin resistance without affecting obesity. Cell Metab. *6*, 386–397.

Solon-Biet, S.M., McMahon, A.C., Ballard, J.W.O., Ruohonen, K., Wu, L.E., Cogger, V.C., Warren, A., Huang, X., Pichaud, N., Melvin, R.G., et al. (2014). The ratio of macronutrients, not caloric intake, dictates cardiometabolic health, aging, and longevity in ad libitum-fed mice. Cell Metab. *19*, 418–430.

Stambolic, V., Suzuki, A., De la Pompa, J.L., Brothers, G.M., Mirtsos, C., Sasaki, T., Ruland, J., Penninger, J.M., Siderovski, D.P., and Mak, T.W. (1998). Negative regulation of PKB/Akt-dependent cell survival by the tumor suppressor PTEN. Cell *95*, 29–39.

Steck, P.A., Pershouse, M.A., Jasser, S.A., Yung, W.K., Lin, H., Ligon, A.H., Langford, L.A., Baumgard, M.L., Hattier, T., Davis, T., et al. (1997). Identification of a candidate tumour suppressor gene, MMAC1, at chromosome 10q23.3 that is mutated in multiple advanced cancers. Nat. Genet. *15*, 356–362.

Steinberg, M.D., Zingg, W. and Angel, A. (1962). Studies of the number and volume of fat cells in adipose tissue. J. Pediatr. *61*, 299–300.

Stephens, L., Anderson, K., Stokoe, D., Erdjument-Bromage, H., Painter, G.F., Holmes, A.B., Gaffney, P.R., Reese, C.B., McCormick, F., Tempst, P., et al. (1998). Protein kinase B kinases that mediate phosphatidylinositol 3,4,5-trisphosphate-dependent activation of protein kinase B. Science *279*, 710–714.

Strissel, K.J., Stancheva, Z., Miyoshi, H., Perfield, J.W., DeFuria, J., Jick, Z., Greenberg, A.S., and Obin, M.S. (2007). Adipocyte death, adipose tissue remodeling, and obesity complications. Diabetes *56*, 2910–2918.

Sunters, A., Fernández De Mattos, S., Stahl, M., Brosens, J.J., Zoumpoulidou, G., Saunders, C.A., Coffer, P.J., Medema, R.H., Coombes, R.C., and Lam, E.W. (2003). FoxO3a transcriptional regulation of bim controls apoptosis in paclitaxel-treated breast cancer cell lines. J. Biol. Chem. *278*, 49795–49805.

Tang, E.D., Nuñez, G., Barr, F.G., and Guan, K.L. (1999). Negative regulation of the forkhead transcription factor FKHR by Akt. J. Biol. Chem. *274*, 16741–16746.

Taniguchi, K., and Karin, M. (2014). IL-6 and related cytokines as the critical lynchpins between inflammation and cancer. Semin. Immunol. *26*, 54–74.

Terauchi, Y., Tsuji, Y., Satoh, S., Minoura, H., Murakami, K., Okuno, A., Inukai, K., Asano, T., Kaburagi, Y., Ueki, K., et al. (1999). Increased insulin sensitivity and hypoglycaemia in mice lacking the p85 alpha subunit of phosphoinositide 3-kinase. Nat. Genet. *21*, 230–235.

Thompson, H.J., Zhu, Z., and Jiang, W. (2003). Dietary energy restriction in breast cancer prevention. J. Mammary Gland Biol. Neoplasia *8*, 133–142.

Tinkum, K.L., White, L.S., Marpegan, L., Herzog, E., Piwnica-Worms, D., and Piwnica-Worms, H. (2013). Forkhead box O1 (FOXO1) protein, but not p53, contributes to robust induction of p21 expression in fasted mice. J. Biol. Chem. *288*, 27999–28008.

Trapnell, C., Roberts, A., Goff, L., Pertea, G., Kim, D., Kelley, D.R., Pimentel, H., Salzberg, S.L., Rinn, J.L., and Pachter, L. (2012). Differential gene and transcript expression analysis of RNA-seq experiments with TopHat and Cufflinks. Nat. Protoc. *7*, 562–578.

Tremblay, F., Brûlé, S., Hee Um, S., Li, Y., Masuda, K., Roden, M., Sun, X.J., Krebs, M., Polakiewicz, R.D., Thomas, G., and Marette, A. (2007). Identification of IRS-1 Ser-1101 as a target of S6K1 in nutrient- and obesity-induced insulin resistance. Proc. Natl. Acad. Sci. USA *104*, 14056–14061.

Trotman, L.C., Wang, X., Alimonti, A., Chen, Z., Teruya-Feldstein, J., Yang, H., Pavletich, N.P., Carver, B.S., Cordon-Cardo, C., Erdjument-Bromage, H., et al. (2007). Ubiquitination regulates PTEN nuclear import and tumor suppression. Cell *128*, 141–156.

Tzatsos, A., and Kandror, K.V. (2006). Nutrients suppress phosphatidylinositol 3-kinase/Akt signaling via raptor-dependent mTOR-mediated insulin receptor substrate 1 phosphorylation. Mol. Cell. Biol. *26*, 63–76.

Uddin, S., Hussain, A.R., Siraj, A.K., Khan, O.S., Bavi, P.P., and Al-Kuraya, K.S. (2011). Role of leptin and its receptors in the pathogenesis of thyroid cancer. Int. J. Clin. Exp. Pathol. *4*, 637–643.

Ueki, K., Yballe, C.M., Brachmann, S.M., Vicent, D., Watt, J.M., Kahn, C.R., and Cantley, L.C. (2002). Increased insulin sensitivity in mice lacking p85beta subunit of phosphoinositide 3-kinase. Proc. Natl. Acad. Sci.USA *99*, 419–424.

Um, S.H., Frigerio, F., Watanabe, M., Picard, F., Joaquin, M., Sticker, M., Fumagalli, S., Allegrini, P.R., Kozma, S.C., Auwerx, J., and Thomas, G. (2004). Absence of S6K1 protects against age- and diet-induced obesity while enhancing insulin sensitivity. Nature *431*, 200–205.

Vanhaesebroeck, B., Guillermet-Guibert, J., Graupera, M., and Bilanges, B. (2010). The emerging mechanisms of isoform-specific PI3K signalling. Nat. Rev. Mol. Cell Biol. *11*, 329–341.

Varady, K.A., and Hellerstein, M.K. (2007). Alternate-day fasting and chronic disease prevention: a review of human and animal trials. Am. J. Clin. Nutr. *86*, 7–13.

Varady, K.A., Bhutani, S., Church, E.C., and Klempel, M.C. (2009). Short-term modified alternate-day fasting: a novel dietary strategy for weight loss and cardioprotection in obese adults. Am. J. Clin. Nutr. *90*, 1138–1143.

Vega, R.B., Huss, J.M., and Kelly, D.P. (2000). The coactivator PGC-1 cooperates with peroxisome proliferator-activated receptor alpha in transcriptional control of nuclear genes encoding mitochondrial fatty acid oxidation enzymes. Mol. Cell. Biol. *20*, 1868–1876.

Vézina, C., Kudelski, A., and Sehgal, S.N. (1975). Rapamycin (AY-22, 989) a new antifungal antibiotic. J. Antibiot. (Tokyo). *28*, 721–726.

Virtanen, K.A., Lidell, M.E., Orava, J., Heglind, M., Westergren, R., Niem, T., Taittonen, M., Laine, J., Savisto, N.J., Enerbäck, S., and Nuutila, P. (2009). Functional brown adipose tissue in healthy adults. N. Engl. J. Med. *360*, 1518–1525.

Virtue, S., Even, P., and Vidal-Puig, A. (2012). Below thermoneutrality, changes in activity do not drive changes in total daily energy expenditure between groups of mice. Cell Metab. *16*, 665–671.

Vogelstein, B., Lane, D., and Levine, A.J. (2000). Surfing the p53 network. Nature *408*, 307–310.

Vurusaner, B., Poli, G., and Basaga, H. (2012). Tumor suppressor genes and ROS: complex networks of interactions. Free Radic. Biol. Med. *52*, 7–18.

Wahli, W., and Michalik, L. (2012). PPARs at the crossroads of lipid signaling and inflammation. Trends Endocrinol. Metab. *23*, 351–363.

Wan, M., Leavens, K.F., Saleh, D., Easton, R.M., Guertin, D.A., Peterson, T.R., Kaestner, K.H., Sabatini, D.M., and Birnbaum, M.J. (2011). Postprandial hepatic lipid metabolism requires signaling through Akt2 independent of the transcription factors FoxA2, FoxO1, and SREBP1c. Cell Metab. *14*, 516–527.

Wan, M., Easton, R.M., Gleason, C.E., Monks, B.R., Ueki, K., Kahn, C.R., and Birnbaum, M.J. (2012). Loss of Akt1 in mice increases energy expenditure and protects against diet-induced obesity. Mol. Cell. Biol. *32*, 96–106.

Wang, L., Harris, T.E., Roth, R.A., and Lawrence, J.C. (2007). PRAS40 regulates mTORC1 kinase activity by functioning as a direct inhibitor of substrate binding. J. Biol. Chem. *282*, 20036–20044.

Wang, R.H., Sengupta, K., Li, C., Kim, H.S., Cao, L., Xiao, C., Kim, S., Xu, X., Zheng, Y., Chilton, B., et al. (2008). Impaired DNA damage response, genome instability, and tumorigenesis in SIRT1 mutant mice. Cancer Cell *14*, 312–323.

Wang, T., Hung, C.C., and Randall, D.J. (2006). The comparative physiology of food deprivation: from feast to famine. Annu. Rev. Physiol. *68*, 223–251.

Wang, X., Li, W., Williams, M., Terada, N., Alessi, D.R., and Proud, C.G. (2001). Regulation of elongation factor 2 kinase by p90RSK1 and p70 S6 kinase. EMBO J. *20*, 4370–4379.

Wang, Y., Li, G., Goode, J., Paz, J.C., Ouyang, K., Screaton, R., Fischer, W.H., Chen, J., Tabas, I., and Montminy, M. (2012). Inositol-1,4,5-trisphosphate receptor regulates hepatic gluconeogenesis in fasting and diabetes. Nature *485*, 128–132.

Wang, Y.A., Elson, A., and Leder, P. (1997). Loss of p21 increases sensitivity to ionizing radiation and delays the onset of lymphoma in atm-deficient mice. Proc. Natl. Acad. Sci. USA *94*, 14590–14595.

Webb, A.E., and Brunet, A. (2014). FOXO transcription factors: key regulators of cellular quality control. Trends Biochem. Sci. *39*, 159–169.

Wei, M., Fabrizio, P., Hu, J., Ge, H., Cheng, C., Li, L., and Longo, V.D. (2008). Life span extension by calorie restriction depends on Rim15 and transcription factors downstream of Ras/PKA, Tor, and Sch9. PLoS Genet. *4*, 0139–0149.

Weindruch, R., Walford, R.L., Fligiel, S., and Guthrie, D. (1986). The retardation of aging in mice by dietary restriction: longevity, cancer, immunity and lifetime energy intake. J. Nutr. *116*, 641–654.

Weisberg, S.P., McCann, D., Desai, M., Rosenbaum, M., Leibel, R.L., and Ferrante Jr., A.W. (2003). Obesity is associated with macrophage accumulation in adipose tissue. J. Clin. Invest. *112*, 1796–1808.

Westerterp, K.R. (2013). Physical activity and physical activity induced energy expenditure in humans: measurement, determinants, and effects. Front. Physiol. *4*, 90.

Whittle, A.J., Carobbio, S., Martins, L., Slawik, M., Hondares, E., Vázquez, M.J., Morgan, D., Csikasz, R.I., Gallego, R., Rodriguez-Cuenca, S., et al. (2012). BMP8B increases brown adipose tissue thermogenesis through both central and peripheral actions. Cell *149*, 871–885.

Workman, P., Clarke, P.A., Raynaud, F.I., and Van Montfort, R.L. (2010). Drugging the PI3 kinome: from chemical tools to drugs in the clinic. Cancer Res. *70*, 2146–2157.

Wu, J., Cohen, P., and Spiegelman, B.M. (2013). Adaptive thermogenesis in adipocytes: is beige the new brown? Genes Dev. *27*, 234–250.

Yamashita, H., Takenoshita, M., Sakurai, M., Bruick, R.K., Henzel, W.J., Shillinglaw, W., Arnot, D., and Uyeda, K. (2001). A glucose-responsive transcription factor that regulates carbohydrate metabolism in the liver. Proc. Natl. Acad. Sci. USA *98*, 9116–9121.

Yan, B., Wang, H., Rabbani, Z.N., Zhao, Y., Li, W., Yuan, Y., Li, F., Dewhirst, M.W., and Li, C.Y. (2006). Tumor necrosis factor-alpha is a potent endogenous mutagen that promotes cellular transformation. Cancer Res. *66*, 11565–11570.

Yang, Y., Ju, D., Zhang, M., and Yang, G. (2008). Interleukin-6 stimulates lipolysis in porcine adipocytes. Endocrine *33*, 261–269.

Yatscoff, R.W., LeGatt, D.F., and Kneteman, N.M. (1993). Therapeutic monitoring of rapamycin: a new immunosuppressive drug. Ther. Drug Monit. *15*, 478–482.

Yecies, J.L., Zhang, H.H., Menon, S., Liu, S., Yecies, D., Lipovsky, A.I., Gorgun, C., Kwiatkowski, D.J., Hotamisligil, G.S., Lee, C.H., and Manning, B.D. (2011). Akt stimulates hepatic SREBP1c and lipogenesis through parallel mTORC1-dependent and independent pathways. Cell Metab. *14*, 21–32.

Yeo, G.S., and Heisler, L.K. (2012). Unraveling the brain regulation of appetite: lessons from genetics. Nat. Neurosci. *15*, 1343–1349.

Yoon, J.C., Puigserver, P., Chen, G., Donovan, J., Wu, Z., Rhee, J., Adelmant, G., Stafford, J., Kahn, C.R., Granner, D.K., et al. (2001). Control of hepatic gluconeogenesis through the transcriptional coactivator PGC-1. Nature *413*, 131–138.

You, H., Pellegrini, M., Tsuchihara, K., Yamamoto, K., Hacker, G., Erlacher, M., Villunger, A., and Mak, T.W. (2006). FOXO3a-dependent regulation of Puma in response to cytokine/growth factor withdrawal. J. Exp. Med. *203*, 1657–1663.

Yu, J., Zhang, Y., Mcilroy, J., Rordorf-Nikolic, T., Orr, G.A., and Backer, J.M. (1998). Regulation of the p85/p110 phosphatidylinositol 3′-kinase: stabilization and inhibition of the p110 α catalytic subunit by the p85 regulatory subunit. Mol. Cell. Biol. *18*, 1379–1387.

Yuan, J.S., Reed, A., Chen, F., and Stewart, C.N. (2006). Statistical analysis of real-time PCR data. BMC Bioinformatics *7*, 85.

Zhande, R., Mitchell, J.J., Wu, J., and Sun, X.J. (2002). Molecular mechanism of insulin-induced degradation of insulin receptor substrate 1. Mol. Cell. Biol. *22*, 1016–1026.

Zhang, C., Liu, J., Liang, Y., Wu, R., Zhao, Y., Hong, X., Lin, M., Yu, H., Liu, L., Levine, A.J., et al. (2013). Tumour-associated mutant p53 drives the Warburg effect. Nat. Commun. *4*, 1–15.

Zhang, H.H., Halbleib, M., Ahmad, F., Manganiello, V.C., and Greenberg, A.S. (2002). Tumor necrosis factor-alpha stimulates lipolysis in differentiated human adipocytes through activation of extracellular signal-related kinase and elevation of intracellular cAMP. Diabetes *51*, 2929–2935.

Zhang, T., Wang, S., Lin, Y., Xu, W., Ye, D., Xiong, Y., Zhao, S., and Guan, K.L. (2012). Acetylation negatively regulates glycogen phosphorylase by recruiting protein phosphatase 1. Cell Metab. *15*, 75–87.

Zhou, B.P., Liao, Y., Xia, W., Zou, Y., Spohn, B., and Hung, M.C. (2001). HER-2/neu induces p53 ubiquitination via Akt-mediated MDM2 phosphorylation. Nat. Cell Biol. *3*, 973–982.

Zhu, W., Abbas, T., and Dutta, A. (2005). Genome Instability in Cancer Development. Cold Spring Harb. Perspect. Biol. *5*, 249–279.

SUPPLEMENTARY MATERIAL

Supplementary Table S1

Differentially expressed genes in p21KO livers versus WT liver controls
DEG: $q < 0.05$

UPREGULATED GENES IN p21KO

UP in p21KO *ad libitum* VS WT *ad libitum*	**UP in p21KO VS WT both conditions**	**UP in p21KO fasting VS WT fasting**
Arrdc3	8430408G22Rik	Lepr
Egr1	Glo1	Cyp2b10
Mup17	Igfbp2	Pdk4
Zbtb16	Rgs16	Acmsd
Dynlt1c,Dynlt1f	Pla2g12a	Cbs
Efna1	Agxt2l1	Hamp2
Dynlt1b	Cobll1	Adcy1
Junb	Wnk4	Ppp1r3g
Dynlt1a		Cyp17a1
Spry4		St5
Nr0b2		Hamp
Eno1,Gm5506		Hspb1
Bcl6		Mt1
Pim1		Mt2
Syvn1		3930402G23Rik
Hsd17b6		Cend1
Il6ra		Ddit4
Nfxl1		Rab44
Mup5		Hba-a2
Rnft2		Txnip
Il1r1		Arl4a
Rnf39		Atf5
Zkscan1		Reps1
Dnajb9		B930025P03Rik
Acsm3		Sulf2
Nr1d1		Krt23
Mup6		Serpine2
Zfp36		Igfbp1
Tgif1		Cpt1b
Pcbp2		Sdsl
Tmem39a		Dnajb2
Selenbp2		Il1rn
Osgin1		Kif21a
Pim3		Sik1
Zfp862		Fam134b
Gdf15		Fgf21
Aadat		Rnf167
Clec2h		Plin5
Mtss1		Chkb
Fzd8		Ablim3
Enpp2		Camk2b
Slc13a2		Scara5
Atp6v0c		1700017B05Rik
Sfpq		4930452B06Rik

Arhgef26
Nox4
Creb3l2
Gigyf2
Golph3l
Ppp2r5e
Pabpc4
4933426M11Rik
Gfpt1
Irs2
G0s2
Xlr3a
Fam193b
Arhgap32
Mup9
Hbb-b1,Hbb-b2
Lifr
Herpud1
Trib3
Cela1
Cdk13
Ces2c
Slc25a34
Map3k5
Eif2ak3
Ep400
Synj2
Cyp2u1
Anks1
Xlr3b
Ehmt1
Nfix
Dsg1c
Ppargc1b
Whsc1l1
Ass1
Hyou1
Fzd5
Myo1e
Sun2
Trib1
Cys1
Rhobtb1
Ppp1r3c
Fam107b
Cpeb2

E030018B13Rik
Tacc2
Slc41a3
Arntl
Accn5
Trp53inp1
Cyp2b13
Josd2
Maff
Hilpda
Dusp8
Ppargc1a
Nrg4
Map3k6
Parp16
Lpin2
Rabggtb
Slc16a10
Rab30
Arhgef40
Arl15
Sorbs3
Cdc42ep5
Aldoa
Tubb2b
Srrm4
Fbxo6
Myom1
Derl3
Grtp1
Cyp39a1
Tbc1d8
Abtb2
Rbpms
Fbxo31
Peg3
Nnmt
Lman2l
Eif4ebp3
Clpx
Nedd4l
Slc20a1
Sf1
Rhbdd2
Tubb2a
Cgref1
Echdc2
Cep110
BC057022
Cdkn1a
Slc25a33
Acacb
Lepre1

		Mcc
		Pde4c
		Peg3as
		Creld2
		Atoh8
		Zfhx2
		Tnfrsf12a
		Rps4y2
		Chpf
		Paip1
		Il3ra
		Tnk2
		Pogk
		Vopp1
		Atf3
		Kctd15
		Ccnf
		Gadd45b
		Eppk1
		Elmod3
		2010003K11Rik
		Nr4a1
		P4ha2

DOWNREGULATED GENES IN p21KO

DOWN in p21KO *ad libitum* VS WT *ad libitum*	**DOWN in p21KO VS WT (both conditions)**	**DOWN in p21KO fasting VS WT fasting**
Fgl1	Apcs	Irf7
Gadd45g	Lcn2	Socs2
Mfsd2a	Orm2	Acot3
Mt1	Saa1	Stat1
Mt2	Saa2	Spp1
Myc	Saa3	H2-Aa
Ppp1r10	Tiam2	Itih4
Hcn3	Apol9a	Ndrg2
Cabyr	Trim30d	Ifi27l1
Apoa4	Pfkfb3	Entpd5
Mvd	Igtp	Sorbs2
Lrg1	Ly6e	H2-Eb1
Fbf1	Tymp	9030619P08Rik
Fdps	Tgtp1	Lyz2
Mid1ip1	Tff3	H2-Ab1
Orm3	Samd9l	Col3a1
1810011O10Rik	Cish	Apol7a
Slc3a1	Ifi44	Clec7a
Cyp4a14	Marco	Chpt1
Acacb	Gbp6	Cd5l
Pmvk	Tgtp2	Tbc1d24
Ppp1r3b	Ifit1	Ly6d
Acsl3	Ifi27l2b	Slc44a3

Nedd9	Gbp10	Cd24a
Apol9b	Thrsp	Arhgap19
Gm5506	Gm4070	Rbfox2
Serpina4-ps1	Axl	Emr1
Usp18	Cd36	Abcd2
Ucp2	Mpeg1	Cybb
Prepl	Pklr	Lgals1
Nnmt	Rtn4	Acly
Prg4	Tmem176a	Cd97
Tmem176b	Prlr	Arhgef9
Chrna4	Col15a1	Iigp1
Dnajb2	Tifa	Vcam1
Tmem51	Wdfy1	Samhd1
Pcsk9	Zbp1	Tlr12
H2-T9	Mmp19	Paqr9
Fads3	Lrtm1	Ces2c
Hmgcs1	Mmd2	1110020G09Rik
Steap4	Ttc23	Lyz1
Orm1	Psmb9	Klhdc7a
Tap1	Gbp3	Ubp1
Hmgcr	Erdr1	Slc39a4
Atp11a	Wsb1	Zfp207
Hbb-b2	Gm4841	Arap1
Aacs	Aqp8	Oxr1
2010003K11Rik	Trim30a	Osbpl3
Extl1	Psmb8	Uap1l1
Fam65b	Ifi47	Olfml1
Smpd3	Itgal	Col1a1
Gm8801	Il18bp	Siglec1
Rgs3	Gbp7	Immt
Shisa5	Parp14	Alas2
Eif4e3	Hacl1	Slc41a2
Oasl1	Slc13a5	Ptprc
Sqle	Slc13a3	Lima1
Tgm1	Fam198a	Lilrb4
Gpr110	Oas1a	Gbp2
Trafd1	Gm12250	Aoah
Fgfr3	Sirpa	Flnb
Pml	Fam46a	Keg1
Lbp	Gas6	Cd52
Gm14403	Irgm2	Cxcl12
Lss	Dmpk	Nckap1l
Sco2	Trim12c	Tmsb4x
Cdhr5	St6gal1	Myof
Cyp26a1	C1qc	Sdc3
Tmie	Gstt3	Gigyf2
Fdft1	Pls1	Ncald
Unkl	AW112010	Ccl5
Ifit3	Csf1r	Scd4
Adar	Ctss	Cxcl13
Acnat2	C1qa	Pik3r1
Rasgef1b	Irgm1	Ubd
Dhx58	Tspan4	Ptprg

Cd151
Srxn1
Tcirg1
Jak3
Serpina7
Ccrn4l
S100a10
Gm7120
Isg15
Trim34a
Cebpe
Fasn
Gstm4
Hn1l
Aldh1b1
Acss2
1300015D01Rik
Gm16551
G6pc
Fam53b
Mtmr11
Slc16a5
Spsb3
Hspb1
Pnpla3
Ddc
Rxrg
C1qtnf1
Irf9
Pgd
Bud13
Gck
Tagap1
Mlkl
Tubb2a
Naip2
Pltp
Serinc2
Ildr2
Josd2
Tor1aip2
Ddx60
Insc
Rap1gap
Isyna1
Hsp90aa1
Slc37a1
Zc3hav1
Gtpbp2
Tceal8
Sc4mol
Tnfsf10
Tgfbr2

Cxcl9
Robo1
Pla2g7
Rtp4
Gsdmd
A230050P20Rik
Tnfrsf19
Kifc3
Gm8979
Cd74
Wwtr1
Fam84b

Lrit1
Il2rg
AF251705
Scd2
Ank3
Arhgap25
Rbm3
Ces1g
Scara3
Ghr
Vwa5a
Slc7a8
Cib3
Ces2d-ps
Cyp2a4
Rps6ka1
Nat8
E330011O21Rik
Rasa4
Klf13
Lyn
Ccr5
Scd3
Sorbs1
Ugt1a9
Clec4a3
Ociad2
Nr3c2
Adcy7
Irf8
Erbb2ip
Rnf152
Clec12a
Aif1
Tlr13
Stk10
Ces2e
Nnt
Lgals3
Cyp3a25
C1qb
Rcbtb2
Zfp809
Lpcat2
Cml5
AI182371
Gbp9
Myo1f
Abcg3
Nr1h4
Pld4
Lphn2
Fyb

Clstn3	Phldb2
Csrp3	Iqgap1
Gm19619	Fam55b
Pvrl2	B3galt1
Dock9	Tstd1
Srp54b,Srp54c	Csf1
Bst2	Cyp2c50
Znrf1	Dcun1d1
Gm7694	Cd68
Mdp1	Klra2
Fam47e	Ahnak
Pdzk1ip1	Gda
Mcm6	Gbp8
Gnat1	Lair1
Gtf2ird1	Hpgds
St6galnac6	Acbd5
D14Ertd449e	Fgd2
Serpina11	Cenpl
Ctgf	Arhgap30
Nlrc5	Acot4
Sgsm1	Rasal2
Fam25c	Lpl
Ube2h	Coro1a
Herc6	Gbp1
Mvk	Igfals
Got1	Pnldc1
Fam129b	Eif4g3
Ifitm2	Hck
Zbtb4	Gbp11
Lgals3bp	Blnk
Nrp2	Capg
Aig1	Cyp2a5
Dhcr7	Hk3
I830012O16Rik	Lgmn
Steap2	Taok3
Cyp4a10	Rdh9
Sun1	Cldn2
St5	Slc15a3
Cpne8	Tfrc
Tmem98	Ly86
Zfp259	Hnmt
Trim21	Gp49a
Plac8	Cxcl16
Oasl2	Tyrobp
Grn	BC013712
Jub	Fam129a
Rras	Laptm5
Xaf1	Anxa2
Nsdhl	Dut
Slc25a25	C730036E19Rik
Trim12a	Syk
Cyb561	Unc119
1700024P16Rik	Adhfe1

Agpat9
Filip1l
Mtap7d1
Sall2
Cyp17a1
Oas1g
Sfxn5
Arhgef19
Gm14431
Ifitm3
Mfge8
Tap2
Ggt6
Elovl6
Gpc1
Cldn14
Golm1
Htatip2
Tm6sf2
AB124611
Ddhd1
Slc17a1
Fam73b
Hba-a1,Hba-a2
Srp54a
Cmpk2
Gm5480
D730039F16Rik
Alas1
Elovl5
Abtb2
Ppap2c
Ppl
Ang
Litaf

Cd48
Lilrb3
Slc2a9
Cd180
Lsp1
Cbr1
Rgn
Itgb2
Adam33
Phka2
Ptprd
Timd4
Gstm3
Gm8989
Adra1b
Fabp5
B430306N03Rik
Herc3
Efha1
Pira2
Gm4951
Idi1
Parp12
S100a11
Magi1
Mpp1
Trim24
Hmox1
Mapkapk3
Lrrc25
Tmtc4
Aifm3
Gng2
Evi2b
Mthfd1l
Mmp15
Clec4a1
1600014C10Rik
Clec4n
Folr2
Aatk
Abr
Marcks
Gna14
Hipk2
Mta3
Cxcl10
Scd1
Ctla2b
Nfib
Vsig4
Cd276
Cyp3a16

Supplementary Table S2

Gene set enrichment analysis of p21KO livers versus WT liver controls
GSEA: *FDR* < 0.25

downregulated in
p21KO *ad libitum* VS WT *ad libitum*

KEGG gene set	FDR
biosynthesis of steroids	0.001
antigen processing and pesentation	0.010
proteosome	0.032
glycolysys/gluconeogenesis	0.062
pentose phosphate pathway	0.106
cell adhesion molecules	0.130
galactose metabolism	0.147
natural killer cell mediated cytotoxicity	0.203
tyrosine metabolism	0.204
adipocytokine signaling pathway	0.214
glycan structures-degradation	0.216
primary immunodeficiency	0.218
DNA replication	0.231
autoimmune thyroid disease	0.234

downregulated in
p21KO 24h fasting VS WT 24h fasting

KEGG gene set	FDR
natural killer cell mediated cytotoxicity	0.002
ECM-receptor interaction	0.009
leucocyte transendothelial migration	0.009
drug metabolism-other enzymes	0.009
type II diabetes mellitus	0.012
B-cell receptor signaling pathway	0.012
toll-like receptor signaling pathway	0.012
focal adhesion	0.017
cell adhesion molecules	0.022
butanoate metabolism	0.028
T-cell receptor signaling pathway	0.039
fc epsilon ri signaling pathway	0.058
pentose and glucuronate interconversions	0.061
primary immunodeficiency	0.068
androgen and estrogen metabolism	0.070
apoptosis	0.088
porphyrin and chlorophyll metabolism	0.089
complement and coagulation cascades	0.090
regulation of actin cytoskeleton	0.092
biosynthesis of steroids	0.092
hematopoietic cell lineage	0.093
pancreatic cancer	0.093
PPAR signaling pathway	0.094
phosphatidylinositol signaling system	0.099
adherens junction	0.101
bile acid biosynthesis	0.104
antigen processing and presentation	0.108
colorectal cancer	0.114
small cell lung cancer	0.114
gamma hexachlorocyclohexane degradation	0.117
dentatorubropallidoluysian atrophy	0.119
mismatch repair	0.120
drug metabolism-cytochrome P450	0.121
drug metabolism-cytochrome P450	0.121
DNA replication	0.123
cytokine-cytokine receptor interaction	0.148
biosynthesis of unsaturated fatty acids	0.161
non-small cell lung cancer	0.171
graft-versus-host disease	0.176
glycosphingolipid biosynthesis	0.179
ABC transporters	0.180
metabolism of xenobiotics by cytochr. P450	0.189

ANNEX

Published articles directly related to this PhD thesis:

Ortega-Molina, A.*, Lopez-Guadamillas, E.*, Mattison, J.E., Mitchell, S.J., Muñoz-Martin, M., Iglesias, G., Gutierrez, V.M., Vaughan, K.L., Szarowicz, M.D., González-García, I., López, M., Cebrián, D., Martinez, S., Pastor, J., de Cabo, R., and Serrano, M. (2015) Pharmacological inhibition of PI3K reduces adiposity and metabolic syndrome in obese mice and monkeys. Cell Metabolism *21*, 558-570. (*Co-first authorship.)

Lopez-Guadamillas, E., Fernandez-Marcos, P.J., Pantoja, C., Muñoz-Martin, M., Martínez, D., Gómez-López, G., Campos, R., Valverde, A.M., and Serrano, M. (2016) $p21^{Cip1}$ plays a critical role in the physiological adaptation to fasting through activation of PPARα. *Under revision in Scientific Reports.*

Other published articles:

Ortega-Molina, A., Efeyan, A., Lopez-Guadamillas, E., Munoz-Martin, M., Gómez-López, G., Cañamero, M., Mulero, F., Martinez, S., Romanos, E., Gonzalez-Barroso, M., Rial, E., Valverde, A.M., Bischoff, J.R., and Serrano, M. (2012). Pten positively regulates brown adipose function, energy expenditure, and longevity. Cell Metabolism *15*, 382–394.